UC Berkeley
UC Berkeley Electronic Theses and Dissertations

## Title

14-3-3σ Expression Identifies Basal-Like Breast Cancer and Regulates Tumor Invasion by Defining Subcellular Regions of Actin Polymerization

## Permalink

https://escholarship.org/uc/item/4wn96899

## Author

Boudreau, Aaron Thomas

## Publication Date

2010

Peer reviewed|Thesis/dissertation

eScholarship.org Powered by the California Digital Library
University of California

# 14-3-3σ Expression Identifies Basal-Like Breast Cancer and Regulates Tumor Invasion by Defining Subcellular Regions of Actin Polymerization

By

Aaron Thomas Boudreau

A dissertation submitted in partial satisfaction of the

requirements for the degree of

Doctor of Philosophy

in

Comparative Biochemistry

in the

Graduate Division

of the

University of California, Berkeley

Committee in charge:

Mina J. Bissell, Distinguished Scientist, co-chair

Professor Fenyong Liu, co-chair

Professor Hei Sook Sul

Professor G. Steven Martin

Fall 2010

Abstract

14-3-3σ Expression Identifies Basal-Like Breast Cancer and Regulates Tumor Invasion by Defining Subcellular Regions of Actin Polymerization

by

Aaron Thomas Boudreau

Doctor of Philosophy in Comparative Biochemistry

University of California, Berkeley

Mina J. Bissell, Distinguished Scientist, co-chair

Professor Fenyong Liu, co-chair

The mammary gland can be thought of as an “organism” with very complicated biology. The normal breast is comprised of a milieu of different cell types and extracellular matrix (ECM) components, the sum of which yield a complex microenvironment and series of biological interactions that are essential for normal development and functional differentiation. Many of these events go awry in breast cancer, a disease best characterized by the loss of tissue structure, morphology, and function - in essence, a loss of microenvironment homeostasis.

Perhaps reflecting the complexity of the normal mammary gland, breast cancer cannot be simply described as a single disease, and is instead thought to be comprised of at least 5 molecular subtypes which have distinct clinical features. Evidence for this is noted in the histological, molecular, intra- and intertumor heterogeneity found in the clinic, the differences in patient response to treatment, and correspondingly, the differences in clinical outcome observed between subgroups of patients. Improving our understanding of the molecular basis of breast tumor heterogeneity can potentially lead to improved diagnosis of breast cancer at earlier stages, identify which patients would benefit most from current treatments or combinations of treatments, and unravel novel biomarkers that, if therapeutically targeted, would improve the clinical management of breast cancer. This would represent a significant advance over current therapeutic strategies that are known to be ineffective against certain subtypes of breast cancer.

Basal-like breast cancer, which accounts for 15-20% of invasive breast carcinomas, represents one subtype of breast cancer that is unresponsive to conventional therapies such as tamoxifen and Herceptin, and which has a particularly aggressive clinical course characterized by poor 5-year survival. This breast cancer subtype presents the most challenging case for current clinical

management, and major effort has been placed towards understanding the molecular basis of basal-like breast cancer progression, origin, and diagnosis. Towards that goal, several animal and culture models of basal breast cancer progression and tumor heterogeneity have been developed, and are currently employed in numerous basic science, translational, and preclinical studies.

To investigate the molecular basis of breast cancer progression, previous work in the Bissell lab has characterized an isogenic culture model of tumor progression, called HMT-3522, which recapitulates many features of basal-like breast tumor progression. Proteomic screening of the cell lines by two-dimensional gel electrophosesis and mass spectrometry identified increased 14-3-3σ protein level during malignant progression in this model. 14-3-3σ belongs to a family of molecular scaffolds known to integrate signaling pathways by binding to phosphorylated serine/threonine motifs found in a spectrum of proteins and regulating their subcellular distributions. There are numerous reports implicating 14-3-3σ as a tumor suppressor in the breast and other organs, yet this has not been sufficiently demonstrated in vivo. In addition, there are many conflicting reports suggesting that 14-3-3σ is not a tumor suppressor, and instead may be related to poor clinical outcome in a subset of breast and other cancers. It is clear that the complicated role for 14-3-3σ in cancer progression or suppression is context-dependent, and the overarching goal of my research has been to characterize the function of 14-3-3σ in breast cancer progression and clinical outcome, particularly within the basal-like breast cancer subtype.

Here, I describe a novel function for 14-3-3σ in promoting basal-like breast cancer cell motility and tumor invasion by regulating cytoskeletal dynamics. Using the HMT-3522 series and an independent isogenic model of basal-like breast cancer progression (the MCF10 series), I discovered 14-3-3σ expression increased as cells transition towards malignancy, and upon shRNA-mediated knockdown, cancer cells with perturbed 14-3-3σ expression show decreased motility and invasion through ECM in culture and diminished tumor invasion in vivo. Immunohistochemical analysis of a tissue microarray showed that 14-3-3σ expression preferentially identified basal-like tumors among 245 invasive breast carcinomas, and in independent breast cancer patient cohorts, 14-3-3σ correlated with metastasis and poor clinical outcome. These data demonstrate that 14-3-3σ expression identifies a subset of aggressive breast carcinomas, namely basal-like breast tumors, and furthermore, that 14-3-3σ functions in these tumors by regulating invasion and migration.

I additionally unravelled a mechanism, supported by several lines of evidence, by which 14-3-3σ regulates basal-like breast cancer migration and invasion. Using a combination of live cell imaging, confocal microscopy, biochemical assays, and transgenic cell lines, I discovered that 14-3-3σ regulates cytoskeletal homeostasis in cells by interacting with G-actin directly and sequestering it from growing F-actin filaments, thus inhibiting its polymerization. Through this interaction, 14-3-3σ retains a soluble, “bioavailable” form of actin

within cells to allow for regulated incorporation into growing filaments, ensuring polarized cell migration can occur. In contrast, basal-like breast cancer cells deficient for 14-3-3σ have elevated rates of actin polymerization, have decreased pools of soluble actin available to be incorporated in a regulated fashion, and as a consequence, have decreased motility and invasion. These phenotypes can be rescued by overexpressing actin, but not a mutant form that is unable to be incorporated into existing actin filaments. This mechanism could explain how 14-3-3σ, by defining the balance of actin polymerization within cells, regulates tumor invasion in basal-like breast cancer.

My data showing that 14-3-3σ is a “functional” marker of basal-like breast tumors and poor clinical outcome does not dispute, but rather reconciles, the literature of whether 14-3-3σ is a tumor suppressor in the breast; I propose that the expression and function of 14-3-3σ in breast cancer is contingent on whether tumors show basal-like differentiation, or are of another molecular subtype. My data implicate 14-3-3σ as a potential therapeutic target against the progression of basal-like breast cancer to metastastic disease, which may be of clinical importance following further validation studies. Furthermore, as the regulation of actin cytoskeletal homeostasis by 14-3-3σ was characterized largely in vitro, the functional interaction of 14-3-3σ and actin may be of importance not only in basal-like breast cancer, but additionally during normal development or during malignant progression in tumors originating from other organs.

Acknowledgements

This work would never have been possible without the superb guidance and mentorship from Mina Bissell, whose support and wisdom has shaped me as a scientist and as a person. I am forever grateful to have been a member of her lab for my graduate work, and will never forget the laughs and the many life lessons.

I would never have survived graduate school without such amazing support and understanding that I have had from my parents, Darlene and Roland Boudreau, my fiancée Nancy Ta Banh, and the rest of my friends and family. You have stood by me and had faith in me through the most challenging period of my life. Thank you to the Banh family for making me feel at home even though I am so far from my own family. I love you all.

I am thankful to Hidetoshi Mori, Alain Beliveau, Roland Meier, Kandice Tanner, Doug Brownfield, Rana Mroue, Ren Xu, Eva Lee, Joni Mott, Irene Kuhn, Virginia Spencer, Mark LaBarge, Rick Schwarz, Genee Lee, Connie Myers, Aylin Rizki, Paraic Kenny, Britta Weigelt, Jason Jung, and all other members of the Bissell laboratory for fruitful discussions, technical advice, and for providing emotional support. It has been an honor to be part of such a stellar team.

I would like to give many thanks to Jorge S. Reis-Filho and members of his laboratory for performing the breast cancer tissue microarray analysis, and additionally would like to thank Joe Gray, Marc Lenburg, Sanjay Kumar, as well as my dissertation committee, Fenyong Liu, G. Steven Martin, and Hei Sook Sul, for providing feedback on my research and very helpful suggestions.

My research has generously been funded by a Department of Defense Predoctoral Fellowship (W81XWH-05-1-0339) and a California Breast Cancer Research Program Dissertation Award (14GB-0007).

This work is dedicated in loving memory to Doris Boudreau, who inspired me to join the fight against breast cancer, and to Melford Crowell, who always had a good story to tell and never failed to make me laugh (did you bring your toothbrush?)

Table of Contents

**1. INTRODUCTION** **1**

1.1. The breast is an “organism” with very complex biology 2

1.2. The complexity of the normal breast is embodied in the heterogeneity of breast tumors. 3

1.3. The basal-like breast cancer (BLBC) molecular subtype is a challenging case for current clinical management. 4

1.4. The development of culture and animal models recapitulating breast tumor heterogeneity 5

1.5. The HMT-3522 and MCF10 isogenic models are useful culture surrogates for understanding BLBC progression 8

1.6. 14-3-3σ is a protein upregulated during HMT-3522 progression. 10

1.7. 14-3-3σ and its complicated biology in cancer. 11

1.8. Hypothesis. 12

**2. MATERIALS AND METHODS** **14**

2.1. Cell Culture 15

2.2. Plasmids 16

2.3. Protein Analysis and Purification 19

2.4. In Vivo Studies 20

2.5. Clinical Analyses 22

2.6. Imaging and Analysis 23

2.7. In Vitro Actin Assays 25

2.8. Statistical Analysis 26

**3. RESULTS** **27**

3.1. 14-3-3σ is a marker of basal-like breast cancer 28

3.2. 14-3-3σ regulates BLBC tumor invasion 31

3.3. 14-3-3σ is a regulator of actin dynamics 34

3.4. 14-3-3σ interacts directly with G-actin and inhibits its polymerization 42

3.5. Future experiments 45

**4. DISCUSSION 47**

4.1. A previously undescribed role for 14-3-3σ in directly inhibiting actin polymerization. 48

4.2. 14-3-3σ and basal-like breast cancer. 49

4.3. 14-3-3σ and poor clinical outcome. 51

4.4. Conclusions. 52

**5. REFERENCES 53**

**6. FIGURES AND FIGURE LEGENDS 81**

# CHAPTER 1. INTRODUCTION

## 1.1. The breast is an "organism" with very complex biology

The breast is comprised of a series of polarized, bilayered epithelial ducts which begin at the nipple, are branched throughout a heterogeneous stroma, and end at terminal ductal lobular units – the functional units of the gland (Cowin and Wysolmerski, 2010; Daniel and Smith, 1999; Nelson and Bissell, 2005; Richert et al., 2000). The inner epithelial cells are known as luminal epithelia, and are involved in milk synthesis during lactation and apical secretion into the ducts. The luminal epithelial cells are surrounded by a discontinuous layer of myoepithelial cells, which provide the coordinated contractile forces necessary to eject secreted milk through the ducts towards the nipple. Myoepithelial cells additionally secrete basement membrane components, in particular laminins, which are involved in the establishment and maintenance of luminal epithelial polarity and function (Gudjonsson et al., 2005); disruption of luminal epithelial cell polarity impairs their ability to express milk proteins in the presence of lactogenic hormones, which can be rescued by placing cells in a laminin-rich extracellular matrix (lrECM) (Gudjonsson et al., 2002). Luminal and myoepithelial cells have characteristic gene expression profiles to instruct their unique roles in mammary function, with one striking feature of myoepithelial cells being the presence of smooth muscle cytoskeletal components that are able to contract in response to oxytocin, whereas a unique feature of luminal epithelial cells is their capacity to respond to lactogenic hormones and synthesize milk proteins as needed (Page et al., 1999; Reversi et al., 2005; Sasadaira et al., 1978; Xu et al., 2009a).

Unique among organs, the majority of breast development occurs postnatally during puberty. Males and females are both born with an undifferentiated mass of breast epithelium called the anlange, which in response to estrogen, progesterone, and other hormones expressed during puberty in females, begins to develop and infiltrate into the surrounding stromal tissue. This infiltration is accompanied by remodeling of the underlying extracellular matrix surrounding the cells, extensive epithelial cell proliferation, and collective migration until the ducts span the entire fat pad (Daniel and Smith, 1999; Fata et al., 2004). Branching ducts never cross paths, presumably due to the secretion of inhibitory factors which act on neighboring ducts to influence their path of migration (Faulkin and Deome, 1960; Nelson et al., 2006; Silberstein and Daniel, 1987). The gland undergoes further development during pregnancy, with lactogenic stimuli directing the epithelia to further proliferate and differentiate, and alveoli become enlarged and eventually synthesize milk. Following birth and weaning, the gland undergoes extensive remodeling and regresses to a state similar to a prenatal gland in order to prepare for subsequent rounds of pregnancy (Stein et al., 2007). These events are tightly regulated by biochemical and mechanical cues within the tissue microenvironment (Alcaraz et al., 2008; Xu et al., 2009b), and cells are poised to respond to the cues as needed - even the fluctuations in estrogenic activity associated with the menstrual cycle are sufficient to modestly influence breast epithelia proliferation and regression (Ferguson and Anderson, 1981; Nazario et al., 1995).

The epithelial ducts are surrounded by a complex stroma comprised of extracellular matrix (ECM) molecules which constantly change during development and pregnancy-related events, and many cell types, including adipocytes, fibroblasts, myofibroblasts, endothelial cells, mesenchymal stem cells, and macrophages among others (Bissell et al., 2005; Fata et al., 2004; Polyak and Kalluri, 2010; Xu et al., 2009a). These cell types participate in extensive heterotypic communication with other cells in their vicinity and their underlying ECM, and the sum of these interactions drive proper gland development and function (Gouon-Evans et al., 2000; Ingman et al., 2006; Landskroner-Eiger et al., 2010). Furthermore, there is clear evidence of a stem/progenitor cell hierarchy being present within the mammary gland whose differentiation is encoded by cues from the tissue microenvironment (LaBarge et al., 2009; Villadsen et al., 2007). Impressively, the mammary gland microenvironment can even cause transdifferentiation of cells originating from other organs (Booth et al., 2008; Boulanger et al., 2007; Bussard et al., 2010). As such, many fundamental questions about the nature of the breast remain unanswered, such as how many cell types exist in the gland, what ECM molecules are involved in functional differentiation, and how does one define breast cell types as unique entities; for instance, what property determines when a progenitor cell is considered a myoepithelial cell? How many of these cell types are transient visitors that leave no lasting impact on gland homeostasis, versus cell types that are absolutely required for development and function?

### 1.2. The complexity of the normal breast is embodied in the heterogeneity of breast tumors.

Given the complexity of normal breast biology, it is not surprising that the biology of breast cancer is also very complicated. Pathologists have known for decades that breast cancer cannot be described as a single disease, and pathological heterogeneity of breast cancer based on tumor morphology, location, grade, lymph node metastasis, and other parameters is well documented and routinely assessed in the clinic (Bloom and Richardson, 1957; Clarke et al., 2005; Ellis et al., 1992; Elston and Ellis, 1993; Erlandson and Rosen, 1982; Fardal et al., 1964; Jackson, 1966; Macdonald, 1966; Moss, 1965; Singletary and Connolly, 2006). In addition, molecular subtypes of breast cancer based on the expression of cell surface molecules such as hormone (estrogen and progesterone) and growth factor (such as HER2/ErbB2) receptors exist in addition to pathological subtypes, and have associated clinical pathology, patient outcome, and treatment regimens (Clark and McGuire, 1988; Fisher et al., 1998; Fisher et al., 1983; Geschickter et al., 1934; Maughan et al., 2010; Mohs, 1940; Paradiso et al., 1990; Pegram et al., 1998; Slamon et al., 1987).

The advent of whole genome expression profiling by microarray analysis has further revealed that there are additional molecular subtypes of breast cancer which bifurcate from estrogen receptor (ER)-positive and ER negative diseases, and these molecular subtypes behave as distinct clinical entities (Fan

et al., 2006; Parker et al., 2009; Perou et al., 2000; Rouzier et al., 2005; Sorlie et al., 2001; Sorlie et al., 2003). Other seminal microarray-based approaches have led to the identification of gene expression signatures which can predict patient outcome independent of other clinical parameters (Foekens et al., 2006; Liu et al., 2007a; Nuyten and van de Vijver, 2006; Paik et al., 2004; van 't Veer et al., 2002; van de Vijver et al., 2002; Wang et al., 2005b); these studies have culminated in the development of expression-based assays (MammaPrint and onco*type*DX) that are in clinical use, and which can predict patients that should be given chemotherapy versus those that would see no additional benefit (Albain et al., 2009; Lo et al., 2010; Paik et al., 2006; Straver et al., 2009). Lastly, in addition to heterogeneity between tumors, it is becoming appreciated that a high degree of molecular and morphological heterogeneity exists even within tumors (Miron et al., 2010; Park et al., 2010; Rakha et al., 2009), further complicating the development of therapeutic strategies and our understanding of disease progression.

The currently accepted molecular subtypes of breast cancer based on gene expression profiling have been largely validated across multiple patient cohorts and array platforms, indicating the biology governing breast cancer heterogeneity observed in large scale genomic profiling is not an artifact of early microarray platform design or of patient selection (Fan et al., 2006; Hu et al., 2006; Sorlie et al., 2003). While the absolute number of subtypes continues to evolve, there are at least two ER-positive “luminal” subtypes (Luminal A and B, with luminal B having significantly worse clinical outcome) and two ER-negative subtypes (“basal-like” and HER2/ErbB2 positive tumors), though additional subtypes of ER-positive and ER-negative tumors (Luminal C and “normal breast-like”, respectively) have emerged in some analyses (Perou et al., 2000; Sorlie et al., 2001; Sotiriou et al., 2003). Nomenclature of the molecular subtypes was assigned largely based on the patterns of gene expression observed in tumors relative to the cell types present in the normal breast, though by no means does this indicate the cell of origin for the tumor – for instance, although basal-like breast cancers (BLBCs) express many markers of basal/myoepithelial cells, many BLBCs are thought to originate from aberrant luminal epithelial progenitor cells rather than myoepithelial cells (Lim et al., 2009), though malignant myoepitheliomas do occur and have a basal-like phenotype (Clarke et al., 2005; Hungermann et al., 2005; Simpson et al., 2004).

### 1.3. The basal-like breast cancer (BLBC) molecular subtype is a challenging case for current clinical management.

Among the molecular subtypes of breast cancer, the basal-like breast cancer (BLBC) subtype accounts for roughly 15-20% of invasive carcinomas and are among the more aggressive of tumor subtypes, with relatively poor 5-year survival in comparison to other subtypes (Perou et al., 2000; Sorlie et al., 2001; Sotiriou et al., 2003). BLBCs are characterized by the lack of ER, progesterone receptor (PR) and HER2/ErbB2 expression (a “triple-negative” immunoprofile),

frequent BRCA1/2 and/or p53 dysfunction, high proliferative index, poor tumor differentiation, central necrotic regions, metaplastic foci, and the expression of epidermal growth factor receptor (EGFR), 'basal' cytokeratins (Cks), and other genes normally restricted to the basal and/or myoepithelial compartment of the nonmalignant breast (Fulford et al., 2006; Nielsen et al., 2004; Perou et al., 2000; Rakha et al., 2007; Rakha et al., 2006; Rakha et al., 2008; Sorlie et al., 2001). In addition, BLBCs are often classified as having a poor prognosis by the 70-gene MammaPrint signature and other gene signatures indicative of poor clinical outcome (Fan et al., 2006). As BLBCs lack ER and HER2/ErbB2 expression, they are not predicted to respond well to tamoxifen, trauztusumab (Herceptin) and other targeted therapeutics available to other breast cancer subtypes. Although polyADP ribose polymerase inhibitors are showing promise in the clinical as a targeted therapy against BRCA1/2-associated BLBC (Fong et al., 2009; Hay et al., 2009), this subtype still presents the most challenging case for current clinical management, and major effort has been placed on understanding the molecular basis governing BLBC progression in order to develop effective targeted therapies for patients.

Several histological surrogates for identifying BLBC have been proposed in order to assess which tumors should be prioritized for aggressive treatment (Cheang et al., 2008; Haffty et al., 2006; Nielsen et al., 2004; Rakha et al., 2007; Sousa et al., 2010). One commonly employed surrogate is "triple-negative" immunohistochemical staining for ER, PR, and HER2/ErbB2 (Haffty et al., 2006), and indeed, the terms "triple-negative" and "basal-like" are often incorrectly used interchangeably in the literature (Rakha et al., 2008). There is growing evidence that while basal-like and triple-negative tumors share a degree of pathological overlap, they also have unique clinical features due to either differences in their underlying biology or tumor miscategorization; poor sample preparation, weak staining, improper scoring/interpretation, and other artifacts can lead to a false positive "triple-negative" immunoprofile (Cheang et al., 2008; Rakha et al., 2007; Rhodes et al., 2000). Other histological surrogates have been proposed, the most widely accepted being the absence of ER and HER2/ErbB2 and the presence of EGFR and/or cytokeratin (Ck) 5/6 staining (Cheang et al., 2008; Nielsen et al., 2004), though there lacks a consensus definition for BLBC. As such, another challenge facing the breast cancer research community is to unravel novel markers of breast cancer subtypes in order to improve tumor detection and classification, and prioritize patient treatment accordingly - ideally markers contributing to disease progression which can be therapeutically targeted in a "personalized-medicine" approach.

### 1.4. The development of culture and animal models recapitulating breast tumor heterogeneity

In order to best understand the molecular basis of cancer progression and heterogeneity, it is ideal to perform experiments using a model that recapitulates the complexities of interactions among cells, tissues, and their microenvironment

as they occur in vivo. Towards that goal, there are dozens of mouse models generated by oncogene transduction and/or targeted deletion of tumor suppressor genes which recapitulate many stages and clinical aspects of breast cancer development and/or progression (Drost and Jonkers, 2009; Sierra, 2009; Taneja et al., 2009). While a full review of all available mouse models is beyond the scope of this work, several examples of mouse strains with high similarity to human breast cancer pathology and which can model specific breast cancer molecular subtypes are established. One popular mouse model due to its rapid tumorigenesis and spontaneous metastasis is the mouse mammary tumor virus (MMTV)-polyoma middle T (PyMT), which form tumors that are of luminal subtype and hence effectively model the majority of human tumors (Guy et al., 1992a; Kouros-Mehr et al., 2008; Kouros-Mehr et al., 2006). The MMTV-PyMT model has recently been employed to show the importance of GATA-3 loss in luminal cancer progression to metastatic disease and the role for GATA3 in maintenance of luminal epithelial cells differentiation (Kouros-Mehr et al., 2008; Kouros-Mehr et al., 2006), validating earlier studies suggesting GATA3 expression correlates with favorable breast cancer clinical outcome (Jenssen et al., 2002; Mehra et al., 2005). Other notable mouse models include the MMTV-HER2/ErbB2 strains popularized by the Muller lab, which have been extensively used to model HER2/ErbB2 human cancer progression, genomic aberration, and therapy response in several studies (Andrechek et al., 2000; Guy et al., 1992b; Hodgson et al., 2005; Lu et al., 2009a; Muller et al., 1988; Shah et al., 2009). Lastly, mouse strains with loss of p53 and BRCA1 function have been generated by independent groups, with tumors formed in these mice being immunohistochemically and pathologically indistinguishable from human basal-like breast tumors (Liu et al., 2007b; McCarthy et al., 2007; Shakya et al., 2008). Despite the availability of mouse models for each of the major breast cancer subtypes, in vivo studies in general are lengthy and are limited in their flexibility for specific experiments such as gene knockdown, combinatorial drug treatment, or kinetic studies, thus using mouse models in the absence of simpler, reductionistic approaches (such as cell culture) may not always be feasible.

Regardless of their inability to recapitulate the complexity of tumor formation and morphology in vivo, studies using established cell lines have yielded much of the present knowledge regarding the properties of breast cancer and its progression due to their flexibility for experiments. However, in order to make effective use of a culture surrogate to study an inherently heterogeneous disease such as breast cancer, one must either use a cell line that is relevant to the breast cancer subtype of interest, or for more generalizable data, enough cell lines to recapitulate the tumor heterogeneity observed in the clinic. A recent molecular profiling analysis on a panel of 51 cell lines has shown that while established cells do not recapitulate the exact molecular spectrum of tumors observed in patients, they can at least sort into basal-like or luminal subtypes that may or may not overexpress HER2/ErbB2, and tend to emulate the clinical features and heterogeneity of their tumor counterparts with respect to drug

response, growth, genomic aberrations, and invasiveness, though are somewhat divergent in their patterns of genomic aberrations (Chin et al., 2006; Neve et al., 2006).

To test the in vivo relevance of results obtained in cell culture studies and monitor tumor-stromal interactions without the burden of generating mouse models, one can perform xenograft experiments by implanting human breast cancer cell lines into immunocompromised mice or organs (Bogden et al., 1979; Clarke, 1996; Greene, 1938; Hendrickson, 1993; Miller, 2000; Miller et al., 1993; Niclou et al., 2008; Rizki et al., 2008). For breast cancer, this is typically accomplished by injecting a mixture of cells and lrECM orthotopically into the mammary fat pad or subcutaneously into the rear flank. Additionally, introducing breast cancer cell lines into the circulatory system of immunocompromised mice, often through either the tail vein or the left ventricle, can be used as a surrogate to measure some elements of metastasis such as extravasation and tropism towards specific organs (Bos et al., 2010; Bos et al., 2009; Conley, 1979; Gupta et al., 2007; Nam et al., 2008; Pang et al., 2009). Due to the relatively short length of time required for xenograft experiments compared to generating trangenic mouse strains and the benefit of cell culture flexibility, xenograft experiments are frequently employed in preclinical or translational studies to measure the contribution of genes and therapeutics to cancer progression (Lu et al., 2009b; Teicher, 2009).

One limitation to xenografts and mouse models, however, is they are not easily amenable to high throughput or multiplexed experiments to test combinations of therapies, in a manner that cell culture is. To overcome this, culturing cells in physiologically relevant 3D microenvironments has been proposed as an ex vivo surrogate for preclinical studies (Park et al., 2006; Weigelt and Bissell, 2008; Weigelt et al., 2010). Culturing nonmalignant mammary epithelial cells in 3D lrECM allows the cells to form growth arrested and polarized structures similar to acini observed in vivo, respond to lactogenic hormones and synthesize milk protein, and distinguishes their growth properties from malignant cells which fail to polarize and continue to proliferate (Barcellos-Hoff et al., 1989; Lee et al., 1985; Lee et al., 1984; Lee et al., 2007; Li et al., 1987; Petersen et al., 1992; Xu et al., 2009a). In a systems-based approach, it was found that breast cancer cell lines cultured in 3D lrECM adopt colony morphologies largely correlating with cell invasiveness, gene expression, molecular subtype, and whether they originated from metastases (Kenny et al., 2007), and high content screens are underway to monitor how the 3D ECM microenvironment influences tumor cell biology and drug response. The advent of more advanced culture techniques, such as xenograft, 3D cell cultures, and heterotypic cell co-cultures (Gudjonsson et al., 2002; Hu et al., 2008; Jedeszko et al., 2009; Manabe et al., 2003; Rozenchan et al., 2009) have aimed to overcome the biological shortcomings of conventional cell culture and are now commonplace. However, another disadvantage of using a collection of cells from different patients (beyond issues of in vivo relevance) is that one cannot look at

events related to tumor progression per se without a nonmalignant comparison from the same patient.

### 1.5. The HMT-3522 and MCF10 isogenic models are useful culture surrogates for understanding BLBC progression

To eliminate confounding factors associated with comparing nonmalignant and cancerous cells from different patients, isogenic cell culture models recapitulating stages of breast cancer progression from nonmalignant to frank malignancy have been established by independent approaches. The MCF10 progression series is comprised of cells that, upon injection into the mammary gland of mice, are nonmalignant (MCF10A), form benign hyperplasia (MCF10neoT), form comedo-type ductal carcinoma in-situ (MCF10DCIS.com), or form invasive carcinomas (MCF10CA1) (Miller et al., 2000; Miller et al., 1993). The series was established by infecting nonmalignant MCF10A cells (originally obtained from a reduction mammoplasty) with viruses expressing constitutively-active H-Ras, to generate MCF10neoT. Serial passaging the MCF10neoT xenografts in mice leads to the eventual formation of a tumor containing mixed DCIS and invasive foci; one such tumor was dissociated and clonal isolates were expanded into the MCF10DCIS.com and MCF10CA1 lines. The cell lines within the MCF10 series have a basal-like gene expression signature and immunohistochemical staining profile (Behbod et al., 2009; Hu et al., 2008), and thus are proposed to be a good model to study BLBC progression. One caveat of the model, however, is that it was established by overexpressing a constitutively-active oncogene that has no reports of being mutated in breast cancer. Nonetheless, this progression model has been used in numerous studies owing to the histological similarity between xenografts and their human breast lesion counterparts, the rarity of other models for DCIS, and due to the ability of the MCF10A to form polarized, acinar-like structures in 3D lrECM cultures (Aranda et al., 2006; Debnath et al., 2003; Hu et al., 2008; Miller et al., 2000; Miller et al., 1993; Muthuswamy et al., 2001).

We have previously described and are actively characterizing another isogenic culture model of human breast tumorigenesis (called HMT-3522) that encompasses nonmalignant (S1), premalignant (S2), preinvasive (S3), and tumorigenic/invasive (T4-2) cell populations (Briand et al., 1996; Briand et al., 1987; Fournier et al., 2006; Kenny and Bissell, 2007; Liu et al., 2006a; Liu et al., 2004; Petersen et al., 1992; Rizki et al., 2007; Rizki et al., 2008; Wang et al., 2002a; Weaver et al., 2002; Weaver et al., 1997). This series has two major advantages over the MCF10 series, the first being that the series was established without exogenous oncogene addition, and secondly, cells are cultured in chemically-defined media lacking serum. Similar to MCF10A, S1 cells were established from a reduction mammoplasty, are nonmalignant, are dependent on exogenous growth factors for proliferation, and form polarized, acinar-like structures when cultured in 3D lrECM (Fournier et al., 2006; Petersen et al., 1992). One hallmark of cancer is the ability for cells to proliferate in the

absence of exogenous growth factors (Hanahan and Weinberg, 2000), and in line with this model, a premalignant population of cells (S2) were selected from S1 cells by culturing them in the absence of epidermal growth factor (EGF) for several generations (Briand et al., 1996). These cells are self-sufficient for EGFR activation, form disorganized, heterogeneously-sized colonies in 3D lrECM, and a rare small-sized tumor in mice. Clonal isolates from S2 cells (S3) were expanded into independent lines based on colony size in 3D lrECM (S3A<S3B<S3C), with S3C in particular having transcriptional and biological features of a preinvasive cell line (Rizki et al., 2007; Rizki et al., 2008). Lastly, serial S2 tumor transplantation and expansion in culture yielded a cell population (T4-2) that forms very large disorganized colonies in 3D lrECM, and is 100% tumorigenic and invasive in vivo (Briand et al., 1996; Rizki et al., 2008; Weaver et al., 1997).

As with the MCF10 series, the HMT-3522 series have basal-like molecular profiles and are thought to best model BLBC progression (Kenny et al., 2007; Rizki et al., 2007; Rizki et al., 2008). Tumors formed from T4-2 xenografts display many cardinal features of human BLBCs, including high histological grade, positivity for cytokeratin (Ck) 5/6, robust EGFR expression, negativity for HER2, ER, and progesterone receptor (PR), high Ki-67 proliferative index, acellular central necrotic regions, squamous differentiation, and aggressive invasion into surrounding soft tissue (Rizki et al., 2008). In addition to modeling tumor progression, the series has been extensively used to model events related to pharmacologic response and corresponding phenotypic reversion; by correcting the elevated signaling observed in T4-2 cells, one can restore the polarity and growth arrest observed in S1 3D lrECM cultures, and can inhibit tumorigenesis in mice (Itoh et al., 2007; Kenny and Bissell, 2003; Liu et al., 2004; Park et al., 2008; Wang et al., 2002a; Wang et al., 1998; Weaver et al., 1997). One caveat to the HMT-3522 series is that many signaling pathways that are altered during tumor progression in this model are either directly or indirectly integrated with EGFR signaling (Kenny and Bissell, 2007; Liu et al., 2004; Rizki et al., 2007; Wang et al., 1998; Weaver et al., 1997) – there is an inherent bias towards the EGFR pathway, which is unsurprising given how the cell lines were established. As one frequent feature of BLBC is elevated EGFR expression (Cheang et al., 2008; Nielsen et al., 2004), this caveat may actually reinforce the utility of the HMT-3522 series as a model for BLBC progression. Interestingly, overexpression of EGFR in S1 cells increases cell proliferation but does not disrupt basal polarity, suggesting that there is more involved in the malignant progression than EGFR amplification (Chen et al., 2009; Wang et al., 1998). Given that the HMT-3522 and the MCF10 series recapitulate many features of basal-like malignant progression, both models are useful tools to dissect molecular events related to breast cancer progression in general or to the BLBC subtype specifically.

### 1.6. 14-3-3σ is a protein upregulated during HMT-3522 progression.

In an attempt to discover novel proteins related to tumor progression, previous unpublished work in the Bissell lab focused on performing 2D gel mass-spectrometry profiling of the HMT-3522 cells when cultured in 3D lrECM. In this analysis, 14-3-3σ emerged as a protein that is expressed 2.3-fold higher in T4-2 cells relative to their non-malignant counterpart, S1. In an independent study using an alternative proteomics approach, 14-3-3σ levels in T4-2 was similarly shown to be 2-fold higher than in S1 cells (Yan et al., 2005); however, in this study, cells were cultured in 2D tissue culture flasks rather than in 3D lrECM. 14-3-3σ belongs to a conserved family of molecular scaffolds comprised of seven known mammalian isoforms (β, γ, ε, η, σ, θ/τ, and ζ) which regulate pathways involved in growth regulation and cell cycle progression through binding and sequestering the subcellular distribution of many ligands (Aitken, 2006; Mhawech, 2005; Porter et al., 2006). Indeed, well over 200 different 14-3-3 ligands have been documented, implicating 14-3-3 proteins as central regulators of many cellular functions. 14-3-3 proteins interact with phosphorylated proteins through consensus phosphoserine motifs that are of sequence RSXpSXP or RXY/FXpSXP (Yaffe et al., 1997), though many examples of phosphorylation-independent interactions and those involving nonclassical epitopes have been documented (Borch et al., 2002; Jin et al., 2004; Ottmann et al., 2007; Petosa et al., 1998).

The crystal structures of all seven mammalian 14-3-3 isoforms and one tobacco 14-3-3 isoform has been published (Gardino et al., 2006; Liu et al., 1995; Ottmann et al., 2009; Wilker et al., 2005; Xiao et al., 1995; Yang et al., 2006c) and reveal a highly conserved molecular blueprint. 14-3-3 functions as a dimer, and each monomer is comprised of 9 alpha-helices that, as a dimer, form a horseshoe-shaped unit. Highly conserved domains in the N-terminus are thought to be involved in dimerization, while the C-terminus helices are implicated in ligand binding (Gardino et al., 2006; Herron et al., 2005; Li et al., 2005; Wilker et al., 2005; Yaffe et al., 1997). 14-3-3σ is the most divergent of the mammalian isoforms, based on both sequence alignment data and on its unique biology. It contains three specific residues facing the ligand binding pocket that are not present in the other six 14-3-3 isoforms; mutating these residues to their analogous residues found in other isoforms allows the protein to interact with cdc25C, normally a ligand for other 14-3-3 isoforms but not 14-3-3σ (Wilker et al., 2005). Additionally, while other 14-3-3 members can heterodimerize, 14-3-3σ and gamma exclusively form homodimers (Wilker et al., 2005). In 14-3-3σ, this homodimerization is mediated by salt bridges and aromatic stacking interactions that are only possible between 14-3-3σ monomers, and performing mutagenesis on these residues allows it to form heterdimers with the remaining six 14-3-3 members and perturbs 14-3-3σ biological activity (Li et al., 2009; Verdoodt et al., 2006; Wilker et al., 2005). These structural studies demonstrated that although 14-3-3 isoforms are highly conserved and have essentially superimposable

crystal structures, there are a sufficient number of subtle differences between the family members to allow specificity and thus unique biology.

### 1.7. 14-3-3σ and its complicated biology in cancer.

Of the seven isoforms, 14-3-3σ and 14-3-3zeta have been implicated the most in breast and other cancers. Two recent studies link 14-3-3zeta expression with breast cancer recurrence, tumorigenesis, and progression from DCIS to invasive carcinoma; interestingly, both studies suggest that the protumorigenic events are related to signaling through the HER2/ErbB2 pathway (Lu et al., 2009a; Neal et al., 2009), suggesting tumor subtype-specific roles for 14-3-3zeta. Expression of this isoform has also been implicated in other tumor types, including the lung (Li et al., 2008), mouth (Matta et al., 2007), head and neck (Matta et al., 2008; Ralhan et al., 2008), and lymphoma (Maxwell et al., 2009) among others.

Less clear is the role for 14-3-3σ in human cancers. This isoform was initially characterized in human mammary epithelial cells, and its expression was shown to be epigenetically regulated in breast tumors through promoter methylation or estrogen-regulated proteolysis (Ferguson et al., 2000; Prasad et al., 1992; Umbricht et al., 2001; Urano et al., 2002; Vercoutter-Edouart et al., 2001). 14-3-3σ promoter methylation occurs in as many as 91% of breast cancers, leading many to predict that 14-3-3σ is a tumor suppressor gene. In further support of this theory, work from the Vogelstein lab has shown that 14-3-3σ functions as an enforcer of the G2/M checkpoint in HCT116 colorectal cancer cells that is upregulated in response to DNA damage (Chan et al., 1999; Hermeking et al., 1997), and it has additionally been shown to facilitate mitotic translation in HeLa and U2OS cells (Wilker et al., 2007). Recent studies have suggested 14-3-3σ is involved in regulating mammary epithelial cell polarity (Ling et al., 2010), which together with the earlier studies mentioned above, compellingly argue that 14-3-3σ is a tumor suppressor.

However, there have been other reports in the literature challenging the dogma of 14-3-3σ acting exclusively as a tumor suppressor gene that is silenced by methylation in cancer. In one such study it was shown that despite the high frequency of promoter methylation observed in breast tumors, protein silencing is an infrequent event in breast cancer (Moreira et al., 2005). This agrees with recent data showing that in a panel of 302 vulval squamous cell carcinomas, only 25% of tumors have low 14-3-3σ protein levels despite 100% of the tumors tested (n = 57) having 14-3-3σ promoter methylation (Wang et al., 2008). In another immunohistochemical study, 14-3-3σ was found to be expressed highly in 10 of 12 cases of BLBCs, and its cytoplasmic localization predicts poor clinical outcome (Simpson et al., 2004). 14-3-3σ expression is elevated in pancreatic (Hustinx et al., 2005; Okada et al., 2006), colorectal (Perathoner et al., 2005), head and neck (Ralhan et al., 2008), and endometrial carcinomas (Nakayama et al., 2005), as well as in various epithelial cancers with squamous differentiation

(Laimer et al., 2009; Mhawech et al., 2005; Nakajima et al., 2003; Wang et al., 2008), suggesting that 14-3-3σ has other (likely tissue-specific) functions related to cancer progression, rather than suppression.

In support of this, it was found that forced 14-3-3σ overexpression in HCT116 colorectal cancer cells, the very cell line where this protein was first demonstrated to regulate the G2/M checkpoint, promotes cell motility (Ide et al., 2007). This observation, in conjunction with that of elevated 14-3-3σ immunohistochemical staining at the invasive front of tumors in patients, suggests a role for 14-3-3σ in facilitating colorectal tumor progression to invasive carcinoma. Forced expression of 14-3-3σ in PANC-1 pancreatic cancer cell lines similarly promotes cell migration and invasion without influencing proliferation (Neupane and Korc, 2008). These studies provide evidence that this molecule can regulate tumor cell migration independently from its cell cycle roles, though there is currently no mechanism to account for this. Intriguingly, there are reports of 14-3-3σ secretion from cells via a non-classical secretion pathway (Ghahary et al., 2004; Leffers et al., 1993), and the presence of 14-3-3σ in interstitial fluid perfusing the breast tumor microenvironment has been demonstrated (Celis et al., 2004); in keratinocytes, this extracellular 14-3-3σ has been shown to stimulate matrix metalloproteinase expression in dermal fibroblasts during wound healing (Ghaffari et al., 2006; Ghahary et al., 2004; Ghahary et al., 2005). These data suggest that 14-3-3σ may modulate cell motility, heterotypic cellular interactions, and ECM remodeling within the tumor microenvironment to regulate tumor invasion.

In agreement with these reports, 14-3-3σ expression has been shown to predict poor clinical outcome in breast, lung, head and neck, pancreatic, colorectal, and oral cancers (Hustinx et al., 2005; Laimer et al., 2009; Matta et al., 2008; Perathoner et al., 2005; Ramirez et al., 2005; Simpson et al., 2004); however, in other malignancies such as endometrial and ovarian cancers, 14-3-3σ expression predicts good clinical outcome (Akahira et al., 2004; Ito et al., 2005). Other studies have shown that 14-3-3σ expression confers drug resistance in breast, pancreatic, and prostate cancer cell lines (Han et al., 2006; Li et al., 2009; Liu et al., 2006b; Neupane and Korc, 2008; Neve et al., 2006). While the link between 14-3-3σ and drug resistance may explain how expression of this protein correlates with poor clinical outcome of certain tumors, the mechanism by which 14-3-3σ contributes to pharmacological response is unclear. What is apparent is that the role for 14-3-3σ in cancer progression or prevention is complicated, highly dependent on tumor type and context, and warrants further characterization.

### 1.8. Hypothesis.

In the normal breast, 14-3-3σ has been shown to be expressed three-fold higher in myoepithelial cells than in luminal cells (Moreira et al., 2005; Simpson et al., 2004). This observation, in conjunction with a pilot study showing high 14-

3-3σ inmmunoreactivity in 10 of 12 BLBCs (Simpson et al., 2004), and previous proteomic data showing elevated 14-3-3σ expression during HMT-3522 BLBC progression (Yan et al., 2005), led me to hypothesize that 14-3-3σ may serve an important function in breast cancer progression, particularly in the basal-like subtype. Furthermore, using the two isogenic breast tumor progression series (HMT-3522 and MCF10) as a model for BLBC progression could provide clues as to what these functions entail. As such, the goal of my PhD research has been to characterize the functions of 14-3-3σ in breast cancer progression, in particular within the BLBC subtype.

# CHAPTER 2. MATERIALS AND METHODS

## 2.1. Cell Culture

### 2.1.1. Media, additives, and substrata

All cell culture media, fetal bovine serum (FBS) and trypsin was obtained either from Gibco or from the UCSF Cell Culture core facility. HMT-3522 cells (S2, S3C, and T4-2) were maintained on flasks coated with acid extracted collagen type I, supplied either as Vitrogen (Celtrix Laboratories) or as PureCol (Advanced BioMatrix). lrECM was obtained either from BD Biosciences (marketed as Matrigel) or from Trevigen (marketed as Cultrex). Each lot of collagen or lrECM was carefully validated prior to use in cultures. Additives used to culture the HMT-3522 cell lines were provided by Sigma (insulin, transferrin, estradiol, prolactin, soybean trypsin inhibitor) or BD Biosciences (sodium selenite, hydrocortisone, EGF).

### 2.1.2. Cell lines

HMT-3522 S1, S2, S3C, and T4-2 were maintained in tissue culture monolayers as previously described (Lee et al., 2007; Petersen et al., 1992; Rizki et al., 2008; Weaver et al., 1997). MCF10neoT and MCF10DCIS.com cells were kindly provided by Dr. Fred Miller (Karmanos Cancer Institute, Detroit, MI) and cultured in the same manner as MCF10A cells (Debnath et al., 2003), which were available from ATCC. BT549, HCC1143, and MDA-MB-231 cell lines were obtained from ATCC and were maintained as previously described (Neve et al., 2006). 293FT cells were obtained commercially (Invitrogen) and cultured as recommended.

### 2.1.3. 3D lrECM cultures

Cells were cultured on top of lrECM as described (Lee et al., 2007). Briefly, a thin coat of lrECM (600uL) was evenly spread onto 35mm dishes, allowed to polymerize, then cells were seeded on top of the gel and cultured for 4-5 days in the presence of growth media containing 5% lrECM. For stellate morphogenesis assays, individual wells of a 24-well plate were coated with 200µL of lrECM and 40,000 cells were seeded on top of the polymerized gel. MCF10DCIS.com cells were cultured in MCF10A 3D assay media (Debnath et al., 2003) for 4 days, then the number of invasive cellular projections per colony were manually counted in 5 independent fields per well. Results presented are the average number of projections per colony for 3 independent wells.

### 2.1.4. Invasion and migration assays

Cell motility was measured as previously described using wound healing or transwell chemotaxis assays (Liu et al., 2006a). In the scratch assay, cells were seeded at quadruple the normal seeding density and grown until confluent, at which point a scratch was made in the monolayer with a p1000 pipet tip. The rate at which the gap closed was measured after 24 hours, with the experiment

performed in triplicate. For transwell chemotaxis assays, 100,000 cells in 300µl media were seeded in 24-well transwell inserts in at least triplicate (8µm pore size), 300µl media was added to the bottom well, and cells were allowed to adhere overnight. 15µl FBS was then added as a chemoattractant, and cells were allowed to migrate for 24 hours. Cells which migrated through the insert to the underside were simultaneously fixed and stained in methanol:water:acetic acid (9:9:2) containing 0.01% Commassie brilliant blue for 20 minutes, rinsed, then the upper side scrubbed with a cotton swab, and the number of cells that passed through to the underside of the membrane were manually counted in 5 independent fields per insert. Alternatively, representative images were collected at low magnification (4x) to cover the majority of the membrane area, and the percentage of membrane area occupied by cells was quantified in ImageJ by thresholding images, then using the "Measure" command. Data were presented relative to control cells in all experiments. Invasion assays were performed the same as transwell chemotaxis assays, except using membranes precoated with lrECM according to the manufacturer's protocol (BD Biosciences). For MDA-MB-231, cells were starved overnight in 0.2% FBS, then passaged using non-proteolytic cell dissociation buffer (Sigma). Following dislodgment, cells were resuspended in Hank's balanced salt solution (Sigma), pelleted, then resuspended in media containing 0.2% FBS. 50,000 cells were seeded in the transwell inserts, and media containing 10% FBS was added to the bottom well the same day. Transwell migration/invasion was quantified 20 hours later.

#### 2.1.5. BrdU proliferation assay

Proliferation in culture was measured by using a BrdU labeling kit (Roche) following the manufacturer's protocol. Cells were pulsed with BrdU for 1hr prior to fixing and immunofluorescence, and nuclei were counterstained with DAPI. The percentage of BrdU-positive nuclei were quantified using a Zeiss Axiovert 200 fluorescence microscope; a total of >200 nuclei were scored, and each experiment was performed in triplicate.

### 2.2. Plasmids

#### 2.2.1. shRNA constructs

For RNA interference, sense and antisense oligonucleotides encoding previously validated shRNAs targeting 14-3-3σ (Wilker et al., 2007) or a scrambled sequence were synthesized. The oligonucleotides were designed to have BglII and HindIII overhangs once annealed, and are as follows:

sh-scrambled sense: 5'- GATCCCC **ACGATCGAGTATCGAGGTA** *TTCAA GAGA* **TACCTCGATACTCGATCGT** TTTTTGGAAA -3'

sh-scrambled antisense: 5'- AGCTTTTCCAAAAA **ACGATCGAGTATCG AGGTA** *TCTCTTGAA* **TACCTCGATACTCGATCGT** GGG -3'

sh-14-3-3σ sense: 5'- GATCCCC **GTGACCATGTTTCCTCTCA** *TTCAA GAGA* **TGAGAGGAAACATGGTCAC** TTTTTGGAAA -3'

sh-14-3-3σ antisense: 5'- AGCTTTTCCAAAAA **GTGACCATGTTTCC TCTCA** *TCTCTTGAA* **TGAGAGGAAACATGGTCAC** GGG -3'

(**bold text -** targeting sequence and its complement, *italics* - loop sequence)

Annealing was performed by diluting sense and antisense oligonucleotides to a final concentration of 0.25µg/µl in minimal restriction buffer (10mM Tris-Cl, 50mM NaCl, 10mM $MgCl_2$, 1mM DTT), followed by incubating samples at 95C for 3 minutes then at 37C for one hour. DNA duplexes were directionally subcloned into pENTR-pTER$^+$ at a 1:10 molar ratio of vector:duplex using DNA Ligation Kit version 2.1 (Takara). Once in pENTR-pTER$^+$, the shRNAs were recombined into pLenti-RNAi-Puro-DEST#2 using LR-Clonase (Invitrogen). Both pENTR/pTER$^+$ and pLenti-RNAi-Puro-DEST#2 were kindly provided by Eric Campeau (Lawrence Berkeley National Laboratory, Berkeley, CA).

2.2.2. 14-3-3σ, actin, and profilin expression constructs

pFlagCMV2-14-3-3σ was kindly provided by Dong-Er Zhang (addgene plasmid #12453), and was used as a PCR template to amplify full-length or C-terminal truncated 14-3-3σ, with and without an N-terminal FLAG epitope. To generate 14-3-3σ$^{\Delta C}$, PCR primers were designed to incorporate a premature stop codon at residue 203. Similarly, human β-actin (wild-type and R62D) and profilin-1 (wild-type and S137D) constructs were obtained from Virginia Spencer (Life Sciences Division, Lawrence Berkeley National Laboratory) and Jieya Shao (Department of Neurology, Washington University School of Medicine), respectively, and were used as PCR templates. Amplicons were incorporated into pCR2.1 TOPO vectors following the manufacturer's protocol (Invitrogen), and then directionally ligated into pENTR1A (Invitrogen; now discontinued) using BamHI and NotI or XhoI restriction sites. YFP was amplified from pEYFP-C1 (Clontech$^{TM}$; now discontinued) using primers allowing an in-frame N-terminal fusion to 14-3-3σ, generating YFP-14-3-3σ in pENTR1A. Once in pENTR1A, plasmids were recombined into either pLenti-CMV/TO-Puro-DEST#2 or pLenti-CMV/TO-Neo-DEST#2 (both kindly provided by Eric Campeau, Lawrence Berkeley National Laboratory, Berkeley, CA) depending on the selection marker necessary, using LR Clonase II. To generate the CMV/TO-Gus control, pENTR1A-Gus (supplied as a positive control with LR Clonase II) was used in the recombination step.

2.2.3. mCherry and LifeAct-mCherry constructs

Wild-type mCherry was PCR amplified from a donor plasmid (pLentiR4R2V5-DEST UbC-mCherry, kindly provided by Curt Hines, Lawrence Berkeley National Laboratory, Berkeley, CA) to incorporate a unique N-terminal NheI site, and was then incorporated into pCR2.1 TOPO. Sense and antisense oligonucleotides encoding the first 17 residues of S. cerevisiae ABP140

(MGVADLIKKFESISKEE), a flexible linker (GDPPVAT) (Riedl et al., 2008), and flanking BamHI and NheI sites were synthesized and annealed as above (see: 2.2.1. shRNA constructs). The oligos used were as follows:

sense: 5'-GATCCATGGGTGTCGCAGATTTGATCAAGAAATTCGAAAGCATCTCAAAGGAAGAAGGCGATCCACCAGTTGCTAC-3'

antisense: 5'-CTAGAAGTAGCAACTGGTGGATCGCCTTCTTCCTTTGAGATGCTTTCGAATTTCTTGATCAAATCTGCGACACCCATG-3'

Duplex oligonucleotides were directionally ligated in frame with the mCherry N-terminus to yield Lifeact-mCherry, which was subsequently cloned into pENTR1A (Invitrogen). Alternatively, mCherry was subcloned into pENTR1A without the LifeAct peptide as a control. Once in pENTR1A, the LifeAct-mCherry was recombined into pLenti as above (see: 2.2.2. 14-3-3σ, actin, and profilin expression constructs).

### 2.2.4. lentivirus production and infection

For lentiviral production, pLenti plasmid obtained as described above (either expressing shRNAs or transgenes) was cotransfected with pLP1, pLP2, and pLP-VSVG plasmids (all from Invitrogen) into 293FT host cells using Fugene6 transfection reagent (Roche) at a 3:1 ratio of Fugene6:DNA. Viral supernatants were collected two days following transfection, 0.45μm filtered, and concentrated by ultracentrifugation at 150,000xg for 2 hours to pellet viral particles, which were then resuspended in 1/100$^{th}$ the original volume and aliquoted. Concentrated virus was diluted 100X in media containing 4μg/mL polybrene, and was added to cells during log-growth phase for infection. Cell lines were stably selected with puromycin or G418 (depending on the pLenti used) beginning two days post-infection.

### 2.2.5. pGex constructs

For recombinant GST-14-3-3σ protein purification, pGEX-2TK 14-3-3σ was kindly provided by Michael Yaffe (Massachusetts Institute of Technology, Cambridge, MA; Addgene plasmid 11944). The control (GST expressing) plasmid was made by excising the 14-3-3σ gene with BamHI and EcoRI restriction endonucleases, then blunt ligating the overhangs of the vector backbone.

### 2.2.6. plasmid sequencing

Prior to use in experiments and subsequent cloning steps, all plasmids were sequence verified using commercial services (Quintara Biosciences, Berkeley, CA; SeqWright Inc, Houston, TX).

## 2.3. Protein Analysis and Purification

### 2.3.1. Antibodies

The antibodies, suppliers, and their dilutions used for western blot analysis are as follows: *From Cell Signaling:* cofilin-pSer3 (3313);1:250, FAK (3285);1:500, FAK-pTyr397 (3283);1:500, Src (2102);1:500, Src-pTyr416 (2101);1:500, LIMK1 (3842);1:500, LIMK1/LIMK2-pThr508/505 (3841);1:250, ERK1/2 (9102);1:1000, ERK1/2-pThr202/Tyr204 (9101);1:250, GSK3β (9332);1:500, GSK3β-pSer9 (9336);1:500, AKT-pSer473 (9271);1:500, profilin-1 (3237);1:500. *From Santa Cruz:* 14-3-3σ (C-18);1:500, 14-3-3σ (N-14);1:500, vimentin (C-20);1:500, Lamin A/C (H-110);1:1000. *From Sigma-Aldrich:* β-actin (AC-15);1:2000, anti-FLAG (M2);1:500. *From BD Biosciences:* E-cadherin (36);1:1000, AKT (7);1:1000. *From Abcam:* cofilin (Ab42824);1:1000.

### 2.3.2. Western blot analysis

Cells grown in monolayers were rinsed in PBS, then lysed in RIPA buffer (1% NP-40, 0.5% deoxycholate, 0.2% SDS, 150mM NaCl, 50mM Tris-HCl pH 7.4; supplemented with fresh protease and phosphatase inhibitor cocktails (EMDBiosciences) immediately prior to use) and clarified at 13,200xg. Cells grown in 3D lrECM were isolated using ice-cold PBS-EDTA (1x PBS, 5mM EDTA, 50mM NaF, 2mM $NaVO_3$, supplemented with fresh protease inhibitor cocktail) (Lee et al., 2007) before lysis as above. Equal amounts of protein (typically 20µg) were resolved on precast Novex 4-20% Tris-Glycine gels (Invitrogen), transferred to nitrocellulose membranes, and then immunoblotted according to recommended durations/temperatures and blocking buffers, at dilutions specified earlier (see: 2.3.1. antibodies). To ensure uniform protein loading in gels and no errors/air bubbles occurred during transfer to nitrocellulose, membranes were stained with Ponceau stain (0.1% Ponceau S in 5% acetic acid) prior to performing western blot analysis. For Triton X-100 soluble and insoluble fractionation, cells were lysed in $10cm^2$ dishes on ice for 5 minutes with 2mL PBS + 1% Triton X-100 and protease inhibitors, the soluble fraction was removed and clarified, while the insoluble cytoskeleton fraction was rinsed with PBS then solubilized with 2mL 8M urea. Equal volumes of soluble and insoluble fractions were loaded, and the ratio of soluble to insoluble actin was calculated following western blot (see: 2.3.6. Quantification).

### 2.3.3. GTPase activity assays

Cells were rapidly lysed in GST-Fish buffer (10% glycerol, 1% NP-40, 100mM NaCl, 2mM $MgCl_2$, 50mM Tris-HCl, pH 7.4, supplemented with fresh protease and phosphatase inhibitors), and all subsequent work prior to SDS-PAGE was performed rapidly on ice. Small GTPase activity was detected by affinity capture assays (Millipore) using agarose beads coated with RBD-GST (for GTP-RhoA) or PAK1-GST (for GTP-Rac1 and GTP-cdc42) according to suggested protocols.

Western blot analysis was performed using Rac1, RhoA, and cdc42 antibodies provided with the respective kits.

#### 2.3.4. FLAG co-immunoprecipitation

For 14-3-3σ co-immunoprecipitation, cells expressing FLAG-tagged proteins (wild type and ΔC mutant) were lysed in IP buffer (1% Triton X-100, 150mM NaCl, 1mM EDTA, 50mM Tris-HCl, pH 7.4; supplemented with fresh protease and phosphatase inhibitor cocktails immediately prior to use). FLAG-tagged proteins and any binding partners were isolated from cell lysates using anti-FLAG M2 affinity gel (Sigma-Aldrich) by following the recommended protocol, and then were resolved by SDS-PAGE for western blot analysis.

#### 2.3.5. Protein purification and bioconjugation

Actin from young rabbit muscle tissue (Pel-Freez) was purified according to previous methods (Pardee and Spudich, 1982). AlexaFluor488-conjugated actin was generated by labeling 1mg of F-actin with AlexaFluor488-TFP ester (Invitrogen) according to the manufacturer's protocol, followed by subsequent cycles of depolymerization, polymerization, and depolymerization to ensure retention of activity following bioconjugation. For purification of recombinant proteins, pGEX-2TK 14-3-3σ (Yaffe et al., 1997) and the GST-expressing control were used to transform BL21(DE3)pLysS cells (Promega), and while cells were in log-growth phase, protein production was induced with 0.25mM IPTG for 4 hours. Pelleted cells were lysed in ice-cold PBS containing 1% Triton X-100 and protease inhibitor cocktail, and recombinant proteins were purified using columns packed with glutathione sepharose 4B according to the manufacturer's protocol (GE Healthcare). Protein purity was assessed by staining gels with SimplyBlue SafeStain (Invitrogen).

#### 2.3.6. Quantification

Quantification of western blot or SimplyBlue-stained gels was performed using ImageJ software. Boxes of equal dimensions were drawn around bands, the band density was measured, and a background spot outside of the region was measured and subtracted from each sample. Experiments were optimized in order to prevent saturation of signal.

### 2.4. In Vivo Studies

#### 2.4.1. Mouse mammary gland sections

Mouse mammary sections from archival formalin-fixed, paraffin-embedded tissue blocks were kindly provided by Jamie Bascom (Lawrence Berkeley National Laboratory, Berkeley, CA). CD-1 mice were used in all studies, and all experiments were approved by the Lawrence Berkeley National Laboratory Animal Research and Welfare Committee. Hormone ablation was achieved by surgical removal of ovaries (ovariectomy) at twelve weeks of age. Briefly, mice

were anesthesized, a vertical incision (4 cm) was made in the skin over the lumbar region along the dorsal midline, then another incision (2 cm) was made into the peritoneum on each side of the mouse where the ovaries are located. Ovaries were surgically removed from the uterine horns by severing the ovarian ligament, the uteri and adipose tissue were carefully pushed back into the body cavity, and incisions were closed by either suture with silk thread or staple. Ovariectomy was followed by one week of postoperative rest before hormone replacement to assure complete depletion of circulating estrogen and progesterone. Subcutaneous injections (100 µL) of estrogen (100 ng/ml), progesterone (100 µg/mL), or vehicle were given to mice in the region between their two scapular bones. Mammary glands were excised and fixed in neutral buffered formalin for immunohistochemical analysis.

#### 2.4.2. Xenograft experiments

For xenografts studies, 5 million cells suspended in 100µL of media + 50% Matrigel were injected subcutaneously into the rear flanks of 8 week old female BALB/c (nu/nu) mice. Tumor sizes were measured three times a week with a caliper until mice were sacrificed after 5-6 weeks of tumor growth. Volume was calculated according to the formula:

$V = \frac{1}{2} L \times W \times W$ (Tomayko and Reynolds, 1989)

Where L is the longest dimension and W is the shortest dimension of the tumor. Tumors were fixed in 4% paraformaldehyde, paraffin embedded, sectioned, and a subset of slides were stained with hematoxylin and Eosin (UCSF Mouse Pathology Core) for histological analysis. These experiments were performed using a protocol approved by the Lawrence Berkeley National Laboratory Animal Research and Welfare Committee.

#### 2.4.3. Immunohistochemistry

Immunohistochemistry of mammary sections and xenografts was performed as previously described for 14-3-3σ (Simpson et al., 2004), except endogenous peroxidases were blocked with 0.3% $H_2O_2$ rather than methanol. Antibody specificity was confirmed by control staining in the absence of primary antibody, or by pretreating the antibody with blocking peptide corresponding to the epitope used to raise the antibody. Ki-67 immunohistochemistry was performed as described (Rizki et al., 2008). Examples of nuclei scored as positive and negative for Ki-67 are shown in Figure 10. All sections were counterstained with hematoxylin. For heat map projection to emphasize staining intensity at the invasive front of tumors, RGB images of T4-2 xenografts were converted to a 16-bit image, inverted, and a 16-color LUT was applied using ImageJ software.

## 2.5. Clinical Analyses

### 2.5.1. Tissue microarray staining and scoring

A tissue microarray (TMA) containing a series of 245 patients was constructed with replicate 0.6 mm cores by a collaborator (Jorge S. Reis-Filho, Institute of Cancer Research, London, UK) using archived tumor samples. All patients in the cohort were diagnosed and managed at the Royal Marsden Hospital between 1994 and 2000. Patients received standard anthracycline-based adjuvant chemotherapy, while endocrine therapy was additionally prescribed for patients with ER-positive tumors. Complete follow-up was available for 244 patients, ranging from 0.5 to 125 months (median = 67 months, mean = 67 months). Tumors were graded according to a modified Bloom-Richardson scoring system (Ellis et al., 1992) and size was categorized according to the TNM staging criteria (Singletary and Connolly, 2006). 3μm sections from the TMAs were mounted on polylysine-coated slides and immunohistochemistry was performed with antibodies raised against the following markers: ER, PR, HER2, EGFR, Ck 5/6, Ck 14, Ck 17, Cyclin D1, Ki-67, p53, topoisomerase II α, caveolin 1, caveolin 2, and FOXA1, as reported elsewhere (Savage et al., 2007; Savage et al., 2008; Tan et al., 2008). TMA sections were also subjected to chromogenic *in situ* hybridisation (CISH) with SpotLight probes for *CCND1*, *MYC*, *HER2*, and *TOP2A*, as previously reported (Arriola et al., 2007; Reis-Filho et al., 2006; Rodriguez-Pinilla et al., 2007). Immunohistochemistry for 14-3-3σ was performed on the TMA cohort as previously described (see: 2.4.3. immunohistochemistry). TMA tissue cores were analysed by three observers at the Institute for Cancer Research (Felipe Geyer, Kay Savage & Jorge S. Reis-Filho) and cytoplasmic and nuclear expression of 14-3-3σ was scored as 0 = negative or weak staining, 1 = core contained no tumour cells or was missing, or + = strong staining (Simpson et al., 2004). The analysis was performed with observers blinded to the results of other immunohistochemical markers and patients' outcome.

### 2.5.2. Microarray data and clinical information sources

Microarray expression data for patients comprising the Netherlands Cancer Institute (NKI) cohort (van de Vijver et al., 2002) were publically available on the Rosetta Inpharmatics server (http://www.rii.com/publications/2002/nejm.html), and updated clinical data for the NKI patients was obtained from a more recent publication (West et al., 2005). Clinical data and microarray data for patients comprising the UCSF cohort (Chin et al., 2006) were kindly provided by Joe Gray. Expression data and available clinical information for the Rotterdam cohort (Wang et al., 2005b) were obtained from the NCBI GEO server (accession number GSE2034). Details outlining the patient selection criteria, age, treatment course, and other information for each cohort can be found in the respective publications.

. 2.5.3. Correlations between 14-3-3σ and clinicopathological parameters

For gene expression data, patients were grouped based on ER status, MammaPrint signature, and molecular subtype using the available clinical information for each patient, and the mean 14-3-3σ expression for patients within each group was calculated. Given the binary nature by which immunohistochemical staining is summarized (present versus absent), correlations between 14-3-3σ protein expression (and subcellular distribution) and other immunohistochemical and histological markers assessed in the tissue microarray analysis were determined using contingency analyses (Fisher's exact test or $\chi^2$ test) as indicated, and were summarized in tabular form (Table 1 and 2). Tumors were classified into molecular subtypes using the immunohistochemical surrogate of Nielsen and colleagues (Nielsen et al., 2004).

2.5.4. Kaplan-Meier analysis

Patients were sorted based on 14-3-3σ expression into 14-3-3σ high (above median) and 14-3-3σ low (below median) groups for Kaplan-Meier survival analysis. Recurrence-free survival was considered the duration from diagnosis to recurrence of any kind (including DCIS, invasive carcinoma, or distant recurrence). For the UCSF cohort, the two probes having the highest Pearson correlation (33322_i_at and 33323_r_at; r = 0.961) were used to categorize 14-3-3σ expression groups. Statistics were calculated using the log-rank method.

## 2.6. Imaging and Analysis

2.6.1. Confocal microscopes

Live and fixed cells were imaged using a custom made spinning disk confocal microscope (Solamere) based on a Zeiss Axiovert 200 microscope fitted with a CSU10 confocal scanhead (Yokogawa) and a cell incubator. Images were captured with a XR Mega 10 Intensified CCD camera (Stanford Photonics) under 63x Plan Apochromat (1.4 numeric aperture) oil immersion lens using QED InVivo imaging software (Media Cybernetics). For colocalization and fluorescence recovery after photobleaching experiments, a Zeiss 710 laser scanning confocal microscope was used. Images were captured under 63x Plan Apochromat (1.4 numeric aperture) oil immersion lens using Zen 2008 imaging software (Zeiss).

2.6.2 Immunofluorescence

Immunofluorescence on formalin-fixed cells was performed according to standard protocols. Antibodies/probes used and their dilution include 14-3-3σ (Santa Cruz, C-18; 1:50), β-catenin (Santa Cruz, H-102; 1:50), β-actin (Sigma, AC-15; 1:100), profilin-1 (Cell Signaling, 3237; 1:100), phalloidin (AlexaFluor488-, 594-, or 633-conjugated, all from Invitrogen; 1:300), AlexaFluor488-, 568-, 594-, or 633-conjugated secondary antibodies (all from Invitrogen; 1:300) ,and 4´,6-

diamidino-2-phenylindole (DAPI; Invitrogen; 1:2000 of 10mg/mL stock). Briefly, cells were fixed in neutral buffered formalin or 4% paraformaldehyde for 30 minutes at room temperature, permeabilized with 0.5% Triton X-100 for 5 minutes at room temperature, then blocked with blocking buffer (PBS + 0.2% Triton X-100 + 5% BSA) for 1 hour. Primary antibodies were diluted in blocking buffer, and cells were incubated with antibodies overnight at 4 C. Cells were rinsed and stained with fluorescently-conjugated secondary antibodies and/or fluorescently-conjugated phalloidin, then nuclei were counterstained with DAPI and mounted with Vectrashield (Vector Labs). For F-actin quantification (Figure 18), the average pixel intensity of the phalloidin channel within a mask encompassing the cell area was calculated using ImageJ software. For 3D image projections (Figure 21), data from confocal stacks (50 z-sections, each < 0.1μm pixel depth) spanning the entire cell volume were used to build a 3D rendering in Imaris software (Bitplane).

### 2.6.3. Live cell F-actin and 14-3-3σ imaging

For live-cell imaging, cells were seeded onto 1.0 chamber coverslips (VWR) previously coated overnight with type I collagen (PureCol; Advanced BioMatrix), and only cells with marginal expression of fluorophores were selected for analysis to minimize artifacts resulting from disrupted endogenous actin dynamics. YFP-14-3-3σ and LifeAct-mCherry transduced cells were grown to a monolayer and scratched with a pipet tip to stimulate directional motility, and the distributions of 14-3-3 and F-actin during cell migration was measured in 4 minute intervals using a spinning disk confocal microscope. Temperature, $CO_2$, and humidity were maintained constant throughout the experiments. Cells which were not viable after the imaging were excluded from analysis. To generate semi-quantitative heat maps, the pixel intensity of the mCherry fluorescence was subtracted from that of the YFP channel for every frame of the movie using ImageJ software, generating a 32-bit differential map to which a 16-color LUT was applied. The maxima and minima were adjusted equally in every frame to compensate for differences in background intensity and fluorophore intensity per cell while avoiding saturation in either channel, giving a positive value where there is higher 14-3-3σ intensity, a negative value where there is higher F-actin intensity, and a neutral value where the intensities are equal.

### 2.6.4. Fluorescence recovery after photobleaching (FRAP)

LifeAct-mCherry, which was previously validated as a useful tool to measure F-actin dynamics by FRAP (Riedl et al., 2008), was introduced into cells by lentiviral transduction as described earlier. FRAP analysis and quantification was performed with the Zeiss LSM 710 confocal microscope, using the bleaching macro within Zen 2008 software. Regions were drawn to measure fluorescence recovery, background intensity, and intensity changes within an unbleached region over time subsequent to bleach cycles. >75% mCherry bleaching was obtained following 30 iterations with 561nm laser at 100% intensity and a

scanning speed of 3; recovery was typically >80% of original intensity. Additionally, a channel for transmitted light was simultaneously collected and analyzed for all the regions of interest, and if drift in focal plan or cell movement was detected by the software, cells were eliminated from further analysis. Recovery kinetics were fitted to an exponential curve, and the kinetic parameter $t_{1/2}$ (the time required for half the bleach recovery) was determined using Zeiss Zen 2008 software.

#### 2.6.5. Colocalization analysis

Cells stained for 14-3-3σ, F-actin, DAPI, and either profilin-1 or β-actin were imaged using a Zeiss 710 LSM with 63x Plan Apochromat (1.4 numeric aperture) oil immersion lens, and colocalization analysis was performed using Imaris software (Bitplane). Briefly, 14-3-3σ immunofluorescence was used to generate a surface mask by automatic threshold detection as previously described (Costes et al., 2004) to exclude sites with a diameter of less than 0.2μm. The Costes colocalization coefficients (Costes et al., 2004) were measured using Imaris and used to assess the non-random staining intensity levels of β-actin, profilin-1, and F-actin with respect to areas occupied by 14-3-3σ within the mask. All pixels contributing to a positive correlation between channels were automatically identified within each cell. To estimate random overlap, one channel was spatially randomized and the resulting correlation between the two channels re-evaluated. By repeating randomization a sufficient number of iterations, the probability of having random overlap for a given amount of correlation could be estimated (Costes et al., 2004). Using this method, all reported colocalizations in this study are statistically significant (i.e. $p<0.05$). Comparable colocalization (or anticolocalization) coefficients were obtained if other cytosolic proteins (such as profilin-1 or β-actin) were used to build the surface mask, and a mask built with the F-actin or DAPI channel resulted in no measurable colocalization. Reported values are the smallest colocalization coefficients measured for n=10 cells; 14-3-3σ, profilin-1, and the β-actin antibody showed no colocalization with F-actin (phalloidin) staining, but significant colocalization to each other.

### 2.7. In Vitro Actin Assays

#### 2.7.1. Actin binding and cosedimentation assays

For GST pull-down actin binding assays, purified actin was diluted to a concentration of 0.1mg/mL (2.38 μM) in GST-Fish buffer and incubated with either GST or GST-14-3-3σ at a 1:1 molar ratio for 1hr at 4C. Recombinant proteins and bound actin (if any) were pulled out of solution using glutathione sepharose 4B (GE Healthcare), resolved by SDS-PAGE, and visualized using SimplyBlue SafeStain (Invitrogen). For cosedimentation assays, actin was incubated in a 8:1 ratio of G-actin:14-3-3σ for 1 hour in G-buffer (2 mM Tris-Cl, 0.2 mM $Na_2ATP$, 0.5 mM 2-mercaptoethanol, 0.2 mM $CaCl_2$, 0.005% azide, pH 8.0), then was polymerized by adding KCl to 50mM, $Mg^{2+}$ to 2mM, and ATP to 1mM. F-actin was pelleted by ultracentrifugation at 150,000xg for 1.5 hours

(Pardee and Spudich, 1982), and the presence or absence of 14-3-3σ which cosedimented with F-actin was assessed by western blot. As a control, actin that was not polymerized was included in the experiment.

#### 2.7.2. Actin polymerization assays

For polymerization assays, 0.1 mg/mL actin was depolymerized into G-actin by dialysis against G-buffer (Pardee and Spudich, 1982), then was incubated for 1 hour with recombinant proteins (1:1 molar ratio), and polymerized by addition of KCl to 50mM, $Mg^{2+}$ to 2mM, and ATP to 1mM concentrations. F-actin was separated from residual G-actin by fractionation at 150,000g for 1.5 hours (Pardee and Spudich, 1982), and the F- and G-actin pools were resolved by SDS-PAGE and quantified by SimplyBlue staining as above. For fluorescent actin polymerization assays, 1μM of AlexaFluor488-conjugated-G-actin (488-G-actin; prepared as described earlier) was pretreated with 4μM of recombinant protein, then polymerized and imaged by confocal microscopy. Alternatively, pretreated 488-G-actin was introduced into cells permeabilized with 0.2mg/mL saponin to measure in situ actin polymerization in the presence of ATP (Symons and Mitchison, 1991). Following 488-G-actin incorporation, cells were fixed and the endogenous F-actin cytoskeleton was counterstained with phalloidin. Background intensity was adjusted by applying a threshold uniformly across all cell fields, and actin incorporation, quantified as the ratio of the 488-actin intensity divided by the phalloidin intensity, was calculated for at least 20 independent cell fields using ImageJ software. To measure the kinetics of actin polymerization from nucleation through steady-state polymerization and up to equilibria, actin conjugated with pyrene was used in polymerization assays and was purchased from Cytoskeleton. 0.05mg/mL of pyrene G-actin was pretreated with GST or GST-14-3-3σ in a 4:1 molar ratio of recombinant proteins:actin, then actin was polymerized following the manufacturer's protocol. Polymerization was monitored in 30s intervals using a GENios fluorescence plate reader (TECAN) with a custom emission filter (410nm bandpass 20, Omega Optics) and 365nm excitation. Unpolymerized G-actin was measured over the time course to correct for photobleaching.

### 2.8. Statistical Analysis

All graphs, including Kaplan-Meier survival curves, were constructed using GraphPad Prism software (version 5.01). All statistics reported are the two-tailed, 95% confidence interval p-values for the statistical test indicated in the respective figure legends.

# CHAPTER 3. RESULTS

### 3.1. 14-3-3σ is a marker of basal-like breast cancer

3.1.1. Rationale

BLBC represents the breast cancer subtype having the fewest clinical management options, as this form of breast cancer does not express therapeutic targets found in other subtypes, and tends to frequently occur as an "interval" cancer that firmly establishes between mammograms and in younger women (Banerjee et al., 2006; Nielsen et al., 2004; Rakha et al., 2006; Rakha et al., 2008). As such, a priority in the breast cancer field is to establish novel methods to improve the detection and treatment of basal-like breast cancers in a manner more readily available to other breast cancer subtypes. BLBC patients have among the worst 5-year clinical outcome of the breast cancer molecular subtypes (Parker et al., 2009; Perou et al., 2000; Sorlie et al., 2001; Sorlie et al., 2003; Sotiriou et al., 2003).

Using the HMT-3522 BLBC progression series, the Bissell lab and others (Yan et al., 2005) have previously demonstrated that 14-3-3σ is expressed highly in malignant T4-2 cells relative to their non-malignant counterpart, S1. The finding that 14-3-3σ expression followed HMT-3522 malignant progression was surprising, given that this molecule is widely described as a tumor suppressor: it is frequently downmodulated in some breast tumors through promoter methylation or proteolysis (Ferguson et al., 2000; Prasad et al., 1992; Umbricht et al., 2001; Urano et al., 2002; Vercoutter-Edouart et al., 2001), and it functions as an enforcer of the G2/M checkpoint in HCT116 colorectal cancer cells (Chan et al., 1999; Hermeking et al., 1997). However, in a pilot immunohistochemical study, 14-3-3σ was found to be expressed highly in 10 of 12 confirmed cases of BLBC and correlated with ER-negative tumors in the rest of the cohort (Simpson et al., 2004). Expression was also reported in the myoepithelial cells of the normal breast (Moreira et al., 2005; Simpson et al., 2004). As BLBC's often express myoepithelial cell markers, I hypothesized that 14-3-3σ expression and function in breast cancer may be contingent on the molecular subtype; specifically, it remains expressed in the BLBC subtype of breast cancer, and thus may serve to identify these tumors. Furthermore, by confirming that 14-3-3σ expression identifies basal tumors in patients, the functions observed for this protein in the HMT-3522 and MCF10 series (if any) may have clinical implications for the eventual therapeutic targeting of these tumors.

3.1.2. 14-3-3σ expression follows malignancy in the HMT-3522 and MCF10 models of BLBC progression.

I confirmed the proteomics data by western blot analysis, and found that 14-3-3σ protein levels correlated well with HMT-3522 progression (Briand et al., 1996; Briand et al., 1987) from S1 (non-malignant), to S2 (pre-malignant and EGF independent), to S3C (pre-invasive and highly proliferative; Rizki et al., 2008), and was highest in T4-2 (tumorigenic and invasive; Figure 1A). Similarly, in the MCF-10 series, 14-3-3σ expression was found to follow tumor progression

(Miller et al., 2000; Miller et al., 1993) from MCF10A (non-malignant), to MCF10neoT (premalignant and hyperproliferative), and to MCF10DCIS.com (which form comedo-type DCIS in vivo) (Figure 1B). These data indicate that 14-3-3σ levels correlate with malignant progression in two independent, isogenic models of BLBC, suggesting that 14-3-3σ expression may be involved in BLBC progression in patients and, if true, that the protein does not function as a tumor suppressor in these tumors.

3.1.3. 14-3-3σ expression is regulated by estrogen

One hallmark feature of BLBCs is their expression of proteins normally restricted to nonmalignant myoepithelial cells, and similar to myoepithelial cells in vivo (Giri et al., 1989; Petersen et al., 1987), their inability to respond to estrogenic stimuli due to the lack of estrogen receptor expression. As mentioned earlier, previous studies have shown that 14-3-3σ expression is predominantly restricted to myoepithelial cells in the normal human breast, a result I confirmed and showed to be the case also in the mouse mammary gland (Figure 2). To investigate whether 14-3-3σ expression in myoepithelial cells of the normal mammary gland is due to differences in hormone responsiveness between the epithelial cell lineages of the mammary gland, 14-3-3σ immunohistochemistry was performed on sections obtained from ovariectomized mice (Figure 3). Upon disruption of estrogenic signaling, a striking increase in the 14-3-3σ immunohistochemical staining was observed in the entire mammary epithelium; in particular, strong expression was no longer restricted to myoepithelial cells. This phenotype could be rescued by exogenous injection of either estrogen or progesterone into ovariectomized mice, indicating the regulation was directly related to estrogenic signaling rather than another systemic event resulting from ovariectomy (Figure 3).

It has previously been shown that 14-3-3σ protein stability may be modulated by Efp, an E3-ligase that is regulated by ER-mediated transcription (Urano et al., 2002). However, whether 14-3-3σ mRNA expression correlates with ER activity independently from its regulation at the protein level has not been previously investigated. To ascertain whether 14-3-3σ mRNA could be shown to inversely correlate with ER, microarray data from three independent breast cancer patient molecular profiling studies (Chin et al., 2006; van de Vijver et al., 2002; Wang et al., 2005b) were downloaded for analysis. In all three patient cohorts, 14-3-3σ mRNA levels were significantly lower in ER-positive tumors in comparison to ER-negative tumors (Figure 4A), indicating that 14-3-3σ mRNA and protein both inversely correlate with estrogen receptor function. These data, in conjunction with the ovariectomy data, indicate that the distribution and expression of 14-3-3σ protein and mRNA in the mammary gland is linked with hormone receptor signaling, and further, provides evidence that once estrogen receptor signaling is compromised as is the case for BLBC, 14-3-3σ expression becomes elevated and no longer restricted to the myoepithelium.

### 3.1.4. 14-3-3σ expression preferentially identifies the BLBC subtype

The finding that 14-3-3σ expression is highest in ER-negative tumors led me to further speculate that it may be a marker of BLBCs. Intriguingly, higher 14-3-3σ expression was observed in tumors that are categorized as poor prognosis by the 70-gene MammaPrint signature, are high grade, or which have p53 or BRCA1 mutation (Figure 4B, and data not shown), clinical features associated with BLBC tumors. To address whether 14-3-3σ expression is higher in BLBC tumors, patients in the Netherlands Cancer Institute cohort (NKI-295) were grouped based on their molecular subtype (West et al., 2005) and the average 14-3-3σ expression for each subtype was measured (Figure 4C). 14-3-3σ expression was significantly higher in BLBC tumors in comparison to other molecular subtypes, and a similar trend was observed for the UCSF-130 breast cancer patient cohort (data not shown). The microarray data provide evidence consistent with the hypothesis that 14-3-3σ expression is a marker of basal tumors – its expression is highest in the basal subtype and in tumors with clinical features of basal tumors.

While the microarray data provide good evidence of a connection between 14-3-3σ expression and BLBCs, they do not indicate whether 14-3-3σ could be used to identify BLBCs in routine clinical samples, such as paraffin-embedded tissue sections. To evaluate the potential for 14-3-3σ as a marker for BLBC in clinical samples, immunohistochemical analysis was performed on a tissue microarray (TMA) spotted with tumor cores from 245 patients to correlate the expression of 14-3-3σ with breast cancer subtypes and clinical outcome. Scoring was performed by a pathologist (Jorge Reis-Filho) and members of his group. This series had been extensively characterized for expression of breast cancer-specific markers in prior studies (Arriola et al., 2007; Reis-Filho et al., 2006; Rodriguez-Pinilla et al., 2007; Savage et al., 2007; Savage et al., 2008; Tan et al., 2008; Thorat et al., 2008).

Strong 14-3-3σ cytoplasmic staining comparable to that of normal breast myoepithelial cells was observed in 16.2% of cases (Table 1). Immunoreactivity correlated positively with high histological grade, with high Ki-67 proliferative index, as well as with expression of several BLBC markers (Ck 5/6, Ck 14, Ck 17, EGFR, and caveolins 1 and 2). In contrast, 14-3-3σ immunoreactivity correlated *inversely* with luminal tumor markers (ER, PR, and FOXA1). When tumors were subclassified into luminal, basal-like, and HER2-positive subtypes using the immunohistochemical surrogate of Nielsen et al (Nielsen et al., 2004), strong 14-3-3σ cytoplasmic staining was observed in 70% (16/23) of BLBC tumors and in only 9% (15/164) of non-basal tumors. Importantly, 94% (16/17) of tumors that are ER-negative and 14-3-3σ-positive were of BLBC subtype. These data demonstrate that 14-3-3σ immunohistochemical staining preferentially identifies BLBC, particularly when used in conjunction with ER status, and suggest that it may be employed among a panel of markers to classify breast tumor subtypes.

It has previously been shown that cytoplasmic 14-3-3σ immunoreactivity within tumors is correlated with poor clinical outcome (Simpson et al., 2004). In this study, I found that 14-3-3σ subcellular distribution correlated well with molecular subtype, with cytoplasmic localization occurring most frequently in basal tumors, whereas HER2+ or luminal tumors tend to either not express this protein or only express it in the nucleus (Table 2, Figure 5A). Similar to the previous report, I further show by Kaplan-Meier analysis that patients having cytoplasmic 14-3-3σ localization have a shorter 5-year survival than patients with nuclear staining (Figure 5B). These data suggest that 14-3-3σ subcellular distribution, and hence function, is linked with breast cancer molecular subtype and most likely clinical outcome.

#### 3.1.5. 14-3-3σ expression is correlated with poor clinical outcome

Evidence was presented earlier that 14-3-3σ is a marker of BLBC, and that its expression may have prognostic significance. To further support that 14-3-3σ expression correlates with poor clinical outcome and that it cannot be generalized as a breast tumor suppressor, I performed Kaplan-Meier analysis on the NKI-295 and UCSF-130 cohorts (Chin et al., 2006; van de Vijver et al., 2002) to correlate 14-3-3σ expression levels with clinical outcome. These were the only microarray datasets with available clinical follow-up available for analysis. In the NKI-295 cohort (van de Vijver et al., 2002), 14-3-3σ mRNA expression correlated with shortened overall, recurrence-free, and metastasis-free survival in patients (Figure 6). A similar trend was observed in the UCSF-130 patient cohort (Chin et al., 2006), robustly indicating that 14-3-3σ expression is linked with poor clinical outcome, and should not be described entirely as a breast tumor suppressor. I have thus validated 14-3-3σ to be a BLBC immunohistochemical marker correlating with poor patient outcome, tumor recurrence, and tumor metastasis in independent cohorts, and concurrently validated the HMT-3522 and MCF10 BLBC progression models as useful surrogates for investigating how 14-3-3σ may be linked to the aggressive clinical features of BLBCs.

### 3.2. 14-3-3σ regulates BLBC tumor invasion

#### 3.2.1. Rationale

The findings that 14-3-3σ expression correlates with malignancy in two models of BLBC progression, that its expression identifies BLBC tumors in patients, and that it correlates with poor clinical outcome, strongly suggest this protein may have pro-tumorigenic functions at least in this subtype of breast cancer. Indeed, recent studies have suggested that this protein may promote invasion and migration of pancreatic, colorectal, and vulval cancer cells (Ide et al., 2007; Li et al., 2009; Neupane and Korc, 2008; Wang et al., 2008) – important prerequisites to metastasis - though there is limited knowledge of the mechanism to account for this. Understanding how 14-3-3σ functions in BLBC progression may allow the development of novel therapeutics targeting progression of this breast cancer subtype. As “function biomarkers” that both

identify a tumor subtype and contributes to its pathology are well known for luminal and HER2+ subtypes, and are presently being targeted by therapeutics in the clinic (tamoxifen and Traustuzumab, respectively), this knowledge may represent an important advance for the BLBC subtype.

During HMT-3522 progression, the cell lines progressively increase their proliferation rate, invasiveness, tumorigenicity, metabolic activity, and growth factor self-sufficiency (Briand et al., 1996; Briand et al., 1987; Petersen et al., 1992; Rizki et al., 2008; Wang et al., 1998; Weaver et al., 1997), though many of these processes are interrelated. In order to understand what function(s) 14-3-3σ may be regulating during these events, I generated lentiviruses expressing shRNA hairpins targeting its expression, and aimed to stably infect T4-2 cells and assess what aspects of malignancy become altered as a consequence of gene knockdown. Based on the previous 14-3-3σ literature and on the changes in cell behavior during progression in the HMT-3522 model, I hypothesized that 14-3-3σ may contribute to BLBC progression either by regulating tumor cell motility and invasion, or by influencing proliferation.

3.2.2. 14-3-3σ regulates T4-2 cell migration and invasion

A previous immunohistochemical study in colorectal cancer has shown that 14-3-3σ staining intensity is highest at the invasive front of the tumors and further, that its expression correlates with tumor invasion in patients (Ide et al., 2007). Given the previous data implicating 14-3-3σ subcellular distribution correlates with tumor subtype and clinical outcome (Figure 5), I performed immunohistochemical analysis on slides prepared from T4-2 xenografts to measure its subcellular distribution and whether increased staining intensity could be observed within specific regions of the tumors. The majority of the tumor displayed homogenous 14-3-3σ cytoplasmic staining and an absence of nuclear staining. Importantly however, increased staining intensity was observed at the invasive front where soft tissue infiltration occurs (Figure 7), suggesting that 14-3-3σ may somehow promote tumor invasion into the surrounding stroma.

To evaluate whether 14-3-3σ may have as yet uncharacterized functions in coordinating invasion and migration of BLBC cells, I generated T4-2 sub-lines stably expressed shRNAs targeting 14-3-3σ (sh-14-3-3σ) or a non-specific sequence (sh-scr). The shRNA targeting 14-3-3σ consistently knocked down protein expression by >80%, which resulted in knockdown cells having decreased migration in scratch assays, decreased transwell migration towards an FBS chemoattractant, and decreased invasion through lrECM-coated transwell inserts (Figure 8).

To assess whether the decreased motility and invasion of cells in culture would hold true in vivo, T4-2 sh-scr and sh-14-3-3σ cells were injected subcutaneously into the rear flanks of immunocompromised mice, and the histology of their tumors was evaluated by hematoxylin and eosin staining. Control cell (T4-2 sh-scr) xenografts show a high degree of invasion into the

surrounding mouse stroma and poor demarcation at the tumor periphery, as well as central necrosis typically associated with proliferative tumors (Figure 9). In contrast, tumors formed from T4-2 sh-14-3-3σ xenografts are characterized by more distinct margins and less perturbation to the adjacent normal mouse tissue in comparison to control xenografts; this was consistently observed in all seven tumors generated in the experiment. The in culture and in vivo data demonstrate that 14-3-3σ indeed has an uncharacterized role in regulating BLBC migration and tumor invasion, emphasizing the importance this protein may play in BLBC progression in patients.

### 3.2.3. 14-3-3σ knockdown does not influence T4-2 proliferation

One possible explanation for the decrease in cell migration and invasion observed in 14-3-3σ knockdown cells is that proliferation is influenced by 14-3-3σ. In other words, impaired motility and invasion are secondary, nonspecific effects resulting from a decrease in cell proliferation. This is an important consideration, given the well-established role for 14-3-3σ in cell cycle regulation (Chan et al., 1999; Hermeking et al., 1997; Wilker et al., 2007). However, it has more recently been shown that 14-3-3σ loss does not result in uncontrolled cell cycle or mistimed G2/M progression in breast tumors relative to tumors having moderate to robust 14-3-3σ expression (Moreira et al., 2005), casting doubt on whether the function for 14-3-3σ in cell cycle regulation can be generalized.

Using BrdU incorporation as a measure of cell cycle progression through S-phase, I observed no significant difference in the proliferation of sh-14-3-3σ cells relative to control cells (Figure 10A). Similarly, no shifts in cell cycle distribution were observed by DNA ploidy flow cytometry analysis (data not shown). One observation from the histological analysis of the xenografts (see Figure 9) was that the degree of central necrosis was comparable in knockdown and control tumors, providing circumstantial evidence that proliferation was not influenced. To directly test whether tumor proliferation was influenced by 14-3-3σ knockdown, I performed Ki-67 immunohistochemical staining on slides obtained from the T4-2 xenografts, and also measured tumor volumes over time. Both measurements demonstrated that T4-2 tumor proliferation in vivo was not influenced by 14-3-3σ knockdown, and neither was tumorigenic frequency (Figure 10B and C). These data indicate that the role for 14-3-3σ in regulating cell migration and tumor invasion described above (section 3.2.2.) occurs independent from cell cycle regulation.

### 3.2.4. 14-3-3σ influences migration and invasion in other BLBC cells

The data showing that 14-3-3σ regulates T4-2 migration and invasion in vivo are in good agreement with the clinical data linking 14-3-3σ expression with poor clinical outcome and metastasis (see Figure 6). However, the data obtained from T4-2 cells alone provides no evidence that this novel role for 14-3-3σ in BLBC can be generalized – it may be an observation limited to the T4-2 cell line, which is why it is important to test whether the same phenotype can be observed

in other cell lines. To test this, I generated sub-lines of MDA-MB-231 (which has basal-like molecular profile; Neve et al., 2006) and MCF10DCIS.com (from the MCF10 series) cells which stably express shRNA hairpins targeting 14-3-3σ or a scrambled sequence, and measured motility and invasion in these cells.

Similar to T4-2 cells, MCF10DCIS.com cells expressing shRNAs targeting 14-3-3σ have decreased motility relative to control cells (Figure 11). However, unlike T4-2 cells, I was not able to test whether invasion through lrECM-coated transwell inserts was influenced by 14-3-3σ knockdown, as even parental MCF10DCIS.com cells were not invasive in this assay (data not shown) perhaps reflecting their propensity to form non-invasive DCIS lesions in xenografts. However, the cells form colonies in 3D lrECM with a "stellate" morphology characterized by multiple invasive projections, and we previously show that stellate morphology correlates with invasiveness (Kenny et al., 2007). Interestingly, MCF10DCIS.com sh-14-3-3σ cells have fewer invasive projections per colony than control cells (Figure 11), suggesting invasiveness is reduced in these cells. In addition, MDA-MB-231 cells expressing shRNA's targeting 14-3-3σ fully recapitulate what was observed in T4-2 cells - knockdown cells have significantly decreased migration and invasion, but do not have altered proliferation (Figure 12). Together, these data indicate that 14-3-3σ regulates invasion and migration independent from proliferation in multiple basal-like cell lines from different clinical origins, suggesting this previously undescribed function may be a fundamental property of BLBC.

In summary, I have shown that 14-3-3σ immunohistochemical staining is most intense at the invasive front of T4-2 tumors, that this protein regulates BLBC cell migration and tumor invasion in vivo, that this function is independent of its previously described roles as a regulator of the cell cycle, and that similar results were observed in other BLBC cell lines. These data are in good agreement with earlier data showing that 14-3-3σ expression correlates with poor clinical outcome and metastasis in patients, and implicate 14-3-3σ as a "functional biomarker" that contributes to BLBC clinical features.

### 3.3. 14-3-3σ is a regulator of actin dynamics

#### 3.3.1. Introduction and rationale

Cell migration is a process of fundamental importance in both normal biology and in cancer (Friedl and Brocker, 2000; Friedl and Wolf, 2003; Kumar and Weaver, 2009; Lauffenburger and Horwitz, 1996; Solnica-Krezel, 2005; Wang et al., 2007; Wang et al., 2005a; Wang and Steinbeisser, 2009; Weijer, 2009). Examples of cell migration in healthy adults occurs during wound repair, burn recovery, and immune response, though perhaps the most dramatic example of cell migration and its importance can be observed in development. Gastrulation defines the interval at which specification of the main germ layers (ectoderm, endoderm, mesoderm, and neural crest cells) occurs, and this specification results largely from collective cell migration and invaginations as

sheets, as well as through epithelial-to-mesechymal transition (EMT) (Acloque et al., 2009; Kalluri and Weinberg, 2009; Micalizzi et al., 2010; Nieto et al., 1994; Solnica-Krezel, 2005; Wang and Steinbeisser, 2009; Weijer, 2009). During EMT, epithelial cells loosen their connection with adjacent cells through deregulation of cadherin-based adhesions, delaminate from the sheet as single cells, and transdifferentiate into mesenchymal cells as measured by expression of specific markers, such as E-cadherin loss and acquisition of vimentin expression. The opposite process, a mesenchymal to epithelial transition (MET) also occurs, illustrating the plasticity of the embryo during development and of cells in general. In cancer, EMT is thought to be a major force driving malignant cell migration and eventual metastasis, and has gained much attention in recent years (Evdokimova et al., 2009; Kalluri and Weinberg, 2009; Moody et al., 2005; Radisky et al., 2005; Wu et al., 2009a; Yang et al., 2004). However, cells can also migrate collectively due to retention of cellular junctions, and several modes of tumor cell migration as single cells and as sheets have been characterized (Bell and Waizbard, 1986; Davidson and Keller, 1999; Enterline and Coman, 1950; Friedl and Wolf, 2003; Jacques et al., 1998; Wolf et al., 2003).

One feature is common to all forms of cell migration – motility requires dramatic deformation and rearrangement of the cytoskeleton in a manner that invokes directionality, and by far the most extensively studied cytoskeletal molecule in this context is actin and its numerous regulatory molecules (Chhabra and Higgs, 2007; Fletcher and Mullins, 2010; Goley and Welch, 2006; Paul and Pollard, 2009; Pellegrin and Mellor, 2007; Wang et al., 2005a). Actins exist as two major forms within the cell – in a globular, unpolymerized form (G-actin) or as organized filaments of polymerized protein (F-actin). Purified actin will undergo self-assembly in the presence of ATP, divalent magnesium, and moderate ionic strength once it is above a critical concentration (Pardee and Spudich, 1982). Interestingly however, biochemical studies have consistently shown that the amount of G-actin found within cells is several orders of magnitude higher than the critical concentration observed in vitro, and G-actin nucleation is a large kinetic hurdle, suggesting that the regulation of actin polymerization and G-actin bioavailability are very tightly regulated (Cooper et al., 1983; Koffer and Daridan, 1985; Sept and McCammon, 2001; Theriot and Mitchison, 1993). Indeed, hundreds of actin binding proteins which regulate actin polymerization and depolymerization in many different ways have been characterized, with the list continuously growing (Carlsson et al., 1977; Hall, 2009; Insall and Machesky, 2009; Narumiya et al., 2009; Paul and Pollard, 2009; Theriot and Mitchison, 1993).

Actin polymerization and assembly into macromolecular structures is a major driving force of cell migration (Chhabra and Higgs, 2007; Higgs and Pollard, 2001; Insall and Machesky, 2009; Pellegrin and Mellor, 2007; Ponti et al., 2004; Theriot and Mitchison, 1991; Theriot et al., 1992; Wang et al., 2007). Several different F-actin structures exist within cells as defined by their localization, associated proteins, and function, though they can broadly be

classified as either branched, such as lammellipodia and ruffles, or linear, such as filopodia and stress fibers (Abercrombie and Ambrose, 1958; Chhabra and Higgs, 2007; Fletcher and Mullins, 2010; Ingram, 1969; Insall and Machesky, 2009; Pellegrin and Mellor, 2007). Some of these structures contribute directly to polarized cell migration by pushing the plasma membrane forward as a sheet (lammellipod) or protrusion (filopod), while other structures are linked to myosin-mediated contractility or maintenance of cell shape (stress fibers). Forward propulsion of the cell requires disassembly and turnover of actin-based structures at the rear of the cell where they are not needed, recycling of monomeric G-actin into the growing ends of F-actin present at the cell's leading edge, and myosin-mediated contractility to result in cell body translocation (Cramer et al., 1997; Lauffenburger and Horwitz, 1996; Ridley et al., 2003; Theriot and Mitchison, 1991; Xu et al., 2003). As one can imagine, a complex, tightly regulated, and multidimensional series of signaling networks for the specification of discreet F-actin structures and their turnover have been elucidated and discussing all of them in detail is well beyond the scope of this work. However, several important core components of actin regulation have been characterized, and are briefly discussed here.

Profilin is a protein that binds to monomeric G-actin, and through this interaction, was previously thought to actively sequester it from the growing ends of F-actin and exclusively function as an inhibitor of actin polymerization (Carlsson et al., 1977; Pollard and Cooper, 1984; Theriot and Mitchison, 1993). More recently, it has been shown that profilin in association with G-actin can bind to FH1-domain containing proteins present at the ends of actin filaments (called formins, which are discussed below), which increases the local concentration of G-actin to the filament ends, resulting in actin polymerization (Kovar et al., 2006; Kovar and Pollard, 2004; Paul and Pollard, 2009; Romero et al., 2004; Shimada et al., 2004; Watanabe et al., 1997; Xu et al., 2004). Cofilin is another actin regulatory protein that binds to F-actin and induces strain on filaments, leading to their disassembly (Andrianantoandro and Pollard, 2006; Hotulainen et al., 2005; Ichetovkin et al., 2000; Wang et al., 2007). One can imagine that if F-actin turnover by cofilin occurs in a deregulated fashion, this disassembly can be counterproductive to directional cell migration; however, filament turnover can also promote de novo actin assembly in sub-regions of cells by concurrently removing capping proteins that bind to the ends of actin filaments and inhibit actin polymerization (DesMarais et al., 2004; Ghosh et al., 2004; Ichetovkin et al., 2002). Cofilin is inactive when phosphorylated at serine 3, and the activation is determined by the balance of kinases (such as LIMK) and phosphatases (such as slingshot) which target the phosphorylation site (Arber et al., 1998; Mouneimne et al., 2006; Niwa et al., 2002; Soosairajah et al., 2005; Yang et al., 1998; Zebda et al., 2000). This is one mechanism by which chemotaxis is thought to occur – chemoattractants activate signaling through growth factor receptors leading to localized activation of slingshot at the cell's leading edge, where it activates cofilin to allow de novo actin assembly and forward protrusion

(Chan et al., 2000; Ghosh et al., 2004; Mouneimne et al., 2006; Wang et al., 2007; Zebda et al., 2000). Cofilin and profilin isoforms are present in all cells, and are thought to exert the most direct influence on the balance of F-actin to G-actin of any protein.

Another core component regulating actin architecture is the Arp2/3 complex. This structure is comprised of at least 7 known proteins that bind to the side of filaments and initiate actin polymerization, leading to formation of side branches at a 70 degree angle with respect to the preexisting filament (Higgs and Pollard, 2001; Insall and Machesky, 2009; Mullins et al., 1998; Pollard and Beltzner, 2002). By itself, the Arp2/3 complex does not form an interaction with F-actin that is strong enough for side branch formation, however the stability of this interaction increases by several orders of magnitude in the presence of active N-WASP or related WASP family members such as SCAR/WAVE (Eden et al., 2002; Goley and Welch, 2006; Hufner et al., 2001; Marchand et al., 2001; Rohatgi et al., 1999). In turn, WASP family members are activated by the small GTPases Rac and cdc42, which are thought to bind to WASP family members and alter their conformation from an autoinhibited state to an active form (Ho et al., 2004; Ishiguro et al., 2004; Jaffe and Hall, 2005; Miki et al., 1998; Nakagawa et al., 2001). Rac and cdc42 similarly undergo an allosteric shift in conformation and are able to regulate target proteins once bound to GTP; the exchange of GDP for GTP is catalyzed by numerous guanine exchange factors (GEFs) and is antagonized by GTPase activating proteins (GAPs), which trigger intrinsic GTPase activity Rac and cdc42 and thus conversion of GTP into GDP (Bernards, 2003; Hall, 2009; Nobes and Hall, 1995; Ridley et al., 1992; Schmidt and Hall, 2002). The balance of GEF to GAP is determined by the activity of growth factor and G-protein coupled receptors, providing another mechanism by which chemoattraction occurs – local activation of receptors by chemoattractants initiates GTPase activation and signaling which culminates in the stabilization of the Arp2/3 complex to F-actin, and subsequent formation of branched actin structures (such as lamellipodia) that promote migration (DesMarais et al., 2004; Insall and Machesky, 2009; Mouneimne et al., 2006; Wang et al., 2007).

Linear actin structures are formed by an alternative signaling pathway that, despite the differences in the end result, shares many parallels with the formation of branched actin structures. Localized activation of growth factor receptors relays signals through adaptor molecules and GEFs/GAPs, which in the correct ratio, leads to the activation (GTP-bound) form of the small GTPase RhoA (Bernards, 2003; Insall and Machesky, 2009; Jaffe and Hall, 2005; Ridley and Hall, 1992; Schmidt and Hall, 2002). However, in contrast to Rac and cdc42, RhoA activates another class of actin-binding proteins called formins (such as mDia1) by alleviating its autoinhibition (Higashida et al., 2004; Li and Higgs, 2003; Watanabe et al., 1997; Zigmond, 2004). Formins promote linear filament extension by several different mechanisms depending on the protein - by competing with capping proteins, by stabilizing the filament structure and protect it from cofilin, or by actively recruiting a profilin:G-actin dimer to the filament ends

(Harris et al., 2004; Higashida et al., 2004; Kovar et al., 2006; Kovar et al., 2003; Kovar and Pollard, 2004; Kovar et al., 2005; Pruyne et al., 2002; Romero et al., 2004; Watanabe et al., 1997; Zigmond et al., 2003). Thus, albeit by different mechanisms, formation of linear actin structures and their regulation during chemoattraction in many ways parallels the formation of branched actin structures. However, there is also growing evidence that the linear and branched actin signaling networks can regulate one another – for instance, RhoA and Rac are mutually inhibitory, while SCAR/WAVE can bind and retain mDia2 in an inactive state to inhibit linear filopodia formation (Beli et al., 2008; El-Sibai et al., 2008; Machacek et al., 2009; Rottner et al., 1999; Wu et al., 2009b).

Given the fundamental importance of actin dynamics in cell migration and that 14-3-3σ is known to regulate many signaling cascades by binding and sequestering phosphorylated proteins, I hypothesized that the decreased migration and invasion observed in 14-3-3σ knockdown cells (see section 3.2) may be due to deregulation in one or more actin signaling pathways. As another 14-3-3 isoform has been recently implicated in EMT (Lu et al., 2009a), I additionally hypothesized that the motility phenotype may be due to reversion of EMT (in other words, MET). As such, I investigated whether cytoskeletal dynamics and cellular adhesion were influenced by 14-3-3σ knockdown, in order to provide a mechanism to explain the motility and invasion phenotypes observed in these cells.

### 3.3.2. 14-3-3σ knockdown does not increase cellular adhesion

As mentioned earlier, one mechanism by which cancer cells are thought to disseminate from tumors and eventually metastasize is through EMT, a process involving decreased association with neighboring cells through disassembly of adherens junctions, and increased motility as a single cell. As the transwell assays measure migration through 8μm pores, the motility and invasive phenotypes quantified by these assays may reflect an increase in cellular adhesion rather than differences in motility rate per se. This would provide evidence that 14-3-3σ regulates EMT, and once absent from cells, the program is reversed.

To assess whether 14-3-3σ regulates adhesion between BLBC cells, T4-2 sh-14-3-3σ and control cells were fixed and stained to measure colocalization of beta-catenin and cortical F-actin at cell-cell contacts (Figure 13). 14-3-3σ knockdown cells display no increased association with neighboring cells; if anything, the adherens junctions in knockdown cells appear more discontinuous and diffuse. Similar data were observed in cells stained with E-cadherin and F-actin, and in live cultures, which had comparable numbers of single cells and showed no obvious increase in cellular adhesion (data not shown). These observations suggest that the motility and invasion phenotypes observed in 14-3-3σ knockdown cells cannot be explained by an increase in cellular adhesion, and most likely not by an induction of MET.

### 3.3.3. 14-3-3σ regulates actin architecture through ligand binding

Cell migration requires dynamic remodeling of the actin cytoskeleton at both the leading and the trailing edges of a cell or a group of cells in response to biochemical and/or mechanical stimuli (Fletcher and Mullins, 2010; Hall, 2009; Kumar and Weaver, 2009; Ridley et al., 2003; Wang et al., 2005a). Given that 14-3-3σ influences motility without affecting cellular adhesion, I next tested whether 14-3-3σ knockdown cells have deregulated actin cytoskeletal architecture. Cells were fixed and stained with fluorescently conjugated phalloidin, a small molecule that binds specifically to F-actin but not G-actin, and were subsequently imaged by confocal microscopy (Figure 14). I observed that 14-3-3σ knockdown cells have a 2-fold higher F-actin content than control cells, suggesting that 14-3-3σ influences cytoskeletal dynamics directly or indirectly.

To address whether 14-3-3σ influences the architecture of microfilaments in a ligand binding mechanism and to eliminate the possibility that the actin phenotype is an off-target effect of shRNA silencing, constructs were generated that enable forced expression of wild-type 14-3-3σ (14-3-3$\sigma^{WT}$) or a C-terminal truncated 14-3-3σ (14-3-3$\sigma^{\Delta C}$; Figure 15A). 14-3-3$\sigma^{\Delta C}$ is the human equivalent of the 14-3-3σ mutation responsible for the repeated-epilation mouse phenotype (Herron et al., 2005; Li et al., 2005), and the truncation eliminates two helices and an acidic region thought to be important for ligand binding to 14-3-3 (Gardino et al., 2006; Wilker et al., 2005; Yaffe et al., 1997). Based on structural analysis, the truncated mutant is proposed to act as a dominant-negative 14-3-3σ, though this has never been demonstrated in the literature and I observed no significant differences in either the motility or invasion of cells expressing the mutant compared to wild-type 14-3-3σ (Figure 16), suggesting it may not function in this way. However, when introduced into sh-14-3-3σ cells, only 14-3-3$\sigma^{WT}$ was able to rescue the deregulated F-actin content in comparison to an unrelated gene (Gus) and to 14-3-3$\sigma^{\Delta C}$ (Figure 15B,C). These data indicate that 14-3-3σ regulates F-actin homeostasis in cells, that this occurs in a ligand binding mechanism, and that the actin phenotype is not an off-target effect of shRNA expression. Given the importance of actin remodeling to cell motility, this observation may account for the migratory and invasive phenotypes described earlier, and was selected for further characterization.

### 3.3.4. 14-3-3σ inhibits actin polymerization downstream of GTPases and other canonical migration signaling pathways.

During cell migration, stimuli from the cell microenvironment promote the localized activation of Rho family GTPases, Rac, Rho, and cdc42, which depending on the stoichiometry of their activity and the activity of other factors such as cofilin, Src, Erk, and LIMK among others, can stimulate the formation of discreet actin structures which drive polarized, directional cell migration (Chhabra and Higgs, 2007; El-Sibai et al., 2008; Hall, 2009; Machacek et al., 2009; Narumiya et al., 2009; Wang et al., 2002b; Wang et al., 2007; Wang et al.,

2005a; Wu et al., 2009b). Considering canonical migration and actin signaling pathways as a starting point, I performed western blot analysis to measure the activation status of these proteins, and was surprised to find that 14-3-3σ knockdown did not influence the level and activation of any of the above signaling molecules nor influence EMT, as E-cadherin and vimentin levels also remain unchanged (Figure 17). These data indicate that 14-3-3σ regulates F-actin homeostasis and cell migration in a ligand-binding manner, though acting most probably downstream of the above canonical signaling pathways in BLBC cells.

3.3.5. 14-3-3σ polarizes away from the leading edge of a cell during migration

During chemotaxis, cells polarize such that factors involved in the formation of actin-dependent protrusions localize to the leading edge of the cell, whereas antagonizing factors or those involved in actinomyosin-based contractility localize to the trailing edge of a cell (Cain and Ridley, 2009; Hall, 2009; Higgs and Pollard, 2001; Machacek et al., 2009; Wang et al., 2002b; Wang et al., 2007; Wu et al., 2009b; Yamana et al., 2006). Understanding how the subcellular distribution of an actin-regulatory protein is regulated in living cells, particularly during migration, can provide additional insight into its function. As such, I developed genetically-encoded probes to monitor the subcellular distribution of 14-3-3σ (YFP-14-3-3σ) and F-actin (Lifeact-mCherry) in living cells. Lifeact is a 17-mer peptide from the actin-binding domain of *S. cerevisiae* Abp140, which preferentially decorates F-actin to act much like a live-cell phalloidin (Riedl et al., 2008). To minimize the chance of disrupting endogenous F-actin dynamics, I only included T4-2 cells weakly expressing each fluorophore for live cell imaging. I found mutually-exclusive subcellular distributions of YFP-14-3-3σ and Lifeact-mCherry comparable to endogenous F-actin and 14-3-3σ (Figure 18), validating the constructs behave as their endogenous counterparts.

Using a spinning-disc confocal microscope fitted with a cell incubator, I were able to visualize 14-3-3σ and F-actin distributions in living cells for time intervals exceeding 24 hours. I found that during cell migration, 14-3-3σ polarizes away from the leading edge of a cell where the most dynamic F-actin remodeling occurs (Figure 19); even 24 hours later, cells that are actively migrating remain polarized (Figure 20), indicating that this gradient is not transient. Similarly, endogenous 14-3-3σ polarizes away from the F-actin-rich leading edge in parental T4-2 cells during migration, but no polarization occurs in stationary cells (Figure 21). These experiments, in conjunction with the increased F-actin content observed in T4-2 sh-14-3-3σ and the mutually-exclusive staining of 14-3-3σ and F-actin, provide additional evidence that this protein may somehow antagonize F-actin, as 14-3-3σ localizes away from regions of the cell where actin remodeling becomes most dramatic in a manner analogous to other actin regulatory proteins.

3.3.6. 14-3-3σ knockdown cells have more rapid actin polymerization, thus depleting the pool of available actin necessary for migration and invasion

The increased F-actin content observed in 14-3-3σ knockdown cells (see Figure 14) and the polarization of 14-3-3σ away from the F-actin rich leading edge of the cell (see Figures 19-21) can be explained by two different models. In the first model, 14-3-3σ in some way inhibits actin polymerization, and to allow the regulated formation of actin-rich protrusions during migration, it becomes polarized away from the leading edge of the cell. In the second model, 14-3-3σ somehow promotes depolymerization of F-actin, and 14-3-3σ polarizes to the rear of the cell during migration in order to promote F-actin disassembly and turnover. The increase in F-actin content and the compromised migration observed in 14-3-3σ knockdown cells can equally be explained by both scenarios - either the polymerization rate is elevated and lacks subcellular specificity and polarity, or there is suppressed depolymerization effectively stalling the cell by preventing filament turnover at the trailing end of the cell. Concluding which of the two models is most likely valid requires the kinetics of actin turnover to be measured in living cells. To do this, I performed fluorescence recovery after photobleaching (FRAP) analysis in cells expressing LifeAct-mCherry, which has been previously validated as an effective probe to measure F-actin dynamics by FRAP (Riedl et al., 2008), and which also effectively measures F-actin treadmilling in my cells (Figure 22A, B). Briefly, FRAP involves selectively photobleaching a subcellular region, then monitoring the time required for uniform staining intensity to be restored as unbleached molecules diffuse or are actively transported into the region (Day and Davidson, 2009; Wu et al., 1977). An increase in actin polymerization would be indicated by a more rapid FRAP, whereas a suppression of actin depolymerization would result in slower FRAP.

On average, I observed that 14-3-3σ knockdown cells showed twice the fluorescence recovery rate than control cells, as indicated by a smaller $t_{1/2}$ rate constant (Figure 22C). This rate constant is defined as the time required for fluorescence intensity to reach half the intensity observed once uniform staining is attained. In other words, a smaller $t_{1/2}$ indicates a shorter time for fluorescence recovery, and as smaller $t_{1/2}$ values were observed for LifeAct-mCherry FRAP in sh-14-3-3σ cells, it can be concluded that 14-3-3σ knockdown cells have an increased rate of actin polymerization compared to control cells rather than a suppressed depolymerization. This explains why an increase in F-actin staining was observed in the sh-14-3-3σ cells (see figure 14) – 14-3-3σ directly or indirectly inhibits actin polymerization.

In order for actin polymerization to occur when and where it is necessary, such as at the leading edge of a cell during migration, pools of soluble, unpolymerized actin must be available when needed. Depletion of the available pool of actin would intuitively inhibit cell motility; actin would no longer be available to be incorporated into filaments in response to extracellular cues, as it is already assimilated into the cytoskeleton, and the rate-limiting factor of motility

in the extreme case may be availability of soluble actin. To measure the amount of soluble actin present within the shRNA-expressing cells, cells were lysed and lysates were fractionated into 1% Triton X-100 soluble and insoluble pools, which can differentiate between bioavailable forms of actin versus actin that is associated with the (insoluble) cytoskeleton. In this analysis, I found that T4-2 sh-14-3-3σ cells have a two-fold lower ratio of soluble to insoluble actin in comparison to control cells (Figure 23). This indicates that the increased polymerization observed in knockdown cells severely depletes their pool of soluble, bioavailable actin, suggesting that 14-3-3σ regulates motility and invasion by ensuring a pool of soluble actin exists within cells – once 14-3-3σ is depleted from cells, actin polymerization becomes deregulated, and cells are unable to form actin-rich migratory protrusions in response to extracellular cues.

#### 3.3.7. Actin overexpression rescues the invasion and migration phenotype

One prediction of this model is that by forcing the expression of actin in T4-2 sh-14-3-3σ cells, one should restore the pool of bioavailable actin, and thus be able to rescue the motility and invasive phenotypes. To test this prediction, constructs were generated that enable forced expression of either wild-type β-actin, or a mutant β-actin (R62D) that is unable to polymerize (Posern et al., 2002). In agreement with the prediction of the model, I found that migration and invasion of T4-2 sh-14-3-3σ cells could both be rescued by forced expression of wild-type actin, but not the polymerization-dead mutant (Figure 24). This indicates that the availability of freely soluble actin is a rate limiting factor for motility and invasion of sh-14-3-3σ cells, supporting the model that 14-3-3σ regulates these processes by ensuring a pool of soluble actin is available.

In summary, the data presented support a mechanism by which 14-3-3σ regulates cell motility and invasion by inhibiting actin polymerization and ensuring a pool of soluble actin exists within cells, thus allowing cells to respond to extracellular cues and undergo directional migration and invasion. However, once 14-3-3σ is depleted from cells, the pool of soluble actin is diminished, and as a consequence, de novo F-actin assembly to allow cell migration and invasion cannot occur. While this mechanism can account for all the phenotypes observed in BLBC cells expressing shRNA hairpins targeting 14-3-3σ, it is missing one key component – whether 14-3-3σ inhibits actin polymerization directly or indirectly.

### 3.4. 14-3-3σ interacts directly with G-actin and inhibits its polymerization

#### 3.4.1. Rationale

In the previous sections, evidence was presented that 14-3-3σ inhibits actin polymerization and regulates directional cell migration and invasion by increasing the pool of available, soluble actin for incorporation into actin filaments. However, one compelling observation was that this occurs downstream or in parallel to several signaling pathways that are central regulators of actin homeostasis (see Figure 17). Furthermore, it has previously

been shown that actin is one of many ligands known to interact with 14-3-3σ by mass spectrometry-based analysis (Wilker et al., 2007). Based on these data, I hypothesized that 14-3-3σ may interact directly with actin in BLBC cells to inhibit its polymerization, and chose to investigate whether these proteins interact in cells using coimmunoprecipitation assays, whether purified 14-3-3σ and actin can interact in vitro, and whether this interaction ultimately regulates actin polymerization.

### 3.4.2. 14-3-3σ interacts directly with actin in BLBC cells and in vitro

To investigate whether 14-3-3σ interacts with actin in cells, I generated constructs allowing the forced expression of FLAG-tagged 14-3-3σ, as well as a C-terminal truncated mutant that is able to dimerize but unable to bind to ligands (see Figure 15A). Cell lines stably expressing FLAG-tagged proteins were lysed, and lysates were used for immunoprecipitation studies. Interestingly, both FLAG-14-3-3$\sigma^{WT}$ and FLAG-14-3-3$\sigma^{\Delta C}$ were able to dimerize with endogenous 14-3-3σ, though only the full-length protein was able to form a stable complex with actin (Figure 25A). This indicates that 14-3-3σ and actin interact in cells, and furthermore, that this interaction requires two full-length 14-3-3σ monomers. To test whether the interaction between 14-3-3σ and actin could additionally be observed in vitro using purified proteins, and by extension, whether the interaction is direct versus as a protein complex, I performed GST pull-down experiments using recombinant GST-14-3-3σ and actin purified from rabbit muscle. Using this assay, I found that recombinant GST-14-3-3σ, but not GST alone, was able to interact with actin in vitro (Figure 25B), indicating that the interaction between 14-3-3σ and actin is direct.

### 3.4.3. 14-3-3σ inhibits actin polymerization in vitro and in situ

While the interaction between actin and 14-3-3σ is compelling, it does not demonstrate that 14-3-3σ plays any role in regulating actin polymerization through this interaction. To test whether interaction with 14-3-3σ is sufficient to inhibit actin polymerization in vitro, purified G-actin was pretreated with an equimolar ratio of either GST or GST-14-3-3σ, then polymerized into F-actin (Pardee and Spudich, 1982) by adding KCl, $Mg^{2+}$, and ATP. Pretreating G-actin with GST-14-3-3σ significantly inhibited actin polymerization, as there was a 2-fold increase in the amount of G-actin remaining in solution following polymerization relative to pretreatment with GST alone (Figure 26A,B). A similar conclusion was reached using AlexaFluor488-conjugated actin (488-actin), where fewer actin fibers were visible following 488-G-actin polymerization when pretreated with GST-14-3-3σ (Figure 26C). These data demonstrate that 14-3-3σ interacts directly with actin in vitro, and that this interaction is sufficient to inhibit the polymerization of G-actin to F-actin in the absence of other cofactors.

To test whether 14-3-3σ antagonizes actin polymerization also in situ, 488-G-actin pretreated with either GST or GST-14-3-3σ was introduced into cells that were gently permeabilized with saponin (Symons and Mitchison, 1991), and

the ratio of actin incorporation into the endogenous F-actin cytoskeleton was measured by counterstaining fixed cells with phalloidin (Figure 27). To do this experiment, I chose two breast cancer cell lines having high and low endogenous 14-3-3σ expression, BT549 and HCC1143, respectively. In BT549, 488-G-actin pretreated with GST-14-3-3σ was incorporated significantly less into the endogenous actin cytoskeleton relative to when 488-G-actin was pretreated with GST alone; this was not observed in HCC1143 cells which have high endogenous 14-3-3σ. The finding suggests that endogenous 14-3-3σ is sufficient to inhibit 488-G-actin incorporation in situ, in agreement with the in vitro experiments.

Actin polymerization in vitro occurs in several distinct stages. There is an initial delay due to the kinetic barrier required for nucleation of actin monomers, followed by a linear growth phase where the concentration of G-actin is in excess and the polymerization occurs at a maximum rate, and then a plateau phase where the rates of actin polymerization and turnover are in equilibrium (Cooper et al., 1983; Sept and McCammon, 2001). The kinetics of actin assembly have been characterized chiefly by measuring the rate of pyrene-conjugated actin polymerization, a technique that is very sensitive and can reproducibly quantify the influence of proteins and drugs on actin polymerization (Kouyama and Mihashi, 1981). Using pyrene-conjugated actin, I found that 14-3-3σ influences actin polymerization kinetics in several ways (Figure 28): by decreasing the maximum rate of polymerization (compare the slopes of the linear region between 1000s and 2500s), by shifting the equilibrium towards less F-actin and more G-actin (compare the plateau heights of the curves), and by increasing the length of time necessary to reach equilibrium (a delay in the plateau phase). The combined in vitro and in situ experiments (Figures 26-28) provide evidence supporting a previously unknown mechanism through which 14-3-3σ regulates actin polymerization directly in cells, leading to coordination of cell migration and invasion by retaining a soluble pool of actin for polymerization.

### 3.4.4. 14-3-3σ inhibits actin polymerization by sequestering G-actin

Several lines of evidence in cells and in vitro indicate that 14-3-3σ interacts directly with actin and inhibits its polymerization. However, one outstanding question remains – does 14-3-3σ inhibit actin polymerization by sequestering G-actin, or by capping actin filaments? To test whether 14-3-3σ interacts with F-actin, I performed an F-actin co-sedimentation assay in which actin was polymerized in the presence of GST-14-3-3σ at an 8:1 molar ratio of actin:14-3-3σ, fractionated into F- and G-actin populations, then tested whether 14-3-3σ would co-sediment with the F-actin pellet following polymerization. Using this assay, I found that 14-3-3σ did not interact with F-actin, as there was no enrichment of 14-3-3σ in the F-actin pellet, nor was there depletion of 14-3-3σ from the supernatant (Figure 29). This experiment indicates that 14-3-3σ most likely does not inhibit actin polymerization by capping F-actin filaments.

Further evidence that 14-3-3σ does not cap actin filaments can be observed by immunofluorescence data, which consistently show that 14-3-3σ and F-actin do not colocalize in cells (Figures 30 and 31, see also Figure 18). Interestingly however, 14-3-3σ shows significant colocalization with a monoclonal antibody against β-actin; this antibody recognizes a non-filamentous form of actin that is most likely G-actin, as it shows no colocalization with phalloidin (Figure 30), and its epitope is lost if cells are extracted with 1% Triton X-100 prior to fixing (data not shown). In addition, 14-3-3σ shows dramatic colocalization with profilin, a G-actin interacting protein that, similar to 14-3-3σ, shows no colocalization with F-actin (Figure 31). Although I cannot definitively conclude that 14-3-3σ preferentially interacts with G-actin in the absence of known binding constants, the co-sedimentation and immunofluorescence data suggest that 14-3-3σ inhibits actin polymerization most likely by binding and sequestering G-actin.

3.4.5. Overexpressing profilin, a G-actin binding protein, phenocopies 14-3-3σ knockdown

To further support the proposed mechanism that 14-3-3σ regulates actin dynamics and migration by binding and sequestering G-actin, I tested whether the phenotypes observed following 14-3-3σ knockdown could be recapitulated by altering the levels of known G-actin binding proteins, such as profilin. To do this experiment, I generated constructs that forced the expression of either wild-type profilin-1 or a mutant (S137D) that is unable to bind to G-actin (Shao et al., 2008), and measured whether motility and actin architecture in the transgenic cells could be influenced in a manner comparable to 14-3-3σ knockdown. Forced expression of profilin-1 increased the polymerization of F-actin in cells, and concomitantly decreased cell motility in chemoattraction assays (Figure 32); this was not observed in cells expressing profilin-1 (S137D), indicating that the phenotypes require interaction with G-actin. These data recapitulate the phenotype observed in 14-3-3σ knockdown cells, providing further evidence to suggest that 14-3-3σ inhibits actin polymerization by sequestering G-actin.

In summary, several lines of evidence are presented which suggest that 14-3-3σ facilitates cell motility by regulating the balance of actin polymerization in cells. Specifically, I demonstrate that 14-3-3σ interacts directly with actin and inhibits its polymerization in vitro, in situ, and in culture, most likely by binding and sequestering G-actin. Several of the phenotypes observed in 14-3-3σ knockdown cells can be recapitulated by overexpressing profilin, which is known to bind G-actin and promote its recruitment to the end of F-actin filaments, providing further evidence that 14-3-3σ regulates actin polymerization through interaction with G-actin.

### 3.5. Future experiments

Due to time constraints, there are several experiments I wish I could have completed in this study, but that are currently being investigated. These include:

- measuring the proteome of 14-3-3σ interacting proteins in BLBCs versus normal myoepithelial cells by mass spectrometry
- measuring the binding constants of 14-3-3σ and G-actin versus F-actin using surface plasmon resonance (Jason-Moller et al., 2006)
- investigating whether 14-3-3σ antagonizes profilin, or vice-versa
- investigate whether the role for 14-3-3σ in BLBCs described here are applicable to other tumors with elevated 14-3-3σ (such as pancreatic cancer)
- assess whether 14-3-3σ influences metastasis in animal models
- understand the role of 14-3-3σ in myoepithelial cells of the normal gland
- define regions of actin that are required for 14-3-3σ interaction

# CHAPTER 4. DISCUSSION

### 4.1. A previously undescribed role for 14-3-3σ in directly inhibiting actin polymerization.

There is a wide body of literature linking actin-regulatory proteins with tumor cell invasion and metastasis (Hall, 2009; Narumiya et al., 2009; Wang et al., 2007; Wang et al., 2005a; see also section 3.3.1). Previous studies describing 14-3-3-mediated actin reorganization have highlighted a number of actin cytoskeletal signaling pathways under regulation by various 14-3-3 family members. 14-3-3zeta can bind to the F-actin severing protein cofilin when phosphorylated at serine-3, protecting cofilin from dephosphorylation by PP2A in vitro (Gohla and Bokoch, 2002). Alternatively, several 14-3-3 isoforms, including gamma, zeta and beta, interact with and sequester the cofilin phosphatase slingshot, leading to stabilization of serine-3 phosphorylated cofilin and establishment of polarized cell movement (Kligys et al., 2007; Nagata-Ohashi et al., 2004; Soosairajah et al., 2005). 14-3-3zeta and 14-3-3beta have also been shown to interact with LIMK1 and TESK1, respectively; kinases responsible for phosphorylating cofilin at serine-3 (Birkenfeld et al., 2003; Toshima et al., 2001). These studies highlight a common theme of 14-3-3-dependent regulation of cofilin phosphorylation, and thus activity, during cell migration.

In addition to the cofilin pathway, a recent study found several 14-3-3 isoforms bind to the AKT substrate Kank, and that Kank inhibits the insulin- and AKT-dependent activation of RhoA and subsequent actin cytoskeletal dynamics through interaction with 14-3-3 (Kakinuma et al., 2008). Activated AKT can interact with both actin and with 14-3-3σ (Vandermoere et al., 2007), and 14-3-3σ has been shown to negatively regulate AKT in MCF-7 cells and to inversely correlate with AKT activity in tumors (Yang et al., 2006a; Yang et al., 2006b). These studies suggest the existence of an alternative 14-3-3-dependent actin regulatory pathway by which AKT activated during chemotaxis is recruited to actin and may locally activate RhoA, but excessive AKT activity is suppressed directly by 14-3-3σ or through AKT-dependent phosphorylation and activation of Kank, which downmodulates RhoA activity via 14-3-3 interaction.

In the course of my research I have unraveled another aspect of how the 14-3-3 family regulates actin architecture. I found the overall activity of LIMK, AKT, cofilin, RhoA, Rac1, cdc42, and other actin cytoskeletal signaling participants were unaffected in T4-2 sh-14-3-3σ cells (Figure 17). However, looking downstream of these signaling pathways, I observed a direct interaction between 14-3-3σ and actin (Figure 25). I show that regions of 14-3-3σ known to be involved in binding to other ligands are also involved in binding actin (Figure 15, 25), and interestingly, despite the fact that the 14-3-3$\sigma^{\Delta C}$ mutant is able to interact with endogenous 14-3-3σ, the heterodimer was unable to interact with actin suggesting that two functional monomers are required for stable actin interactions. Using purified molecules, I show 14-3-3σ inhibits actin polymerization in vitro by perturbing the kinetics of polymerization and shifting the quilibrium levels of G- and F-actin (Figure 26, 28). By introducing fluorescently

labeled G-actin into permeabilized cells, I found that 14-3-3σ inhibits actin polymerization also in situ (Figure 27).

Using live cell imaging and FRAP analysis, I show that during cell migration, 14-3-3σ polarizes away from the migratory front where actin remodeling is most dramatic (Figure 19-21), and that the actin polymerization rate increases in cells deficient for 14-3-3σ (Figure 22). This depletes the pool of soluble, bioavailable actin required for polarized motility (Figure 23), and overexpressing actin in 14-3-3σ knockdown cells rescues their impaired motility and invasion (Figure 24). Based on the observed lack of interaction and colocalization with F-actin, and conversely, the strong colocalization with G-actin and profilin (Figure 29-31), I propose that 14-3-3σ directly inhibits actin polymerization by sequestering G-actin and competing with profilin. To my knowledge, this is the first biochemical and functional demonstration of any 14-3-3 family member regulating actin dynamics independent of other actin-regulatory factors. Actin remodeling and contractility is necessary for cell migration both during development and metastasis (see section 3.3.1), and I propose that 14-3-3 regulation of actin dynamics may play a fundamental role in cell migration both during development and cancer progression. Intriguingly, *S. cerevisiae* strains with dominant-negative or temperature-sensitive mutations to *BMH1* or *BMH2*, genes encoding yeast 14-3-3 homologues, have disrupted actin cytoskeletal integrity and polarity (Lottersberger et al., 2006; Roth et al., 1999), suggesting that F-actin regulation by 14-3-3 is conserved during evolution.

### 4.2. 14-3-3σ and basal-like breast cancer.

Several reports have suggested that in primary breast cancers and cell lines, 14-3-3σ function is silenced either through proteolysis via an estrogen-responsive E3 ligase, or through promoter methylation which is observable in as high as 91% of breast tumors (Ferguson et al., 2000; Prasad et al., 1992; Umbricht et al., 2001; Urano et al., 2002; Vercoutter-Edouart et al., 2001). However, more recent studies have shown that the methylation status of 14-3-3σ promoter does not accurately assess protein silencing. Immunohistochemical analysis has shown that despite the high frequency of 14-3-3σ promoter methylation in breast cancer, silencing on the protein level is an infrequent event occurring in only 3 of 68 tumors (Moreira et al., 2005). Similar data were also shown in vulval epithelial carcinomas (Wang et al., 2008), questioning whether 14-3-3σ promoter methylation can be used as evidence that the protein functions as a tumor suppressor. Other frequently cited evidence that 14-3-3σ is a tumor suppressor is its role as a regulator of the cell cycle in HCT116 colorectal cancer cells (Chan et al., 1999; Hermeking et al., 1997), though I see no evidence that 14-3-3σ regulates BLBC cell cycle (Figure 10) which has also been observed in clinical samples (Moreira et al., 2005). Despite the considerable literature suggesting 14-3-3σ is a tumor suppressor, it is surprising that to my knowledge, there are no reports of its overexpression resulting in the suppression of tumors in vivo.

One caveat to early papers describing declined 14-3-3σ expression in breast cancer is that expression was normalized to non-malignant cell lines derived from reduction mammoplasty (primary HMECs, MCF-10A, and 184) (Ferguson et al., 2000; Prasad et al., 1992; Vercoutter-Edouart et al., 2001). Primary mammary epithelial cells rapidly adopt myoepithelial/basal-like gene expression profiles when cultured on tissue culture plastic in the absence of selective growth media (Dairkee et al., 1986; DiRenzo et al., 2002; O'Hare et al., 1991), and 14-3-3σ has at least three-fold higher expression in myoepithelial cells than luminal epithelial cells – a trend consistent in pathologically normal tissue, in premalignant lesions, and in normal tissue adjacent to primary breast tumors (Figure 2; Moreira et al., 2005; Simpson et al., 2004). Indeed, primary cultures derived from the tissue of a breast cancer patient with weak 14-3-3σ tumor immunoreactivity have robust 14-3-3σ expression after 6 passages in culture, indicating rapid population drift towards myoepithelial gene expression profile (Moreira et al., 2005). Given that tumors stain relatively homogenous for 14-3-3σ (Moreira et al., 2005) and that >80% of tumors lack basal/myoepithelial-like differentiation (Cheang et al., 2008; Lakhani and O'Hare, 2001; Nielsen et al., 2004; Perou et al., 2000; Sorlie et al., 2001; Sorlie et al., 2003), comparing gene expression profiles between a homogenous “non-myoepithelial” population and a homogenous “myoepithelial” population would artificially identify several lineage-specific markers, including 14-3-3σ.

By staining a tissue microarray derived from 245 cases of invasive breast carcinoma, I show clearly that 14-3-3σ cytoplasmic expression is highest in patients with basal-like breast cancers, with expression having positive correlation with all markers of basal-like breast cancers and inverse correlation with the markers of luminal tumors that were tested (Table 1). I found strong 14-3-3σ staining detected 16 of 23 (70%) basal tumors and 15 of 164 (9%) non-basal tumors. Whereas the presence of 14-3-3σ in a subset of non-basal tumors limits the utility of 14-3-3σ as a single marker to identify BLBCs, I found that 16 of 17 tumors that are 14-3-3σ-positive and ER-negative were of basal-like subtype. When used in conjunction with ER negativity, cytoplasmic 14-3-3σ staining may thus be employed as an immunohistochemical surrogate for BLBCs. Interestingly, 14-3-3σ cytoplasmic expression in ER-positive tumors is associated with poorer clinical outcome than nuclear expression (Simpson et al., 2004); I obtained similar data in this cohort by showing that cytoplasmic staining correlates with poorer clinical outcome than nuclear staining, and furthermore, that subcellular distribution is linked with tumor molecular subtype (Figure 5).

During the transition to invasive breast carcinoma, the myoepithelium, itself thought to act as a natural “tumor suppressor, becomes discontinuous or is lost entirely, and in the majority of cases, tumor cells of luminal epithelial gene expression predominate (Barsky and Karlin, 2005; Hu et al., 2008; Lakhani and Bissell, 2005; Lakhani and O'Hare, 2001; Perou et al., 2000). As mentioned earlier, 14-3-3σ expression is approximately 3-fold lower in the luminal epithelium versus myoepithelial cells of the normal breast (Moreira et al., 2005; Simpson et

al., 2004), and furthermore, genes that are expressed at low levels in tissues become sensitive to step-wise epigenetic modifications culminating in promoter methylation (Leu et al., 2004; Oyer et al., 2009). Thus, it is plausible that the 14-3-3σ 'downmodulation' and promoter methylation frequently observed in breast cancers may be due to a combination of myoepithelium loss, clonal expansion of a cell lineage with low expression prior to malignancy, progressive epigenetic silencing, and proteolysis in the case of non-basal breast cancer subtypes. Alternatively, it has recently been proposed that basal-like tumors originate from aberrant luminal epithelial precursor cells (Lim et al., 2009), and the expression of 14-3-3σ both in myoepithelial cells and in basal-like tumors suggests that this protein may be expressed in a common progenitor cell type, with 14-3-3σ expression diminishing during the differentiation of precursor cells into ductal and alveolar luminal epithelia. In either case, it follows that 14-3-3σ expression and function in breast cancer would correlate with breast cancer subtype, and my data strongly suggest this to be the case.

### 4.3. 14-3-3σ and poor clinical outcome.

In three independent patient cohorts, I observed that 14-3-3σ correlates with poor patient outcome (Figure 5, 6). Of the seven mammalian 14-3-3 isoforms, only 14-3-3σ and 14-3-3ζ expression correlated with shortened overall, metastasis-free, and recurrence-free survival in the NKI cohort (data not shown), and 14-3-3ζ has recently been implicated in the progression from HER2-positive ductal carcinoma in situ to invasive carcinoma by promoting epithelial to mesenchymal transition (Lu et al., 2009a). The correlation between 14-3-3σ and poor clinical outcome is supported most strongly by the NKI cohort, although it should be noted that the UCSF cohort have both fewer patients and decreased metastasis frequency in these patients in comparison to the NKI cohort (data not shown), the combination of which could explain why the metastasis-free survival in the UCSF cohort failed to reach statistical significance. The correlation between 14-3-3σ and poor outcome may stem from this protein being a marker of a breast cancer subtype that inherently has aggressive clinical behavior. Nevertheless, I show that 14-3-3σ is directly linked to cell migration and invasion in culture and in vivo independent of proliferation, and that its expression in tumors is highest at the invasive front where soft tissue infiltration occurs. (Figures 7-12). Similar results have recently been reported for colorectal cancer where forced expression of 14-3-3σ in HCT116 cells increases their motility (Ide et al., 2007), despite this being the very cell line in which 14-3-3σ was previously shown to regulate the G2/M checkpoint and potentially be a tumor suppressor (Chan et al., 1999; Hermeking et al., 1997). This study also showed an increased 14-3-3σ staining intensity at the invasive front of colorectal cancers, analogous to my observations in T4-2 tumors (Figure 7). I further provide a mechanism by which 14-3-3σ promotes cell migration and tumor invasion in vivo by directly regulating actin polymerization (Figures 22-28).

### 4.4. Conclusions.

The finding that 14-3-3σ expression is highest in basal-like breast tumors, a breast cancer subtype that inherently has an aggressive clinical behavior, and that 14-3-3σ mechanistically regulates actin dynamics, suggests that this molecule could be an important element of basal-like tumor progression. My data showing that 14-3-3σ is a marker of basal-like breast tumors does not dispute, but rather reconciles, the literature of whether 14-3-3σ is silenced in breast cancer or not: I propose that "silencing" of 14-3-3σ in breast cancer is contingent on whether tumors show basal-like differentiation or luminal differentiation, and the previously described 14-3-3σ downregulation frequency in breast cancer is in good agreement with the frequency of non-basal tumors. I show that 14-3-3σ directly interacts with actin and inhibits its polymerization in vitro and in situ to regulate motility and tumor invasion in vivo, thus providing a molecular basis by which 14-3-3σ may contribute to basal tumor progression to invasive carcinoma. These data implicate 14-3-3σ as a potential therapeutic target, prognostic indicator, and "functional biomarker" of BLBC, which may be of clinical importance following further validation studies.

# CHAPTER 5. REFERENCES

Abercrombie, M., and Ambrose, E. J. 1958. Interference microscope studies of cell contacts in tissue culture. Exp Cell Res *15*, 332-345.

Acloque, H., Adams, M. S., Fishwick, K., Bronner-Fraser, M., and Nieto, M. A. 2009. Epithelial-mesenchymal transitions: the importance of changing cell state in development and disease. J Clin Invest *119*, 1438-1449.

Aitken, A. 2006. 14-3-3 proteins: a historic overview. Semin Cancer Biol *16*, 162-172.

Akahira, J., Sugihashi, Y., Suzuki, T., Ito, K., Niikura, H., Moriya, T., Nitta, M., Okamura, H., Inoue, S., Sasano, H., Okamura, K., and Yaegashi, N. 2004. Decreased expression of 14-3-3 sigma is associated with advanced disease in human epithelial ovarian cancer: its correlation with aberrant DNA methylation. Clin Cancer Res *10*, 2687-2693.

Albain, K. S., Barlow, W. E., Shak, S., Hortobagyi, G. N., Livingston, R. B., Yeh, I. T., Ravdin, P., Bugarini, R., Baehner, F. L., Davidson, N. E., Sledge, G. W., Winer, E. P., Hudis, C., Ingle, J. N., Perez, E. A., Pritchard, K. I., Shepherd, L., Gralow, J. R., Yoshizawa, C., Allred, D. C., Osborne, C. K., and Hayes, D. F. 2009. Prognostic and predictive value of the 21-gene recurrence score assay in postmenopausal women with node-positive, oestrogen-receptor-positive breast cancer on chemotherapy: a retrospective analysis of a randomised trial. Lancet Oncol *11*, 55-65.

Alcaraz, J., Xu, R., Mori, H., Nelson, C. M., Mroue, R., Spencer, V. A., Brownfield, D., Radisky, D. C., Bustamante, C., and Bissell, M. J. 2008. Laminin and biomimetic extracellular elasticity enhance functional differentiation in mammary epithelia. EMBO J *27*, 2829-2838.

Andrechek, E. R., Hardy, W. R., Siegel, P. M., Rudnicki, M. A., Cardiff, R. D., and Muller, W. J. 2000. Amplification of the neu/erbB-2 oncogene in a mouse model of mammary tumorigenesis. Proc Natl Acad Sci U S A *97*, 3444-3449.

Andrianantoandro, E., and Pollard, T. D. 2006. Mechanism of actin filament turnover by severing and nucleation at different concentrations of ADF/cofilin. Mol Cell *24*, 13-23.

Aranda, V., Haire, T., Nolan, M. E., Calarco, J. P., Rosenberg, A. Z., Fawcett, J. P., Pawson, T., and Muthuswamy, S. K. 2006. Par6-aPKC uncouples ErbB2 induced disruption of polarized epithelial organization from proliferation control. Nat Cell Biol *8*, 1235-1245.

Arber, S., Barbayannis, F. A., Hanser, H., Schneider, C., Stanyon, C. A., Bernard, O., and Caroni, P. 1998. Regulation of actin dynamics through phosphorylation of cofilin by LIM-kinase. Nature *393*, 805-809.

Arriola, E., Rodriguez-Pinilla, S. M., Lambros, M. B., Jones, R. L., James, M., Savage, K., Smith, I. E., Dowsett, M., and Reis-Filho, J. S. 2007. Topoisomerase II alpha amplification may predict benefit from adjuvant anthracyclines in HER2 positive early breast cancer. Breast Cancer Res Treat *106*, 181-189.

Banerjee, S., Reis-Filho, J. S., Ashley, S., Steele, D., Ashworth, A., Lakhani, S. R., and Smith, I. E. 2006. Basal-like breast carcinomas: clinical outcome and response to chemotherapy. J Clin Pathol *59*, 729-735.

Barcellos-Hoff, M. H., Aggeler, J., Ram, T. G., and Bissell, M. J. 1989. Functional differentiation and alveolar morphogenesis of primary mammary cultures on reconstituted basement membrane. Development *105*, 223-235.

Barsky, S. H., and Karlin, N. J. 2005. Myoepithelial cells: autocrine and paracrine suppressors of breast cancer progression. J Mammary Gland Biol Neoplasia *10*, 249-260.

Behbod, F., Kittrell, F. S., Lamarca, H., Edwards, D., Kerbawy, S., Heestand, J. C., Young, E., Mukhopadhyay, P., Yeh, H. W., Allred, D. C., Hu, M., Polyak, K., Rosen, J. M., and Medina, D. 2009. An intra-ductal human-in-mouse transplantation model mimics the subtypes of ductal carcinoma in situ. Breast Cancer Res *11*, R66.

Beli, P., Mascheroni, D., Xu, D., and Innocenti, M. 2008. WAVE and Arp2/3 jointly inhibit filopodium formation by entering into a complex with mDia2. Nat Cell Biol *10*, 849-857.

Bell, C. D., and Waizbard, E. 1986. Variability of cell size in primary and metastatic human breast carcinoma. Invasion Metastasis *6*, 11-20.

Bernards, A. 2003. GAPs galore! A survey of putative Ras superfamily GTPase activating proteins in man and Drosophila. Biochim Biophys Acta *1603*, 47-82.

Birkenfeld, J., Betz, H., and Roth, D. 2003. Identification of cofilin and LIM-domain-containing protein kinase 1 as novel interaction partners of 14-3-3 zeta. Biochem J *369*, 45-54.

Bissell, M. J., Kenny, P. A., and Radisky, D. C. 2005. Microenvironmental regulators of tissue structure and function also regulate tumor induction and progression: the role of extracellular matrix and its degrading enzymes. Cold Spring Harb Symp Quant Biol *70*, 343-356.

Bloom, H. J., and Richardson, W. W. 1957. Histological grading and prognosis in breast cancer; a study of 1409 cases of which 359 have been followed for 15 years. Br J Cancer *11*, 359-377.

Bogden, A. E., Haskell, P. M., LePage, D. J., Kelton, D. E., Cobb, W. R., and Esber, H. J. 1979. Growth of human tumor xenografts implanted under the renal capsule of normal immunocompetent mice. Exp Cell Biol *47*, 281-293.

Booth, B. W., Mack, D. L., Androutsellis-Theotokis, A., McKay, R. D., Boulanger, C. A., and Smith, G. H. 2008. The mammary microenvironment alters the differentiation repertoire of neural stem cells. Proc Natl Acad Sci U S A *105*, 14891-14896.

Borch, J., Bych, K., Roepstorff, P., Palmgren, M. G., and Fuglsang, A. T. 2002. Phosphorylation-independent interaction between 14-3-3 protein and the plant plasma membrane H+-ATPase. Biochem Soc Trans *30*, 411-415.

Bos, P. D., Nguyen, D. X., and Massague, J. 2010. Modeling metastasis in the mouse. Curr Opin Pharmacol.

Bos, P. D., Zhang, X. H., Nadal, C., Shu, W., Gomis, R. R., Nguyen, D. X., Minn, A. J., van de Vijver, M. J., Gerald, W. L., Foekens, J. A., and Massague, J. 2009. Genes that mediate breast cancer metastasis to the brain. Nature *459*, 1005-1009.

Boulanger, C. A., Mack, D. L., Booth, B. W., and Smith, G. H. 2007. Interaction with the mammary microenvironment redirects spermatogenic cell fate in vivo. Proc Natl Acad Sci U S A *104*, 3871-3876.

Briand, P., Nielsen, K. V., Madsen, M. W., and Petersen, O. W. 1996. Trisomy 7p and malignant transformation of human breast epithelial cells following epidermal growth factor withdrawal. Cancer Res *56*, 2039-2044.

Briand, P., Petersen, O. W., and Van Deurs, B. 1987. A new diploid nontumorigenic human breast epithelial cell line isolated and propagated in chemically defined medium. In Vitro Cell Dev Biol *23*, 181-188.

Bussard, K. M., Boulanger, C. A., Booth, B. W., Bruno, R. D., and Smith, G. H. 2010. Reprogramming Human Cancer Cells in the Mouse Mammary Gland. Cancer Res.

Cain, R. J., and Ridley, A. J. 2009. Phosphoinositide 3-kinases in cell migration. Biol Cell *101*, 13-29.

Carlsson, L., Nystrom, L. E., Sundkvist, I., Markey, F., and Lindberg, U. 1977. Actin polymerizability is influenced by profilin, a low molecular weight protein in non-muscle cells. J Mol Biol *115*, 465-483.

Celis, J. E., Gromov, P., Cabezon, T., Moreira, J. M., Ambartsumian, N., Sandelin, K., Rank, F., and Gromova, I. 2004. Proteomic characterization of the interstitial fluid perfusing the breast tumor microenvironment: a novel resource for biomarker and therapeutic target discovery. Mol Cell Proteomics *3*, 327-344.

Chan, A. Y., Bailly, M., Zebda, N., Segall, J. E., and Condeelis, J. S. 2000. Role of cofilin in epidermal growth factor-stimulated actin polymerization and lamellipod protrusion. J Cell Biol *148*, 531-542.

Chan, T. A., Hermeking, H., Lengauer, C., Kinzler, K. W., and Vogelstein, B. 1999. 14-3-3σ is required to prevent mitotic catastrophe after DNA damage. Nature *401*, 616-620.

Cheang, M. C., Voduc, D., Bajdik, C., Leung, S., McKinney, S., Chia, S. K., Perou, C. M., and Nielsen, T. O. 2008. Basal-like breast cancer defined by five biomarkers has superior prognostic value than triple-negative phenotype. Clin Cancer Res *14*, 1368-1376.

Chen, A., Cuevas, I., Kenny, P. A., Miyake, H., Mace, K., Ghajar, C., Boudreau, A., Bissell, M., and Boudreau, N. 2009. Endothelial cell migration and vascular endothelial growth factor expression are the result of loss of breast tissue polarity. Cancer Res *69*, 6721-6729.

Chhabra, E. S., and Higgs, H. N. 2007. The many faces of actin: matching assembly factors with cellular structures. Nat Cell Biol *9*, 1110-1121.

Chin, K., DeVries, S., Fridlyand, J., Spellman, P. T., Roydasgupta, R., Kuo, W. L., Lapuk, A., Neve, R. M., Qian, Z., Ryder, T., Chen, F., Feiler, H., Tokuyasu, T., Kingsley, C., Dairkee, S., Meng, Z., Chew, K., Pinkel, D.,

Jain, A., Ljung, B. M., Esserman, L., Albertson, D. G., Waldman, F. M., and Gray, J. W. 2006. Genomic and transcriptional abberations linked to breast cancer pathophysiologies. Cancer Cell *10*, 529-542.

Clark, G. M., and McGuire, W. L. 1988. Steroid receptors and other prognostic factors in primary breast cancer. Semin Oncol *15*, 20-25.

Clarke, C., Sandle, J., and Lakhani, S. R. 2005. Myoepithelial cells: pathology, cell separation and markers of myoepithelial differentiation. J Mammary Gland Biol Neoplasia *10*, 273-280.

Clarke, R. 1996. Human breast cancer cell line xenografts as models of breast cancer. The immunobiologies of recipient mice and the characteristics of several tumorigenic cell lines. Breast Cancer Res Treat *39*, 69-86.

Conley, F. K. 1979. Development of a metastatic brain tumor model in mice. Cancer Res *39*, 1001-1007.

Cooper, J. A., Buhle, E. L., Jr., Walker, S. B., Tsong, T. Y., and Pollard, T. D. 1983. Kinetic evidence for a monomer activation step in actin polymerization. Biochemistry *22*, 2193-2202.

Costes, S. V., Daelemans, D., Cho, E. H., Dobbin, Z., Pavlakis, G., and Lockett, S. 2004. Automatic and quantitative measurement of protein-protein colocalization in live cells. Biophys J *86*, 3993-4003.

Cowin, P., and Wysolmerski, J. 2010. Molecular mechanisms guiding embryonic mammary gland development. Cold Spring Harb Perspect Biol *2*, a003251.

Cramer, L. P., Siebert, M., and Mitchison, T. J. 1997. Identification of novel graded polarity actin filament bundles in locomoting heart fibroblasts: implications for the generation of motile force. J Cell Biol *136*, 1287-1305.

Dairkee, S. H., Blayney-Moore, C. M., Smith, H. S., and Hackett, A. J. 1986. Concurrent expression of basal and luminal epithelial markers in cultures of normal human breast analyzed using monoclonal antibodies. Differentiation *32*, 93-100.

Daniel, C. W., and Smith, G. H. 1999. The mammary gland: a model for development. J Mammary Gland Biol Neoplasia *4*, 3-8.

Davidson, L. A., and Keller, R. E. 1999. Neural tube closure in Xenopus laevis involves medial migration, directed protrusive activity, cell intercalation and convergent extension. Development *126*, 4547-4556.

Day, R. N., and Davidson, M. W. 2009. The fluorescent protein palette: tools for cellular imaging. Chem Soc Rev *38*, 2887-2921.

Debnath, J., Muthuswamy, S. K., and Brugge, J. S. 2003. Morphogenesis and oncogenesis of MCF-10A mammary epithelial acini grown in three-dimensional basement membrane cultures. Methods *30*, 256-268.

DesMarais, V., Macaluso, F., Condeelis, J., and Bailly, M. 2004. Synergistic interaction between the Arp2/3 complex and cofilin drives stimulated lamellipod extension. J Cell Sci *117*, 3499-3510.

DiRenzo, J., Signoretti, S., Nakamura, N., Rivera-Gonzalez, R., Sellers, W., Loda, M., and Brown, M. 2002. Growth factor requirements and basal

phenotype of an immortalized mammary epithelial cell line. Cancer Res *62*, 89-98.

Drost, R. M., and Jonkers, J. 2009. Preclinical mouse models for BRCA1-associated breast cancer. Br J Cancer *101*, 1651-1657.

Eden, S., Rohatgi, R., Podtelejnikov, A. V., Mann, M., and Kirschner, M. W. 2002. Mechanism of regulation of WAVE1-induced actin nucleation by Rac1 and Nck. Nature *418*, 790-793.

El-Sibai, M., Pertz, O., Pang, H., Yip, S. C., Lorenz, M., Symons, M., Condeelis, J. S., Hahn, K. M., and Backer, J. M. 2008. RhoA/ROCK-mediated switching between Cdc42- and Rac1-dependent protrusion in MTLn3 carcinoma cells. Exp Cell Res *314*, 1540-1552.

Ellis, I. O., Galea, M., Broughton, N., Locker, A., Blamey, R. W., and Elston, C. W. 1992. Pathological prognostic factors in breast cancer. II. Histological type. Relationship with survival in a large study with long-term follow-up. Histopathology *20*, 479-489.

Elston, E. W., and Ellis, I. O. 1993. Method for grading breast cancer. J Clin Pathol *46*, 189-190.

Enterline, H. T., and Coman, D. R. 1950. The ameboid motility of human and animal neoplastic cells. Cancer *3*, 1033-1038.

Erlandson, R. A., and Rosen, P. P. 1982. Infiltrating myoepithelioma of the breast. Am J Surg Pathol *6*, 785-793.

Evdokimova, V., Tognon, C., Ng, T., Ruzanov, P., Melnyk, N., Fink, D., Sorokin, A., Ovchinnikov, L. P., Davicioni, E., Triche, T. J., and Sorensen, P. H. 2009. Translational activation of snail1 and other developmentally regulated transcription factors by YB-1 promotes an epithelial-mesenchymal transition. Cancer Cell *15*, 402-415.

Fan, C., Oh, D. S., Wessels, L., Weigelt, B., Nuyten, D. S., Nobel, A. B., van't Veer, L. J., and Perou, C. M. 2006. Concordance among gene-expression-based predictors for breast cancer. N Engl J Med *355*, 560-569.

Fardal, R. W., Kierland, R. R., Clagett, O. T., and Woolner, L. B. 1964. Prognosis in Cutaneous Paget's Disease. Postgrad Med *36*, 584-593.

Fata, J. E., Werb, Z., and Bissell, M. J. 2004. Regulation of mammary gland branching morphogenesis by the extracellular matrix and its remodeling enzymes. Breast Cancer Res *6*, 1-11.

Faulkin, L. J., Jr., and Deome, K. B. 1960. Regulation of growth and spacing of gland elements in the mammary fat pad of the C3H mouse. J Natl Cancer Inst *24*, 953-969.

Ferguson, A. T., Evron, E., Umbricht, C. B., Pandita, T. K., Chan, T. A., Hermeking, H., Marks, J. R., Lambers, A. R., Futreal, P. A., Stampfer, M. R., and Sukumar, S. 2000. High frequency of hypermethylation at the 14-3-3 sigma locus leads to gene silencing in breast cancer. Proc Natl Acad Sci U S A *97*, 6049-6054.

Ferguson, D. J., and Anderson, T. J. 1981. Morphological evaluation of cell turnover in relation to the menstrual cycle in the "resting" human breast. Br J Cancer *44*, 177-181.

Fisher, B., Costantino, J. P., Wickerham, D. L., Redmond, C. K., Kavanah, M., Cronin, W. M., Vogel, V., Robidoux, A., Dimitrov, N., Atkins, J., Daly, M., Wieand, S., Tan-Chiu, E., Ford, L., and Wolmark, N. 1998. Tamoxifen for prevention of breast cancer: report of the National Surgical Adjuvant Breast and Bowel Project P-1 Study. J Natl Cancer Inst *90*, 1371-1388.

Fisher, B., Redmond, C., Brown, A., Wickerham, D. L., Wolmark, N., Allegra, J., Escher, G., Lippman, M., Savlov, E., Wittliff, J., and et al. 1983. Influence of tumor estrogen and progesterone receptor levels on the response to tamoxifen and chemotherapy in primary breast cancer. J Clin Oncol *1*, 227-241.

Fletcher, D. A., and Mullins, R. D. 2010. Cell mechanics and the cytoskeleton. Nature *463*, 485-492.

Foekens, J. A., Atkins, D., Zhang, Y., Sweep, F. C., Harbeck, N., Paradiso, A., Cufer, T., Sieuwerts, A. M., Talantov, D., Span, P. N., Tjan-Heijnen, V. C., Zito, A. F., Specht, K., Hoefler, H., Golouh, R., Schittulli, F., Schmitt, M., Beex, L. V., Klijn, J. G., and Wang, Y. 2006. Multicenter validation of a gene expression-based prognostic signature in lymph node-negative primary breast cancer. J Clin Oncol *24*, 1665-1671.

Fong, P. C., Boss, D. S., Yap, T. A., Tutt, A., Wu, P., Mergui-Roelvink, M., Mortimer, P., Swaisland, H., Lau, A., O'Connor, M. J., Ashworth, A., Carmichael, J., Kaye, S. B., Schellens, J. H., and de Bono, J. S. 2009. Inhibition of poly(ADP-ribose) polymerase in tumors from BRCA mutation carriers. N Engl J Med *361*, 123-134.

Fournier, M. V., Martin, K. J., Kenny, P. A., Xhaja, K., Bosch, I., Yaswen, P., and Bissell, M. J. 2006. Gene expression signature in organized and growth-arrested mammary acini predicts good outcome in breast cancer. Cancer Res *66*, 7095-7102.

Friedl, P., and Brocker, E. B. 2000. The biology of cell locomotion within three-dimensional extracellular matrix. Cell Mol Life Sci *57*, 41-64.

Friedl, P., and Wolf, K. 2003. Tumour-cell invasion and migration: diversity and escape mechanisms. Nat Rev Cancer *3*, 362-374.

Fulford, L. G., Easton, D. F., Reis-Filho, J. S., Sofronis, A., Gillett, C. E., Lakhani, S. R., and Hanby, A. 2006. Specific morphological features predictive for the basal phenotype in grade 3 invasive ductal carcinoma of breast. Histopathology *49*, 22-34.

Gardino, A. K., Smerdon, S. J., and Yaffe, M. B. 2006. Structural determinants of 14-3-3 binding specificities and regulation of subcellular localization of 14-3-3-ligand complexes: a comparison of the X-ray crystal structures of all human 14-3-3 isoforms. Semin Cancer Biol *16*, 173-182.

Geschickter, C. F., Lewis, D., and Hartman, C. G. 1934. Tumors of the breast related to the oestrin hormone. Am J Cancer *21*, 828-859.

Ghaffari, A., Li, Y., Karami, A., Ghaffari, M., Tredget, E. E., and Ghahary, A. 2006. Fibroblast extracellular matrix gene expression in response to keratinocyte-releasable stratifin. J Cell Biochem *98*, 383-393.

Ghahary, A., Karimi-Busheri, F., Marcoux, Y., Li, Y., Tredget, E. E., Taghi Kilani, R., Li, L., Zheng, J., Karami, A., Keller, B. O., and Weinfeld, M. 2004. Keratinocyte-releasable stratifin functions as a potent collagenase-stimulating factor in fibroblasts. J Invest Dermatol *122*, 1188-1197.

Ghahary, A., Marcoux, Y., Karimi-Busheri, F., Li, Y., Tredget, E. E., Kilani, R. T., Lam, E., and Weinfeld, M. 2005. Differentiated keratinocyte-releasable stratifin (14-3-3 sigma) stimulates MMP-1 expression in dermal fibroblasts. J Invest Dermatol *124*, 170-177.

Ghosh, M., Song, X., Mouneimne, G., Sidani, M., Lawrence, D. S., and Condeelis, J. S. 2004. Cofilin promotes actin polymerization and defines the direction of cell motility. Science *304*, 743-746.

Giri, D. D., Dundas, S. A., Nottingham, J. F., and Underwood, J. C. 1989. Oestrogen receptors in benign epithelial lesions and intraduct carcinomas of the breast: an immunohistological study. Histopathology *15*, 575-584.

Gohla, A., and Bokoch, G. M. 2002. 14-3-3 regulates actin dynamics by stabilizing phosphorylated cofilin. Curr Biol *12*, 1704-1710.

Goley, E. D., and Welch, M. D. 2006. The ARP2/3 complex: an actin nucleator comes of age. Nat Rev Mol Cell Biol *7*, 713-726.

Gouon-Evans, V., Rothenberg, M. E., and Pollard, J. W. 2000. Postnatal mammary gland development requires macrophages and eosinophils. Development *127*, 2269-2282.

Greene, H. S. 1938. Heterologous Transplantation of Human and Other Mammalian Tumors. Science *88*, 357-358.

Gudjonsson, T., Adriance, M. C., Sternlicht, M. D., Petersen, O. W., and Bissell, M. J. 2005. Myoepithelial cells: their origin and function in breast morphogenesis and neoplasia. J Mammary Gland Biol Neoplasia *10*, 261-272.

Gudjonsson, T., Ronnov-Jessen, L., Villadsen, R., Rank, F., Bissell, M. J., and Petersen, O. W. 2002. Normal and tumor-derived myoepithelial cells differ in their ability to interact with luminal breast epithelial cells for polarity and basement membrane deposition. J Cell Sci *115*, 39-50.

Gupta, G. P., Nguyen, D. X., Chiang, A. C., Bos, P. D., Kim, J. Y., Nadal, C., Gomis, R. R., Manova-Todorova, K., and Massague, J. 2007. Mediators of vascular remodelling co-opted for sequential steps in lung metastasis. Nature *446*, 765-770.

Guy, C. T., Cardiff, R. D., and Muller, W. J. 1992a. Induction of mammary tumors by expression of polyomavirus middle T oncogene: a transgenic mouse model for metastatic disease. Mol Cell Biol *12*, 954-961.

Guy, C. T., Webster, M. A., Schaller, M., Parsons, T. J., Cardiff, R. D., and Muller, W. J. 1992b. Expression of the neu protooncogene in the mammary epithelium of transgenic mice induces metastatic disease. Proc Natl Acad Sci U S A *89*, 10578-10582.

Haffty, B. G., Yang, Q., Reiss, M., Kearney, T., Higgins, S. A., Weidhaas, J., Harris, L., Hait, W., and Toppmeyer, D. 2006. Locoregional relapse and distant metastasis in conservatively managed triple negative early-stage breast cancer. J Clin Oncol *24*, 5652-5657.

Hall, A. 2009. The cytoskeleton and cancer. Cancer Metastasis Rev.

Han, B., Xie, H., Chen, Q., and Zhang, J. T. 2006. Sensitizing hormone-refractory prostate cancer cells to drug treatment by targeting 14-3-3σ. Mol Cancer Ther *5*, 903-912.

Hanahan, D., and Weinberg, R. A. 2000. The hallmarks of cancer. Cell *100*, 57-70.

Harris, E. S., Li, F., and Higgs, H. N. 2004. The mouse formin, FRLalpha, slows actin filament barbed end elongation, competes with capping protein, accelerates polymerization from monomers, and severs filaments. J Biol Chem *279*, 20076-20087.

Hay, T., Matthews, J. R., Pietzka, L., Lau, A., Cranston, A., Nygren, A. O., Douglas-Jones, A., Smith, G. C., Martin, N. M., O'Connor, M., and Clarke, A. R. 2009. Poly(ADP-ribose) polymerase-1 inhibitor treatment regresses autochthonous Brca2/p53-mutant mammary tumors in vivo and delays tumor relapse in combination with carboplatin. Cancer Res *69*, 3850-3855.

Hendrickson, E. A. 1993. The SCID mouse: relevance as an animal model system for studying human disease. Am J Pathol *143*, 1511-1522.

Hermeking, H., Lengauer, C., Polyak, K., He, T. C., Zhang, L., Thiagalingam, S., Kinzler, K. W., and Vogelstein, B. 1997. 14-3-3 sigma is a p53-regulated inhibitor of G2/M progression. Mol Cell *1*, 3-11.

Herron, B. J., Liddell, R. A., Parker, A., Grant, S., Kinne, J., Fisher, J. K., and Siracusa, L. D. 2005. A mutation in stratifin is responsible for the repeated epilation (Er) phenotype in mice. Nat Genet *37*, 1210-1212.

Higashida, C., Miyoshi, T., Fujita, A., Oceguera-Yanez, F., Monypenny, J., Andou, Y., Narumiya, S., and Watanabe, N. 2004. Actin polymerization-driven molecular movement of mDia1 in living cells. Science *303*, 2007-2010.

Higgs, H. N., and Pollard, T. D. 2001. Regulation of actin filament network formation through ARP2/3 complex: activation by a diverse array of proteins. Annu Rev Biochem *70*, 649-676.

Ho, H. Y., Rohatgi, R., Lebensohn, A. M., Le, M., Li, J., Gygi, S. P., and Kirschner, M. W. 2004. Toca-1 mediates Cdc42-dependent actin nucleation by activating the N-WASP-WIP complex. Cell *118*, 203-216.

Hodgson, J. G., Malek, T., Bornstein, S., Hariono, S., Ginzinger, D. G., Muller, W. J., and Gray, J. W. 2005. Copy number aberrations in mouse breast tumors reveal loci and genes important in tumorigenic receptor tyrosine kinase signaling. Cancer Res *65*, 9695-9704.

Hotulainen, P., Paunola, E., Vartiainen, M. K., and Lappalainen, P. 2005. Actin-depolymerizing factor and cofilin-1 play overlapping roles in promoting rapid F-actin depolymerization in mammalian nonmuscle cells. Mol Biol Cell *16*, 649-664.

Hu, M., Yao, J., Carroll, D. K., Weremowicz, S., Chen, H., Carrasco, D., Richardson, A., Violette, S., Nikolskaya, T., Nikolsky, Y., Bauerlein, E. L., Hahn, W. C., Gelman, R. S., Allred, C., Bissell, M. J., Schnitt, S., and Polyak, K. 2008. Regulation of in situ to invasive breast carcinoma transition. Cancer Cell *13*, 394-406.

Hu, Z., Fan, C., Oh, D. S., Marron, J. S., He, X., Qaqish, B. F., Livasy, C., Carey, L. A., Reynolds, E., Dressler, L., Nobel, A., Parker, J., Ewend, M. G., Sawyer, L. R., Wu, J., Liu, Y., Nanda, R., Tretiakova, M., Ruiz Orrico, A., Dreher, D., Palazzo, J. P., Perreard, L., Nelson, E., Mone, M., Hansen, H., Mullins, M., Quackenbush, J. F., Ellis, M. J., Olopade, O. I., Bernard, P. S., and Perou, C. M. 2006. The molecular portraits of breast tumors are conserved across microarray platforms. BMC Genomics *7*, 96.

Hufner, K., Higgs, H. N., Pollard, T. D., Jacobi, C., Aepfelbacher, M., and Linder, S. 2001. The verprolin-like central (vc) region of Wiskott-Aldrich syndrome protein induces Arp2/3 complex-dependent actin nucleation. J Biol Chem *276*, 35761-35767.

Hungermann, D., Buerger, H., Oehlschlegel, C., Herbst, H., and Boecker, W. 2005. Adenomyoepithelial tumours and myoepithelial carcinomas of the breast--a spectrum of monophasic and biphasic tumours dominated by immature myoepithelial cells. BMC Cancer *5*, 92.

Hustinx, S. R., Fukushima, N., Zahurak, M. L., Riall, T. S., Maitra, A., Brosens, L., Cameron, J. L., Yeo, C. J., Offerhaus, G. J., Hruban, R. H., and Goggins, M. 2005. Expression and prognostic significance of 14-3-3σ and ERM family protein expression in periampullary neoplasms. Cancer Biol Ther *4*, 596-601.

Ichetovkin, I., Grant, W., and Condeelis, J. 2002. Cofilin produces newly polymerized actin filaments that are preferred for dendritic nucleation by the Arp2/3 complex. Curr Biol *12*, 79-84.

Ichetovkin, I., Han, J., Pang, K. M., Knecht, D. A., and Condeelis, J. S. 2000. Actin filaments are severed by both native and recombinant dictyostelium cofilin but to different extents. Cell Motil Cytoskeleton *45*, 293-306.

Ide, M., Saito, K., Tsutsumi, S., Tsuboi, K., Yamaguchi, S., Asao, T., Kuwano, H., and Nakajima, T. 2007. Over-expression of 14-3-3σ in budding colorectal cancer cells modulates cell migration in the presence of tenascin-C. Oncol Rep *18*, 1451-1456.

Ingman, W. V., Wyckoff, J., Gouon-Evans, V., Condeelis, J., and Pollard, J. W. 2006. Macrophages promote collagen fibrillogenesis around terminal end buds of the developing mammary gland. Dev Dyn *235*, 3222-3229.

Ingram, V. M. 1969. A side view of moving fibroblasts. Nature *222*, 641-644.

Insall, R. H., and Machesky, L. M. 2009. Actin dynamics at the leading edge: from simple machinery to complex networks. Dev Cell *17*, 310-322.

Ishiguro, K., Cao, Z., Ilasca, M. L., Ando, T., and Xavier, R. 2004. Wave2 activates serum response element via its VCA region and functions downstream of Rac. Exp Cell Res *301*, 331-337.

Ito, K., Suzuki, T., Akahira, J., Sakuma, M., Saitou, S., Okamoto, S., Niikura, H., Okamura, K., Yaegashi, N., Sasano, H., and Inoue, S. 2005. 14-3-3σ in endometrial cancer--a possible prognostic marker in early-stage cancer. Clin Cancer Res *11*, 7384-7391.

Itoh, M., Nelson, C. M., Myers, C. A., and Bissell, M. J. 2007. Rap1 integrates tissue polarity, lumen formation, and tumorigenic potential in human breast epithelial cells. Cancer Res *67*, 4759-4766.

Jackson, S. M. 1966. Carcinoma of the breast--the significance of supraclavicular lymph node metastases. Clin Radiol *17*, 107-114.

Jacques, T. S., Relvas, J. B., Nishimura, S., Pytela, R., Edwards, G. M., Streuli, C. H., and ffrench-Constant, C. 1998. Neural precursor cell chain migration and division are regulated through different beta1 integrins. Development *125*, 3167-3177.

Jaffe, A. B., and Hall, A. 2005. Rho GTPases: biochemistry and biology. Annu Rev Cell Dev Biol *21*, 247-269.

Jason-Moller, L., Murphy, M., and Bruno, J. 2006. Overview of Biacore systems and their applications. Curr Protoc Protein Sci *Chapter 19*, Unit 19 13.

Jedeszko, C., Victor, B. C., Podgorski, I., and Sloane, B. F. 2009. Fibroblast hepatocyte growth factor promotes invasion of human mammary ductal carcinoma in situ. Cancer Res *69*, 9148-9155.

Jenssen, T. K., Kuo, W. P., Stokke, T., and Hovig, E. 2002. Associations between gene expressions in breast cancer and patient survival. Hum Genet *111*, 411-420.

Jin, J., Smith, F. D., Stark, C., Wells, C. D., Fawcett, J. P., Kulkarni, S., Metalnikov, P., O'Donnell, P., Taylor, P., Taylor, L., Zougman, A., Woodgett, J. R., Langeberg, L. K., Scott, J. D., and Pawson, T. 2004. Proteomic, functional, and domain-based analysis of in vivo 14-3-3 binding proteins involved in cytoskeletal regulation and cellular organization. Curr Biol *14*, 1436-1450.

Kakinuma, N., Roy, B. C., Zhu, Y., Wang, Y., and Kiyama, R. 2008. Kank regulates RhoA-dependent formation of actin stress fibers and cell migration via 14-3-3 in PI3K-Akt signaling. J Cell Biol *181*, 537-549.

Kalluri, R., and Weinberg, R. A. 2009. The basics of epithelial-mesenchymal transition. J Clin Invest *119*, 1420-1428.

Kenny, P. A., and Bissell, M. J. 2003. Tumor reversion: correction of malignant behavior by microenvironmental cues. Int J Cancer *107*, 688-695.

Kenny, P. A., and Bissell, M. J. 2007. Targeting TACE-dependent EGFR ligand shedding in breast cancer. J Clin Invest *117*, 337-345.

Kenny, P. A., Lee, G. Y., Myers, C. A., Neve, R. M., Semeiks, J. R., Spellman, P. T., Lorenz, K., Lee, E. H., Barcellos-Hoff, M. H., Petersen, O. W., Gray, J. W., and Bissell, M. J. 2007. The morphologies of breast cancer cell lines in three-dimensional assays correlate with their profiles of gene expression. Mol Oncol *1*, 84-96.

Kligys, K., Claiborne, J. N., DeBiase, P. J., Hopkinson, S. B., Wu, Y., Mizuno, K., and Jones, J. C. 2007. The slingshot family of phosphatases mediates

Rac1 regulation of cofilin phosphorylation, laminin-332 organization, and motility behavior of keratinocytes. J Biol Chem *282*, 32520-32528.

Koffer, A., and Daridan, M. 1985. Actin-regulating activities in cultured BHK cells. J Cell Sci *75*, 239-257.

Kouros-Mehr, H., Bechis, S. K., Slorach, E. M., Littlepage, L. E., Egeblad, M., Ewald, A. J., Pai, S. Y., Ho, I. C., and Werb, Z. 2008. GATA-3 links tumor differentiation and dissemination in a luminal breast cancer model. Cancer Cell *13*, 141-152.

Kouros-Mehr, H., Slorach, E. M., Sternlicht, M. D., and Werb, Z. 2006. GATA-3 maintains the differentiation of the luminal cell fate in the mammary gland. Cell *127*, 1041-1055.

Kouyama, T., and Mihashi, K. 1981. Fluorimetry study of N-(1-pyrenyl)iodoacetamide-labelled F-actin. Local structural change of actin protomer both on polymerization and on binding of heavy meromyosin. Eur J Biochem *114*, 33-38.

Kovar, D. R., Harris, E. S., Mahaffy, R., Higgs, H. N., and Pollard, T. D. 2006. Control of the assembly of ATP- and ADP-actin by formins and profilin. Cell *124*, 423-435.

Kovar, D. R., Kuhn, J. R., Tichy, A. L., and Pollard, T. D. 2003. The fission yeast cytokinesis formin Cdc12p is a barbed end actin filament capping protein gated by profilin. J Cell Biol *161*, 875-887.

Kovar, D. R., and Pollard, T. D. 2004. Insertional assembly of actin filament barbed ends in association with formins produces piconewton forces. Proc Natl Acad Sci U S A *101*, 14725-14730.

Kovar, D. R., Wu, J. Q., and Pollard, T. D. 2005. Profilin-mediated competition between capping protein and formin Cdc12p during cytokinesis in fission yeast. Mol Biol Cell *16*, 2313-2324.

Kumar, S., and Weaver, V. M. 2009. Mechanics, malignancy, and metastasis: The force journey of a tumor cell. Cancer Metastasis Rev.

LaBarge, M. A., Nelson, C. M., Villadsen, R., Fridriksdottir, A., Ruth, J. R., Stampfer, M. R., Petersen, O. W., and Bissell, M. J. 2009. Human mammary progenitor cell fate decisions are products of interactions with combinatorial microenvironments. Integr Biol (Camb) *1*, 70-79.

Laimer, K., Blassnig, N., Spizzo, G., Kloss, F., Rasse, M., Obrist, P., Schafer, G., Perathoner, A., Margreiter, R., and Amberger, A. 2009. Prognostic significance of 14-3-3σ expression in oral squamous cell carcinoma (OSCC). Oral Oncol *45*, 127-134.

Lakhani, S., and Bissell, M. 2005. Introduction: the role of myoepithelial cells in integration of form and function in the mammary gland. J Mammary Gland Biol Neoplasia *10*, 197-198.

Lakhani, S. R., and O'Hare, M. J. 2001. The mammary myoepithelial cell--Cinderella or ugly sister? Breast Cancer Res *3*, 1-4.

Landskroner-Eiger, S., Park, J., Israel, D., Pollard, J. W., and Scherer, P. E. 2010. Morphogenesis of the developing mammary gland: Stage-dependent impact of adipocytes. Dev Biol.

Lauffenburger, D. A., and Horwitz, A. F. 1996. Cell migration: a physically integrated molecular process. Cell *84*, 359-369.

Lee, E. Y., Lee, W. H., Kaetzel, C. S., Parry, G., and Bissell, M. J. 1985. Interaction of mouse mammary epithelial cells with collagen substrata: regulation of casein gene expression and secretion. Proc Natl Acad Sci U S A *82*, 1419-1423.

Lee, E. Y., Parry, G., and Bissell, M. J. 1984. Modulation of secreted proteins of mouse mammary epithelial cells by the collagenous substrata. J Cell Biol *98*, 146-155.

Lee, G. Y., Kenny, P. A., Lee, E. H., and Bissell, M. J. 2007. Three-dimensional culture models of normal and malignant breast epithelial cells. Nat Methods *4*, 359-365.

Leffers, H., Madsen, P., Rasmussen, H. H., Honore, B., Andersen, A. H., Walbum, E., Vandekerckhove, J., and Celis, J. E. 1993. Molecular cloning and expression of the transformation sensitive epithelial marker stratifin. A member of a protein family that has been involved in the protein kinase C signalling pathway. J Mol Biol *231*, 982-998.

Leu, Y. W., Yan, P. S., Fan, M., Jin, V. X., Liu, J. C., Curran, E. M., Welshons, W. V., Wei, S. H., Davuluri, R. V., Plass, C., Nephew, K. P., and Huang, T. H. 2004. Loss of estrogen receptor signaling triggers epigenetic silencing of downstream targets in breast cancer. Cancer Res *64*, 8184-8192.

Li, F., and Higgs, H. N. 2003. The mouse Formin mDia1 is a potent actin nucleation factor regulated by autoinhibition. Curr Biol *13*, 1335-1340.

Li, M. L., Aggeler, J., Farson, D. A., Hatier, C., Hassell, J., and Bissell, M. J. 1987. Influence of a reconstituted basement membrane and its components on casein gene expression and secretion in mouse mammary epithelial cells. Proc Natl Acad Sci U S A *84*, 136-140.

Li, Q., Lu, Q., Estepa, G., and Verma, I. M. 2005. Identification of 14-3-3s mutation causing cutaneous abnormality in repeated-epilation mutant mouse. Proc Natl Acad Sci U S A *102*, 15977-15982.

Li, Z., Liu, J. Y., and Zhang, J. T. 2009. 14-3-3σ, the double-edged sword of human cancers. Am J Transl Res *1*, 326-340.

Li, Z., Zhao, J., Du, Y., Park, H. R., Sun, S. Y., Bernal-Mizrachi, L., Aitken, A., Khuri, F. R., and Fu, H. 2008. Down-regulation of 14-3-3zeta suppresses anchorage-independent growth of lung cancer cells through anoikis activation. Proc Natl Acad Sci U S A *105*, 162-167.

Lim, E., Vaillant, F., Wu, D., Forrest, N. C., Pal, B., Hart, A. H., Asselin-Labat, M. L., Gyorki, D. E., Ward, T., Partanen, A., Feleppa, F., Huschtscha, L. I., Thorne, H. J., Fox, S. B., Yan, M., French, J. D., Brown, M. A., Smyth, G. K., Visvader, J. E., and Lindeman, G. J. 2009. Aberrant luminal progenitors as the candidate target population for basal tumor development in BRCA1 mutation carriers. Nat Med *15*, 907-913.

Ling, C., Zuo, D., Xue, B., Muthuswamy, S., and Muller, W. J. 2010. A novel role for 14-3-3σ in regulating epithelial cell polarity. Genes Dev *24*, 947-956.

Liu, D., Bienkowska, J., Petosa, C., Collier, R. J., Fu, H., and Liddington, R. 1995. Crystal structure of the zeta isoform of the 14-3-3 protein. Nature *376*, 191-194.

Liu, H., Radisky, D. C., Nelson, C. M., Zhang, H., Fata, J. E., Roth, R. A., and Bissell, M. J. 2006a. Mechanism of Akt1 inhibition of breast cancer cell invasion reveals a protumorigenic role for TSC2. Proc Natl Acad Sci U S A *103*, 4134-4139.

Liu, H., Radisky, D. C., Wang, F., and Bissell, M. J. 2004. Polarity and proliferation are controlled by distinct signaling pathways downstream of PI3-kinase in breast epithelial tumor cells. J Cell Biol *164*, 603-612.

Liu, R., Wang, X., Chen, G. Y., Dalerba, P., Gurney, A., Hoey, T., Sherlock, G., Lewicki, J., Shedden, K., and Clarke, M. F. 2007a. The prognostic role of a gene signature from tumorigenic breast-cancer cells. N Engl J Med *356*, 217-226.

Liu, X., Holstege, H., van der Gulden, H., Treur-Mulder, M., Zevenhoven, J., Velds, A., Kerkhoven, R. M., van Vliet, M. H., Wessels, L. F., Peterse, J. L., Berns, A., and Jonkers, J. 2007b. Somatic loss of BRCA1 and p53 in mice induces mammary tumors with features of human BRCA1-mutated basal-like breast cancer. Proc Natl Acad Sci U S A *104*, 12111-12116.

Liu, Y., Liu, H., Han, B., and Zhang, J. T. 2006b. Identification of 14-3-3σ as a contributor to drug resistance in human breast cancer cells using functional proteomic analysis. Cancer Res *66*, 3248-3255.

Lo, S. S., Mumby, P. B., Norton, J., Rychlik, K., Smerage, J., Kash, J., Chew, H. K., Gaynor, E. R., Hayes, D. F., Epstein, A., and Albain, K. S. 2010. Prospective multicenter study of the impact of the 21-gene recurrence score assay on medical oncologist and patient adjuvant breast cancer treatment selection. J Clin Oncol *28*, 1671-1676.

Lottersberger, F., Panza, A., Lucchini, G., Piatti, S., and Longhese, M. P. 2006. The Saccharomyces cerevisiae 14-3-3 proteins are required for the G1/S transition, actin cytoskeleton organization and cell wall integrity. Genetics *173*, 661-675.

Lu, J., Guo, H., Treekitkarnmongkol, W., Li, P., Zhang, J., Shi, B., Ling, C., Zhou, X., Chen, T., Chiao, P. J., Feng, X., Seewaldt, V. L., Muller, W. J., Sahin, A., Hung, M. C., and Yu, D. 2009a. 14-3-3zeta Cooperates with ErbB2 to promote ductal carcinoma in situ progression to invasive breast cancer by inducing epithelial-mesenchymal transition. Cancer Cell *16*, 195-207.

Lu, J., Steeg, P. S., Price, J. E., Krishnamurthy, S., Mani, S. A., Reuben, J., Cristofanilli, M., Dontu, G., Bidaut, L., Valero, V., Hortobagyi, G. N., and Yu, D. 2009b. Breast cancer metastasis: challenges and opportunities. Cancer Res *69*, 4951-4953.

Macdonald, I. 1966. The natural history of mammary carcinoma. Am J Surg *111*, 435-442.

Machacek, M., Hodgson, L., Welch, C., Elliott, H., Pertz, O., Nalbant, P., Abell, A., Johnson, G. L., Hahn, K. M., and Danuser, G. 2009. Coordination of Rho GTPase activities during cell protrusion. Nature *461*, 99-103.

Manabe, Y., Toda, S., Miyazaki, K., and Sugihara, H. 2003. Mature adipocytes, but not preadipocytes, promote the growth of breast carcinoma cells in collagen gel matrix culture through cancer-stromal cell interactions. J Pathol *201*, 221-228.

Marchand, J. B., Kaiser, D. A., Pollard, T. D., and Higgs, H. N. 2001. Interaction of WASP/Scar proteins with actin and vertebrate Arp2/3 complex. Nat Cell Biol *3*, 76-82.

Matta, A., Bahadur, S., Duggal, R., Gupta, S. D., and Ralhan, R. 2007. Over-expression of 14-3-3zeta is an early event in oral cancer. BMC Cancer *7*, 169.

Matta, A., DeSouza, L. V., Shukla, N. K., Gupta, S. D., Ralhan, R., and Siu, K. W. 2008. Prognostic significance of head-and-neck cancer biomarkers previously discovered and identified using iTRAQ-labeling and multidimensional liquid chromatography-tandem mass spectrometry. J Proteome Res *7*, 2078-2087.

Maughan, K. L., Lutterbie, M. A., and Ham, P. S. 2010. Treatment of breast cancer. Am Fam Physician *81*, 1339-1346.

Maxwell, S. A., Li, Z., Jaya, D., Ballard, S., Ferrell, J., and Fu, H. 2009. 14-3-3zeta mediates resistance of diffuse large B cell lymphoma to an anthracycline-based chemotherapeutic regimen. J Biol Chem *284*, 22379-22389.

McCarthy, A., Savage, K., Gabriel, A., Naceur, C., Reis-Filho, J. S., and Ashworth, A. 2007. A mouse model of basal-like breast carcinoma with metaplastic elements. J Pathol *211*, 389-398.

Mehra, R., Varambally, S., Ding, L., Shen, R., Sabel, M. S., Ghosh, D., Chinnaiyan, A. M., and Kleer, C. G. 2005. Identification of GATA3 as a breast cancer prognostic marker by global gene expression meta-analysis. Cancer Res *65*, 11259-11264.

Mhawech, P. 2005. 14-3-3 proteins--an update. Cell Res *15*, 228-236.

Mhawech, P., Greloz, V., Assaly, M., and Herrmann, F. 2005. Immunohistochemical expression of 14-3-3 sigma protein in human urological and gynecological tumors using a multi-tumor microarray analysis. Pathol Int *55*, 77-82.

Micalizzi, D. S., Farabaugh, S. M., and Ford, H. L. 2010. Epithelial-mesenchymal transition in cancer: parallels between normal development and tumor progression. J Mammary Gland Biol Neoplasia *15*, 117-134.

Miki, H., Suetsugu, S., and Takenawa, T. 1998. WAVE, a novel WASP-family protein involved in actin reorganization induced by Rac. EMBO J *17*, 6932-6941.

Miller, F. R. 2000. Xenograft models of premalignant breast disease. J Mammary Gland Biol Neoplasia *5*, 379-391.

Miller, F. R., Santner, S. J., Tait, L., and Dawson, P. J. 2000. MCF10DCIS.com xenograft model of human comedo ductal carcinoma in situ. J Natl Cancer Inst *92*, 1185-1186.

Miller, F. R., Soule, H. D., Tait, L., Pauley, R. J., Wolman, S. R., Dawson, P. J., and Heppner, G. H. 1993. Xenograft model of progressive human proliferative breast disease. J Natl Cancer Inst *85*, 1725-1732.

Miron, A., Varadi, M., Carrasco, D., Li, H., Luongo, L., Kim, H. J., Park, S. Y., Cho, E. Y., Lewis, G., Kehoe, S., Iglehart, J. D., Dillon, D., Allred, D. C., Macconaill, L., Gelman, R., and Polyak, K. 2010. PIK3CA mutations in in situ and invasive breast carcinomas. Cancer Res *70*, 5674-5678.

Mohs, F. E. 1940. The effect of the sex hormones on the growth of transplanted mammary adenofibroma in rats. Am J Cancer *38*, 212-216.

Moody, S. E., Perez, D., Pan, T. C., Sarkisian, C. J., Portocarrero, C. P., Sterner, C. J., Notorfrancesco, K. L., Cardiff, R. D., and Chodosh, L. A. 2005. The transcriptional repressor Snail promotes mammary tumor recurrence. Cancer Cell *8*, 197-209.

Moreira, J. M., Ohlsson, G., Rank, F. E., and Celis, J. E. 2005. Down-regulation of the tumor suppressor protein 14-3-3σ is a sporadic event in cancer of the breast. Mol Cell Proteomics *4*, 555-569.

Moss, N. H. 1965. Cancer of the Male Breast. Prog Clin Cancer *10*, 515-526.

Mouneimne, G., DesMarais, V., Sidani, M., Scemes, E., Wang, W., Song, X., Eddy, R., and Condeelis, J. 2006. Spatial and temporal control of cofilin activity is required for directional sensing during chemotaxis. Curr Biol *16*, 2193-2205.

Muller, W. J., Sinn, E., Pattengale, P. K., Wallace, R., and Leder, P. 1988. Single-step induction of mammary adenocarcinoma in transgenic mice bearing the activated c-neu oncogene. Cell *54*, 105-115.

Mullins, R. D., Heuser, J. A., and Pollard, T. D. 1998. The interaction of Arp2/3 complex with actin: nucleation, high affinity pointed end capping, and formation of branching networks of filaments. Proc Natl Acad Sci U S A *95*, 6181-6186.

Muthuswamy, S. K., Li, D., Lelievre, S., Bissell, M. J., and Brugge, J. S. 2001. ErbB2, but not ErbB1, reinitiates proliferation and induces luminal repopulation in epithelial acini. Nat Cell Biol *3*, 785-792.

Nagata-Ohashi, K., Ohta, Y., Goto, K., Chiba, S., Mori, R., Nishita, M., Ohashi, K., Kousaka, K., Iwamatsu, A., Niwa, R., Uemura, T., and Mizuno, K. 2004. A pathway of neuregulin-induced activation of cofilin-phosphatase Slingshot and cofilin in lamellipodia. J Cell Biol *165*, 465-471.

Nakagawa, H., Miki, H., Ito, M., Ohashi, K., Takenawa, T., and Miyamoto, S. 2001. N-WASP, WAVE and Mena play different roles in the organization of actin cytoskeleton in lamellipodia. J Cell Sci *114*, 1555-1565.

Nakajima, T., Shimooka, H., Weixa, P., Segawa, A., Motegi, A., Jian, Z., Masuda, N., Ide, M., Sano, T., Oyama, T., Tsukagoshi, H., Hamanaka, K., and Maeda, M. 2003. Immunohistochemical demonstration of 14-3-3 sigma protein in normal human tissues and lung cancers, and the preponderance of its strong expression in epithelial cells of squamous cell lineage. Pathol Int *53*, 353-360.

Nakayama, H., Sano, T., Motegi, A., Oyama, T., and Nakajima, T. 2005. Increasing 14-3-3 sigma expression with declining estrogen receptor alpha and estrogen-responsive finger protein expression defines malignant progression of endometrial carcinoma. Pathol Int *55*, 707-715.

Nam, D. H., Jeon, H. M., Kim, S., Kim, M. H., Lee, Y. J., Lee, M. S., Kim, H., Joo, K. M., Lee, D. S., Price, J. E., Bang, S. I., and Park, W. Y. 2008. Activation of notch signaling in a xenograft model of brain metastasis. Clin Cancer Res *14*, 4059-4066.

Narumiya, S., Tanji, M., and Ishizaki, T. 2009. Rho signaling, ROCK and mDia1, in transformation, metastasis and invasion. Cancer Metastasis Rev.

Nazario, A. C., De Lima, G. R., Simoes, M. J., and Novo, N. F. 1995. Cell kinetics of the human mammary lobule during the proliferative and secretory phase of the menstrual cycle. Bull Assoc Anat (Nancy) *79*, 23-27.

Neal, C. L., Yao, J., Yang, W., Zhou, X., Nguyen, N. T., Lu, J., Danes, C. G., Guo, H., Lan, K. H., Ensor, J., Hittelman, W., Hung, M. C., and Yu, D. 2009. 14-3-3zeta overexpression defines high risk for breast cancer recurrence and promotes cancer cell survival. Cancer Res *69*, 3425-3432.

Nelson, C. M., and Bissell, M. J. 2005. Modeling dynamic reciprocity: engineering three-dimensional culture models of breast architecture, function, and neoplastic transformation. Semin Cancer Biol *15*, 342-352.

Nelson, C. M., Vanduijn, M. M., Inman, J. L., Fletcher, D. A., and Bissell, M. J. 2006. Tissue geometry determines sites of mammary branching morphogenesis in organotypic cultures. Science *314*, 298-300.

Neupane, D., and Korc, M. 2008. 14-3-3σ Modulates pancreatic cancer cell survival and invasiveness. Clin Cancer Res *14*, 7614-7623.

Neve, R. M., Chin, K., Fridlyand, J., Yeh, J., Baehner, F. L., Fevr, T., Clark, L., Bayani, N., Coppe, J. P., Tong, F., Speed, T., Spellman, P. T., DeVries, S., Lapuk, A., Wang, N. J., Kuo, W. L., Stilwell, J. L., Pinkel, D., Albertson, D. G., Waldman, F. M., McCormick, F., Dickson, R. B., Johnson, M. D., Lippman, M., Ethier, S., Gazdar, A., and Gray, J. W. 2006. A collection of breast cancer cell lines for the study of functionally distinct cancer subtypes. Cancer Cell *10*, 515-527.

Niclou, S. P., Danzeisen, C., Eikesdal, H. P., Wiig, H., Brons, N. H., Poli, A. M., Svendsen, A., Torsvik, A., Enger, P. O., Terzis, J. A., and Bjerkvig, R. 2008. A novel eGFP-expressing immunodeficient mouse model to study tumor-host interactions. FASEB J *22*, 3120-3128.

Nielsen, T. O., Hsu, F. D., Jensen, K., Cheang, M., Karaca, G., Hu, Z., Hernandez-Boussard, T., Livasy, C., Cowan, D., Dressler, L., Akslen, L. A., Ragaz, J., Gown, A. M., Gilks, C. B., van de Rijn, M., and Perou, C. M. 2004. Immunohistochemical and clinical characterization of the basal-like subtype of invasive breast carcinoma. Clin Cancer Res *10*, 5367-5374.

Nieto, M. A., Sargent, M. G., Wilkinson, D. G., and Cooke, J. 1994. Control of cell behavior during vertebrate development by Slug, a zinc finger gene. Science *264*, 835-839.

Niwa, R., Nagata-Ohashi, K., Takeichi, M., Mizuno, K., and Uemura, T. 2002. Control of actin reorganization by Slingshot, a family of phosphatases that dephosphorylate ADF/cofilin. Cell *108*, 233-246.

Nobes, C. D., and Hall, A. 1995. Rho, rac, and cdc42 GTPases regulate the assembly of multimolecular focal complexes associated with actin stress fibers, lamellipodia, and filopodia. Cell *81*, 53-62.

Nuyten, D. S., and van de Vijver, M. J. 2006. Gene expression signatures to predict the development of metastasis in breast cancer. Breast Dis *26*, 149-156.

O'Hare, M. J., Ormerod, M. G., Monaghan, P., Lane, E. B., and Gusterson, B. A. 1991. Characterization in vitro of luminal and myoepithelial cells isolated from the human mammary gland by cell sorting. Differentiation *46*, 209-221.

Okada, T., Masuda, N., Fukai, Y., Shimura, T., Nishida, Y., Hosouchi, Y., Kashiwabara, K., Nakajima, T., and Kuwano, H. 2006. Immunohistochemical expression of 14-3-3 sigma protein in intraductal papillary-mucinous tumor and invasive ductal carcinoma of the pancreas. Anticancer Res *26*, 3105-3110.

Ottmann, C., Weyand, M., Sassa, T., Inoue, T., Kato, N., Wittinghofer, A., and Oecking, C. 2009. A structural rationale for selective stabilization of anti-tumor interactions of 14-3-3 proteins by cotylenin A. J Mol Biol *386*, 913-919.

Ottmann, C., Yasmin, L., Weyand, M., Veesenmeyer, J. L., Diaz, M. H., Palmer, R. H., Francis, M. S., Hauser, A. R., Wittinghofer, A., and Hallberg, B. 2007. Phosphorylation-independent interaction between 14-3-3 and exoenzyme S: from structure to pathogenesis. EMBO J *26*, 902-913.

Oyer, J. A., Chu, A., Brar, S., and Turker, M. S. 2009. Aberrant epigenetic silencing is triggered by a transient reduction in gene expression. PLoS One *4*, e4832.

Page, M. J., Amess, B., Townsend, R. R., Parekh, R., Herath, A., Brusten, L., Zvelebil, M. J., Stein, R. C., Waterfield, M. D., Davies, S. C., and O'Hare, M. J. 1999. Proteomic definition of normal human luminal and myoepithelial breast cells purified from reduction mammoplasties. Proc Natl Acad Sci U S A *96*, 12589-12594.

Paik, S., Shak, S., Tang, G., Kim, C., Baker, J., Cronin, M., Baehner, F. L., Walker, M. G., Watson, D., Park, T., Hiller, W., Fisher, E. R., Wickerham, D. L., Bryant, J., and Wolmark, N. 2004. A multigene assay to predict recurrence of tamoxifen-treated, node-negative breast cancer. N Engl J Med *351*, 2817-2826.

Paik, S., Tang, G., Shak, S., Kim, C., Baker, J., Kim, W., Cronin, M., Baehner, F. L., Watson, D., Bryant, J., Costantino, J. P., Geyer, C. E., Jr., Wickerham, D. L., and Wolmark, N. 2006. Gene expression and benefit of chemotherapy in women with node-negative, estrogen receptor-positive breast cancer. J Clin Oncol *24*, 3726-3734.

Pang, H., Flinn, R., Patsialou, A., Wyckoff, J., Roussos, E. T., Wu, H., Pozzuto, M., Goswami, S., Condeelis, J. S., Bresnick, A. R., Segall, J. E., and Backer, J. M. 2009. Differential enhancement of breast cancer cell motility and metastasis by helical and kinase domain mutations of class IA phosphoinositide 3-kinase. Cancer Res *69*, 8868-8876.

Paradiso, A., Tommasi, S., Mangia, A., Lorusso, V., Simone, G., and De Lena, M. 1990. Tumor-proliferative activity, progesterone receptor status, estrogen receptor level, and clinical outcome of estrogen receptor-positive advanced breast cancer. Cancer Res *50*, 2958-2962.

Pardee, J. D., and Spudich, J. A. 1982. Purification of muscle actin. Methods Enzymol *85 Pt B*, 164-181.

Park, C. C., Zhang, H., Pallavicini, M., Gray, J. W., Baehner, F., Park, C. J., and Bissell, M. J. 2006. Beta1 integrin inhibitory antibody induces apoptosis of breast cancer cells, inhibits growth, and distinguishes malignant from normal phenotype in three dimensional cultures and in vivo. Cancer Res *66*, 1526-1535.

Park, C. C., Zhang, H. J., Yao, E. S., Park, C. J., and Bissell, M. J. 2008. Beta1 integrin inhibition dramatically enhances radiotherapy efficacy in human breast cancer xenografts. Cancer Res *68*, 4398-4405.

Park, S. Y., Gonen, M., Kim, H. J., Michor, F., and Polyak, K. 2010. Cellular and genetic diversity in the progression of in situ human breast carcinomas to an invasive phenotype. J Clin Invest *120*, 636-644.

Parker, J. S., Mullins, M., Cheang, M. C., Leung, S., Voduc, D., Vickery, T., Davies, S., Fauron, C., He, X., Hu, Z., Quackenbush, J. F., Stijleman, I. J., Palazzo, J., Marron, J. S., Nobel, A. B., Mardis, E., Nielsen, T. O., Ellis, M. J., Perou, C. M., and Bernard, P. S. 2009. Supervised risk predictor of breast cancer based on intrinsic subtypes. J Clin Oncol *27*, 1160-1167.

Paul, A. S., and Pollard, T. D. 2009. Review of the mechanism of processive actin filament elongation by formins. Cell Motil Cytoskeleton *66*, 606-617.

Pegram, M. D., Lipton, A., Hayes, D. F., Weber, B. L., Baselga, J. M., Tripathy, D., Baly, D., Baughman, S. A., Twaddell, T., Glaspy, J. A., and Slamon, D. J. 1998. Phase II study of receptor-enhanced chemosensitivity using recombinant humanized anti-p185HER2/neu monoclonal antibody plus cisplatin in patients with HER2/neu-overexpressing metastatic breast cancer refractory to chemotherapy treatment. J Clin Oncol *16*, 2659-2671.

Pellegrin, S., and Mellor, H. 2007. Actin stress fibres. J Cell Sci *120*, 3491-3499.

Perathoner, A., Pirkebner, D., Brandacher, G., Spizzo, G., Stadlmann, S., Obrist, P., Margreiter, R., and Amberger, A. 2005. 14-3-3σ expression is an independent prognostic parameter for poor survival in colorectal carcinoma patients. Clin Cancer Res *11*, 3274-3279.

Perou, C. M., Sorlie, T., Eisen, M. B., van de Rijn, M., Jeffrey, S. S., Rees, C. A., Pollack, J. R., Ross, D. T., Johnsen, H., Akslen, L. A., Fluge, O., Pergamenschikov, A., Williams, C., Zhu, S. X., Lonning, P. E., Borresen-Dale, A. L., Brown, P. O., and Botstein, D. 2000. Molecular portraits of human breast tumours. Nature *406*, 747-752.

Petersen, O. W., Hoyer, P. E., and van Deurs, B. 1987. Frequency and distribution of estrogen receptor-positive cells in normal, nonlactating human breast tissue. Cancer Res *47*, 5748-5751.

Petersen, O. W., Ronnov-Jessen, L., Howlett, A. R., and Bissell, M. J. 1992. Interaction with basement membrane serves to rapidly distinguish growth and differentiation pattern of normal and malignant human breast epithelial cells. Proc Natl Acad Sci U S A *89*, 9064-9068.

Petosa, C., Masters, S. C., Bankston, L. A., Pohl, J., Wang, B., Fu, H., and Liddington, R. C. 1998. 14-3-3zeta binds a phosphorylated Raf peptide and an unphosphorylated peptide via its conserved amphipathic groove. J Biol Chem *273*, 16305-16310.

Pollard, T. D., and Beltzner, C. C. 2002. Structure and function of the Arp2/3 complex. Curr Opin Struct Biol *12*, 768-774.

Pollard, T. D., and Cooper, J. A. 1984. Quantitative analysis of the effect of Acanthamoeba profilin on actin filament nucleation and elongation. Biochemistry *23*, 6631-6641.

Polyak, K., and Kalluri, R. 2010. The Role of the Microenvironment in Mammary Gland Development and Cancer. Cold Spring Harb Perspect Biol.

Ponti, A., Machacek, M., Gupton, S. L., Waterman-Storer, C. M., and Danuser, G. 2004. Two distinct actin networks drive the protrusion of migrating cells. Science *305*, 1782-1786.

Porter, G. W., Khuri, F. R., and Fu, H. 2006. Dynamic 14-3-3/client protein interactions integrate survival and apoptotic pathways. Semin Cancer Biol *16*, 193-202.

Posern, G., Sotiropoulos, A., and Treisman, R. 2002. Mutant actins demonstrate a role for unpolymerized actin in control of transcription by serum response factor. Mol Biol Cell *13*, 4167-4178.

Prasad, G. L., Valverius, E. M., McDuffie, E., and Cooper, H. L. 1992. Complementary DNA cloning of a novel epithelial cell marker protein, HME1, that may be down-regulated in neoplastic mammary cells. Cell Growth Differ *3*, 507-513.

Pruyne, D., Evangelista, M., Yang, C., Bi, E., Zigmond, S., Bretscher, A., and Boone, C. 2002. Role of formins in actin assembly: nucleation and barbed-end association. Science *297*, 612-615.

Radisky, D. C., Levy, D. D., Littlepage, L. E., Liu, H., Nelson, C. M., Fata, J. E., Leake, D., Godden, E. L., Albertson, D. G., Nieto, M. A., Werb, Z., and Bissell, M. J. 2005. Rac1b and reactive oxygen species mediate MMP-3-induced EMT and genomic instability. Nature *436*, 123-127.

Rakha, E. A., El-Sayed, M. E., Green, A. R., Paish, E. C., Lee, A. H., and Ellis, I. O. 2007. Breast carcinoma with basal differentiation: a proposal for pathology definition based on basal cytokeratin expression. Histopathology *50*, 434-438.

Rakha, E. A., Gill, M. S., El-Sayed, M. E., Khan, M. M., Hodi, Z., Blamey, R. W., Evans, A. J., Lee, A. H., and Ellis, I. O. 2009. The biological and clinical

characteristics of breast carcinoma with mixed ductal and lobular morphology. Breast Cancer Res Treat *114*, 243-250.

Rakha, E. A., Putti, T. C., Abd El-Rehim, D. M., Paish, C., Green, A. R., Powe, D. G., Lee, A. H., Robertson, J. F., and Ellis, I. O. 2006. Morphological and immunophenotypic analysis of breast carcinomas with basal and myoepithelial differentiation. J Pathol *208*, 495-506.

Rakha, E. A., Reis-Filho, J. S., and Ellis, I. O. 2008. Basal-like breast cancer: a critical review. J Clin Oncol *26*, 2568-2581.

Ralhan, R., Desouza, L. V., Matta, A., Chandra Tripathi, S., Ghanny, S., Datta Gupta, S., Bahadur, S., and Siu, K. W. 2008. Discovery and verification of head-and-neck cancer biomarkers by differential protein expression analysis using iTRAQ labeling, multidimensional liquid chromatography, and tandem mass spectrometry. Mol Cell Proteomics *7*, 1162-1173.

Ramirez, J. L., Rosell, R., Taron, M., Sanchez-Ronco, M., Alberola, V., de Las Penas, R., Sanchez, J. M., Moran, T., Camps, C., Massuti, B., Sanchez, J. J., Salazar, F., and Catot, S. 2005. 14-3-3σ methylation in pretreatment serum circulating DNA of cisplatin-plus-gemcitabine-treated advanced non-small-cell lung cancer patients predicts survival: The Spanish Lung Cancer Group. J Clin Oncol *23*, 9105-9112.

Reis-Filho, J. S., Savage, K., Lambros, M. B., James, M., Steele, D., Jones, R. L., and Dowsett, M. 2006. Cyclin D1 protein overexpression and CCND1 amplification in breast carcinomas: an immunohistochemical and chromogenic in situ hybridisation analysis. Mod Pathol *19*, 999-1009.

Reversi, A., Cassoni, P., and Chini, B. 2005. Oxytocin receptor signaling in myoepithelial and cancer cells. J Mammary Gland Biol Neoplasia *10*, 221-229.

Rhodes, A., Jasani, B., Barnes, D. M., Bobrow, L. G., and Miller, K. D. 2000. Reliability of immunohistochemical demonstration of oestrogen receptors in routine practice: interlaboratory variance in the sensitivity of detection and evaluation of scoring systems. J Clin Pathol *53*, 125-130.

Richert, M. M., Schwertfeger, K. L., Ryder, J. W., and Anderson, S. M. 2000. An atlas of mouse mammary gland development. J Mammary Gland Biol Neoplasia *5*, 227-241.

Ridley, A. J., and Hall, A. 1992. The small GTP-binding protein rho regulates the assembly of focal adhesions and actin stress fibers in response to growth factors. Cell *70*, 389-399.

Ridley, A. J., Paterson, H. F., Johnston, C. L., Diekmann, D., and Hall, A. 1992. The small GTP-binding protein rac regulates growth factor-induced membrane ruffling. Cell *70*, 401-410.

Ridley, A. J., Schwartz, M. A., Burridge, K., Firtel, R. A., Ginsberg, M. H., Borisy, G., Parsons, J. T., and Horwitz, A. R. 2003. Cell migration: integrating signals from front to back. Science *302*, 1704-1709.

Riedl, J., Crevenna, A. H., Kessenbrock, K., Yu, J. H., Neukirchen, D., Bista, M., Bradke, F., Jenne, D., Holak, T. A., Werb, Z., Sixt, M., and Wedlich-

Soldner, R. 2008. Lifeact: a versatile marker to visualize F-actin. Nat Methods *5*, 605-607.

Rizki, A., Mott, J. D., and Bissell, M. J. 2007. Polo-like kinase 1 is involved in invasion through extracellular matrix. Cancer Res *67*, 11106-11110.

Rizki, A., Weaver, V. M., Lee, S. Y., Rozenberg, G. I., Chin, K., Myers, C. A., Bascom, J. L., Mott, J. D., Semeiks, J. R., Grate, L. R., Mian, I. S., Borowsky, A. D., Jensen, R. A., Idowu, M. O., Chen, F., Chen, D. J., Petersen, O. W., Gray, J. W., and Bissell, M. J. 2008. A human breast cell model of preinvasive to invasive transition. Cancer Res *68*, 1378-1387.

Rodriguez-Pinilla, S. M., Jones, R. L., Lambros, M. B., Arriola, E., Savage, K., James, M., Pinder, S. E., and Reis-Filho, J. S. 2007. MYC amplification in breast cancer: a chromogenic in situ hybridisation study. J Clin Pathol *60*, 1017-1023.

Rohatgi, R., Ma, L., Miki, H., Lopez, M., Kirchhausen, T., Takenawa, T., and Kirschner, M. W. 1999. The interaction between N-WASP and the Arp2/3 complex links Cdc42-dependent signals to actin assembly. Cell *97*, 221-231.

Romero, S., Le Clainche, C., Didry, D., Egile, C., Pantaloni, D., and Carlier, M. F. 2004. Formin is a processive motor that requires profilin to accelerate actin assembly and associated ATP hydrolysis. Cell *119*, 419-429.

Roth, D., Birkenfeld, J., and Betz, H. 1999. Dominant-negative alleles of 14-3-3 proteins cause defects in actin organization and vesicle targeting in the yeast Saccharomyces cerevisiae. FEBS Lett *460*, 411-416.

Rottner, K., Hall, A., and Small, J. V. 1999. Interplay between Rac and Rho in the control of substrate contact dynamics. Curr Biol *9*, 640-648.

Rouzier, R., Perou, C. M., Symmans, W. F., Ibrahim, N., Cristofanilli, M., Anderson, K., Hess, K. R., Stec, J., Ayers, M., Wagner, P., Morandi, P., Fan, C., Rabiul, I., Ross, J. S., Hortobagyi, G. N., and Pusztai, L. 2005. Breast cancer molecular subtypes respond differently to preoperative chemotherapy. Clin Cancer Res *11*, 5678-5685.

Rozenchan, P. B., Carraro, D. M., Brentani, H., de Carvalho Mota, L. D., Bastos, E. P., e Ferreira, E. N., Torres, C. H., Katayama, M. L., Roela, R. A., Lyra, E. C., Soares, F. A., Folgueira, M. A., Goes, J. C., and Brentani, M. M. 2009. Reciprocal changes in gene expression profiles of cocultured breast epithelial cells and primary fibroblasts. Int J Cancer *125*, 2767-2777.

Sasadaira, H., Kameya, T., Shimosato, Y., Baba, K., and Amemiya, R. 1978. Immunohistochemical identification of actomyosin-containing (myoepithelial) cells in non-neoplastic and neoplastic tissues. Acta Pathol Jpn *28*, 345-355.

Savage, K., Lambros, M. B., Robertson, D., Jones, R. L., Jones, C., Mackay, A., James, M., Hornick, J. L., Pereira, E. M., Milanezi, F., Fletcher, C. D., Schmitt, F. C., Ashworth, A., and Reis-Filho, J. S. 2007. Caveolin 1 is overexpressed and amplified in a subset of basal-like and metaplastic breast carcinomas: a morphologic, ultrastructural, immunohistochemical, and in situ hybridization analysis. Clin Cancer Res *13*, 90-101.

Savage, K., Leung, S., Todd, S. K., Brown, L. A., Jones, R. L., Robertson, D., James, M., Parry, S., Rodrigues Pinilla, S. M., Huntsman, D., and Reis-Filho, J. S. 2008. Distribution and significance of caveolin 2 expression in normal breast and invasive breast cancer: an immunofluorescence and immunohistochemical analysis. Breast Cancer Res Treat *110*, 245-256.

Schmidt, A., and Hall, A. 2002. Guanine nucleotide exchange factors for Rho GTPases: turning on the switch. Genes Dev *16*, 1587-1609.

Sept, D., and McCammon, J. A. 2001. Thermodynamics and kinetics of actin filament nucleation. Biophys J *81*, 667-674.

Shah, C., Miller, T. W., Wyatt, S. K., McKinley, E. T., Olivares, M. G., Sanchez, V., Nolting, D. D., Buck, J. R., Zhao, P., Ansari, M. S., Baldwin, R. M., Gore, J. C., Schiff, R., Arteaga, C. L., and Manning, H. C. 2009. Imaging biomarkers predict response to anti-HER2 (ErbB2) therapy in preclinical models of breast cancer. Clin Cancer Res *15*, 4712-4721.

Shakya, R., Szabolcs, M., McCarthy, E., Ospina, E., Basso, K., Nandula, S., Murty, V., Baer, R., and Ludwig, T. 2008. The basal-like mammary carcinomas induced by Brca1 or Bard1 inactivation implicate the BRCA1/BARD1 heterodimer in tumor suppression. Proc Natl Acad Sci U S A *105*, 7040-7045.

Shao, J., Welch, W. J., Diprospero, N. A., and Diamond, M. I. 2008. Phosphorylation of profilin by ROCK1 regulates polyglutamine aggregation. Mol Cell Biol *28*, 5196-5208.

Shimada, A., Nyitrai, M., Vetter, I. R., Kuhlmann, D., Bugyi, B., Narumiya, S., Geeves, M. A., and Wittinghofer, A. 2004. The core FH2 domain of diaphanous-related formins is an elongated actin binding protein that inhibits polymerization. Mol Cell *13*, 511-522.

Sierra, A. 2009. Animal models of breast cancer for the study of pathogenesis and therapeutic insights. Clin Transl Oncol *11*, 721-727.

Silberstein, G. B., and Daniel, C. W. 1987. Reversible inhibition of mammary gland growth by transforming growth factor-beta. Science *237*, 291-293.

Simpson, P. T., Gale, T., Reis-Filho, J. S., Jones, C., Parry, S., Steele, D., Cossu, A., Budroni, M., Palmieri, G., and Lakhani, S. R. 2004. Distribution and significance of 14-3-3σ, a novel myoepithelial marker, in normal, benign, and malignant breast tissue. J Pathol *202*, 274-285.

Singletary, S. E., and Connolly, J. L. 2006. Breast cancer staging: working with the sixth edition of the AJCC Cancer Staging Manual. CA Cancer J Clin *56*, 37-47; quiz 50-31.

Slamon, D. J., Clark, G. M., Wong, S. G., Levin, W. J., Ullrich, A., and McGuire, W. L. 1987. Human breast cancer: correlation of relapse and survival with amplification of the HER-2/neu oncogene. Science *235*, 177-182.

Solnica-Krezel, L. 2005. Conserved patterns of cell movements during vertebrate gastrulation. Curr Biol *15*, R213-228.

Soosairajah, J., Maiti, S., Wiggan, O., Sarmiere, P., Moussi, N., Sarcevic, B., Sampath, R., Bamburg, J. R., and Bernard, O. 2005. Interplay between

components of a novel LIM kinase-slingshot phosphatase complex regulates cofilin. EMBO J *24*, 473-486.

Sorlie, T., Perou, C. M., Tibshirani, R., Aas, T., Geisler, S., Johnsen, H., Hastie, T., Eisen, M. B., van de Rijn, M., Jeffrey, S. S., Thorsen, T., Quist, H., Matese, J. C., Brown, P. O., Botstein, D., Eystein Lonning, P., and Borresen-Dale, A. L. 2001. Gene expression patterns of breast carcinomas distinguish tumor subclasses with clinical implications. Proc Natl Acad Sci U S A *98*, 10869-10874.

Sorlie, T., Tibshirani, R., Parker, J., Hastie, T., Marron, J. S., Nobel, A., Deng, S., Johnsen, H., Pesich, R., Geisler, S., Demeter, J., Perou, C. M., Lonning, P. E., Brown, P. O., Borresen-Dale, A. L., and Botstein, D. 2003. Repeated observation of breast tumor subtypes in independent gene expression data sets. Proc Natl Acad Sci U S A *100*, 8418-8423.

Sotiriou, C., Neo, S. Y., McShane, L. M., Korn, E. L., Long, P. M., Jazaeri, A., Martiat, P., Fox, S. B., Harris, A. L., and Liu, E. T. 2003. Breast cancer classification and prognosis based on gene expression profiles from a population-based study. Proc Natl Acad Sci U S A *100*, 10393-10398.

Sousa, B., Paredes, J., Milanezi, F., Lopes, N., Martins, D., Dufloth, R., Vieira, D., Albergaria, A., Veronese, L., Carneiro, V., Carvalho, S., Costa, J. L., Zeferino, L., and Schmitt, F. 2010. P-cadherin, vimentin and CK14 for identification of basal-like phenotype in breast carcinomas: an immunohistochemical study. Histol Histopathol *25*, 963-974.

Stein, T., Salomonis, N., and Gusterson, B. A. 2007. Mammary gland involution as a multi-step process. J Mammary Gland Biol Neoplasia *12*, 25-35.

Straver, M. E., Glas, A. M., Hannemann, J., Wesseling, J., van de Vijver, M. J., Rutgers, E. J., Vrancken Peeters, M. J., van Tinteren, H., Van't Veer, L. J., and Rodenhuis, S. 2009. The 70-gene signature as a response predictor for neoadjuvant chemotherapy in breast cancer. Breast Cancer Res Treat *119*, 551-558.

Symons, M. H., and Mitchison, T. J. 1991. Control of actin polymerization in live and permeabilized fibroblasts. J Cell Biol *114*, 503-513.

Tan, D. S., Marchio, C., Jones, R. L., Savage, K., Smith, I. E., Dowsett, M., and Reis-Filho, J. S. 2008. Triple negative breast cancer: molecular profiling and prognostic impact in adjuvant anthracycline-treated patients. Breast Cancer Res Treat *111*, 27-44.

Taneja, P., Frazier, D. P., Kendig, R. D., Maglic, D., Sugiyama, T., Kai, F., Taneja, N. K., and Inoue, K. 2009. MMTV mouse models and the diagnostic values of MMTV-like sequences in human breast cancer. Expert Rev Mol Diagn *9*, 423-440.

Teicher, B. A. 2009. In vivo/ex vivo and in situ assays used in cancer research: a brief review. Toxicol Pathol *37*, 114-122.

Theriot, J. A., and Mitchison, T. J. 1991. Actin microfilament dynamics in locomoting cells. Nature *352*, 126-131.

Theriot, J. A., and Mitchison, T. J. 1993. The three faces of profilin. Cell *75*, 835-838.

Theriot, J. A., Mitchison, T. J., Tilney, L. G., and Portnoy, D. A. 1992. The rate of actin-based motility of intracellular Listeria monocytogenes equals the rate of actin polymerization. Nature *357*, 257-260.

Thorat, M. A., Marchio, C., Morimiya, A., Savage, K., Nakshatri, H., Reis-Filho, J. S., and Badve, S. 2008. Forkhead box A1 expression in breast cancer is associated with luminal subtype and good prognosis. J Clin Pathol *61*, 327-332.

Tomayko, M. M., and Reynolds, C. P. 1989. Determination of subcutaneous tumor size in athymic (nude) mice. Cancer Chemother Pharmacol *24*, 148-154.

Toshima, J. Y., Toshima, J., Watanabe, T., and Mizuno, K. 2001. Binding of 14-3-3beta regulates the kinase activity and subcellular localization of testicular protein kinase 1. J Biol Chem *276*, 43471-43481.

Umbricht, C. B., Evron, E., Gabrielson, E., Ferguson, A., Marks, J., and Sukumar, S. 2001. Hypermethylation of 14-3-3 sigma (stratifin) is an early event in breast cancer. Oncogene *20*, 3348-3353.

Urano, T., Saito, T., Tsukui, T., Fujita, M., Hosoi, T., Muramatsu, M., Ouchi, Y., and Inoue, S. 2002. Efp targets 14-3-3 sigma for proteolysis and promotes breast tumour growth. Nature *417*, 871-875.

van 't Veer, L. J., Dai, H., van de Vijver, M. J., He, Y. D., Hart, A. A., Mao, M., Peterse, H. L., van der Kooy, K., Marton, M. J., Witteveen, A. T., Schreiber, G. J., Kerkhoven, R. M., Roberts, C., Linsley, P. S., Bernards, R., and Friend, S. H. 2002. Gene expression profiling predicts clinical outcome of breast cancer. Nature *415*, 530-536.

van de Vijver, M. J., He, Y. D., van't Veer, L. J., Dai, H., Hart, A. A., Voskuil, D. W., Schreiber, G. J., Peterse, J. L., Roberts, C., Marton, M. J., Parrish, M., Atsma, D., Witteveen, A., Glas, A., Delahaye, L., van der Velde, T., Bartelink, H., Rodenhuis, S., Rutgers, E. T., Friend, S. H., and Bernards, R. 2002. A gene-expression signature as a predictor of survival in breast cancer. N Engl J Med *347*, 1999-2009.

Vandermoere, F., El Yazidi-Belkoura, I., Demont, Y., Slomianny, C., Antol, J., Lemoine, J., and Hondermarck, H. 2007. Proteomics exploration reveals that actin is a signaling target of the kinase Akt. Mol Cell Proteomics *6*, 114-124.

Vercoutter-Edouart, A. S., Lemoine, J., Le Bourhis, X., Louis, H., Boilly, B., Nurcombe, V., Revillion, F., Peyrat, J. P., and Hondermarck, H. 2001. Proteomic analysis reveals that 14-3-3σ is down-regulated in human breast cancer cells. Cancer Res *61*, 76-80.

Verdoodt, B., Benzinger, A., Popowicz, G. M., Holak, T. A., and Hermeking, H. 2006. Characterization of 14-3-3σ dimerization determinants: requirement of homodimerization for inhibition of cell proliferation. Cell Cycle *5*, 2920-2926.

Villadsen, R., Fridriksdottir, A. J., Ronnov-Jessen, L., Gudjonsson, T., Rank, F., LaBarge, M. A., Bissell, M. J., and Petersen, O. W. 2007. Evidence for a stem cell hierarchy in the adult human breast. J Cell Biol *177*, 87-101.

Wang, F., Hansen, R. K., Radisky, D., Yoneda, T., Barcellos-Hoff, M. H., Petersen, O. W., Turley, E. A., and Bissell, M. J. 2002a. Phenotypic reversion or death of cancer cells by altering signaling pathways in three-dimensional contexts. J Natl Cancer Inst *94*, 1494-1503.

Wang, F., Herzmark, P., Weiner, O. D., Srinivasan, S., Servant, G., and Bourne, H. R. 2002b. Lipid products of PI(3)Ks maintain persistent cell polarity and directed motility in neutrophils. Nat Cell Biol *4*, 513-518.

Wang, F., Weaver, V. M., Petersen, O. W., Larabell, C. A., Dedhar, S., Briand, P., Lupu, R., and Bissell, M. J. 1998. Reciprocal interactions between beta1-integrin and epidermal growth factor receptor in three-dimensional basement membrane breast cultures: a different perspective in epithelial biology. Proc Natl Acad Sci U S A *95*, 14821-14826.

Wang, W., Eddy, R., and Condeelis, J. 2007. The cofilin pathway in breast cancer invasion and metastasis. Nat Rev Cancer *7*, 429-440.

Wang, W., Goswami, S., Sahai, E., Wyckoff, J. B., Segall, J. E., and Condeelis, J. S. 2005a. Tumor cells caught in the act of invading: their strategy for enhanced cell motility. Trends Cell Biol *15*, 138-145.

Wang, Y., Klijn, J. G., Zhang, Y., Sieuwerts, A. M., Look, M. P., Yang, F., Talantov, D., Timmermans, M., Meijer-van Gelder, M. E., Yu, J., Jatkoe, T., Berns, E. M., Atkins, D., and Foekens, J. A. 2005b. Gene-expression profiles to predict distant metastasis of lymph-node-negative primary breast cancer. Lancet *365*, 671-679.

Wang, Y., and Steinbeisser, H. 2009. Molecular basis of morphogenesis during vertebrate gastrulation. Cell Mol Life Sci *66*, 2263-2273.

Wang, Z., Trope, C. G., Suo, Z., Troen, G., Yang, G., Nesland, J. M., and Holm, R. 2008. The clinicopathological and prognostic impact of 14-3-3 sigma expression on vulvar squamous cell carcinomas. BMC Cancer *8*, 308.

Watanabe, N., Madaule, P., Reid, T., Ishizaki, T., Watanabe, G., Kakizuka, A., Saito, Y., Nakao, K., Jockusch, B. M., and Narumiya, S. 1997. p140mDia, a mammalian homolog of Drosophila diaphanous, is a target protein for Rho small GTPase and is a ligand for profilin. EMBO J *16*, 3044-3056.

Weaver, V. M., Lelievre, S., Lakins, J. N., Chrenek, M. A., Jones, J. C., Giancotti, F., Werb, Z., and Bissell, M. J. 2002. beta4 integrin-dependent formation of polarized three-dimensional architecture confers resistance to apoptosis in normal and malignant mammary epithelium. Cancer Cell *2*, 205-216.

Weaver, V. M., Petersen, O. W., Wang, F., Larabell, C. A., Briand, P., Damsky, C., and Bissell, M. J. 1997. Reversion of the malignant phenotype of human breast cells in three-dimensional culture and in vivo by integrin blocking antibodies. J Cell Biol *137*, 231-245.

Weigelt, B., and Bissell, M. J. 2008. Unraveling the microenvironmental influences on the normal mammary gland and breast cancer. Semin Cancer Biol *18*, 311-321.

Weigelt, B., Lo, A. T., Park, C. C., Gray, J. W., and Bissell, M. J. 2010. HER2 signaling pathway activation and response of breast cancer cells to HER2-

targeting agents is dependent strongly on the 3D microenvironment. Breast Cancer Res Treat *122*, 35-43.

Weijer, C. J. 2009. Collective cell migration in development. J Cell Sci *122*, 3215-3223.

West, R. B., Nuyten, D. S., Subramanian, S., Nielsen, T. O., Corless, C. L., Rubin, B. P., Montgomery, K., Zhu, S., Patel, R., Hernandez-Boussard, T., Goldblum, J. R., Brown, P. O., van de Vijver, M., and van de Rijn, M. 2005. Determination of stromal signatures in breast carcinoma. PLoS Biol *3*, e187.

Wilker, E. W., Grant, R. A., Artim, S. C., and Yaffe, M. B. 2005. A structural basis for 14-3-3σ functional specificity. J Biol Chem *280*, 18891-18898.

Wilker, E. W., van Vugt, M. A., Artim, S. A., Huang, P. H., Petersen, C. P., Reinhardt, H. C., Feng, Y., Sharp, P. A., Sonenberg, N., White, F. M., and Yaffe, M. B. 2007. 14-3-3σ controls mitotic translation to facilitate cytokinesis. Nature *446*, 329-332.

Wolf, K., Mazo, I., Leung, H., Engelke, K., von Andrian, U. H., Deryugina, E. I., Strongin, A. Y., Brocker, E. B., and Friedl, P. 2003. Compensation mechanism in tumor cell migration: mesenchymal-amoeboid transition after blocking of pericellular proteolysis. J Cell Biol *160*, 267-277.

Wu, E. S., Jacobson, K., and Papahadjopoulos, D. 1977. Lateral diffusion in phospholipid multibilayers measured by fluorescence recovery after photobleaching. Biochemistry *16*, 3836-3841.

Wu, Y., Deng, J., Rychahou, P. G., Qiu, S., Evers, B. M., and Zhou, B. P. 2009a. Stabilization of snail by NF-kappaB is required for inflammation-induced cell migration and invasion. Cancer Cell *15*, 416-428.

Wu, Y. I., Frey, D., Lungu, O. I., Jaehrig, A., Schlichting, I., Kuhlman, B., and Hahn, K. M. 2009b. A genetically encoded photoactivatable Rac controls the motility of living cells. Nature *461*, 104-108.

Xiao, B., Smerdon, S. J., Jones, D. H., Dodson, G. G., Soneji, Y., Aitken, A., and Gamblin, S. J. 1995. Structure of a 14-3-3 protein and implications for coordination of multiple signalling pathways. Nature *376*, 188-191.

Xu, J., Wang, F., Van Keymeulen, A., Herzmark, P., Straight, A., Kelly, K., Takuwa, Y., Sugimoto, N., Mitchison, T., and Bourne, H. R. 2003. Divergent signals and cytoskeletal assemblies regulate self-organizing polarity in neutrophils. Cell *114*, 201-214.

Xu, R., Boudreau, A., and Bissell, M. J. 2009a. Tissue architecture and function: dynamic reciprocity via extra- and intra-cellular matrices. Cancer Metastasis Rev.

Xu, R., Nelson, C. M., Muschler, J. L., Veiseh, M., Vonderhaar, B. K., and Bissell, M. J. 2009b. Sustained activation of STAT5 is essential for chromatin remodeling and maintenance of mammary-specific function. J Cell Biol *184*, 57-66.

Xu, Y., Moseley, J. B., Sagot, I., Poy, F., Pellman, D., Goode, B. L., and Eck, M. J. 2004. Crystal structures of a Formin Homology-2 domain reveal a tethered dimer architecture. Cell *116*, 711-723.

Yaffe, M. B., Rittinger, K., Volinia, S., Caron, P. R., Aitken, A., Leffers, H., Gamblin, S. J., Smerdon, S. J., and Cantley, L. C. 1997. The structural basis for 14-3-3:phosphopeptide binding specificity. Cell *91*, 961-971.

Yamana, N., Arakawa, Y., Nishino, T., Kurokawa, K., Tanji, M., Itoh, R. E., Monypenny, J., Ishizaki, T., Bito, H., Nozaki, K., Hashimoto, N., Matsuda, M., and Narumiya, S. 2006. The Rho-mDia1 pathway regulates cell polarity and focal adhesion turnover in migrating cells through mobilizing Apc and c-Src. Mol Cell Biol *26*, 6844-6858.

Yan, Y., Weaver, V. M., and Blair, I. A. 2005. Analysis of protein expression during oxidative stress in breast epithelial cells using a stable isotope labeled proteome internal standard. J Proteome Res *4*, 2007-2014.

Yang, H., Wen, Y. Y., Zhao, R., Lin, Y. L., Fournier, K., Yang, H. Y., Qiu, Y., Diaz, J., Laronga, C., and Lee, M. H. 2006a. DNA damage-induced protein 14-3-3 sigma inhibits protein kinase B/Akt activation and suppresses Akt-activated cancer. Cancer Res *66*, 3096-3105.

Yang, H., Zhang, Y., Zhao, R., Wen, Y. Y., Fournier, K., Wu, H. B., Yang, H. Y., Diaz, J., Laronga, C., and Lee, M. H. 2006b. Negative cell cycle regulator 14-3-3σ stabilizes p27 Kip1 by inhibiting the activity of PKB/Akt. Oncogene *25*, 4585-4594.

Yang, J., Mani, S. A., Donaher, J. L., Ramaswamy, S., Itzykson, R. A., Come, C., Savagner, P., Gitelman, I., Richardson, A., and Weinberg, R. A. 2004. Twist, a master regulator of morphogenesis, plays an essential role in tumor metastasis. Cell *117*, 927-939.

Yang, N., Higuchi, O., Ohashi, K., Nagata, K., Wada, A., Kangawa, K., Nishida, E., and Mizuno, K. 1998. Cofilin phosphorylation by LIM-kinase 1 and its role in Rac-mediated actin reorganization. Nature *393*, 809-812.

Yang, X., Lee, W. H., Sobott, F., Papagrigoriou, E., Robinson, C. V., Grossmann, J. G., Sundstrom, M., Doyle, D. A., and Elkins, J. M. 2006c. Structural basis for protein-protein interactions in the 14-3-3 protein family. Proc Natl Acad Sci U S A *103*, 17237-17242.

Zebda, N., Bernard, O., Bailly, M., Welti, S., Lawrence, D. S., and Condeelis, J. S. 2000. Phosphorylation of ADF/cofilin abolishes EGF-induced actin nucleation at the leading edge and subsequent lamellipod extension. J Cell Biol *151*, 1119-1128.

Zigmond, S. H. 2004. Formin-induced nucleation of actin filaments. Curr Opin Cell Biol *16*, 99-105.

Zigmond, S. H., Evangelista, M., Boone, C., Yang, C., Dar, A. C., Sicheri, F., Forkey, J., and Pring, M. 2003. Formin leaky cap allows elongation in the presence of tight capping proteins. Curr Biol *13*, 1820-1823.

# CHAPTER 6. FIGURES AND FIGURE LEGENDS

**Figure 1: 14-3-3σ expression follows malignancy in the HMT-3522 model of basal-like breast cancer (BLBC) progression.** (A) Lysates from cells grown for 4 days in tissue culture polystyrene (2D) or on top of basement membrane extract (3D Matrigel) were resolved by SDS-PAGE and analyzed for 14-3-3σ expression by western blot analysis. Actin and E-cadherin are provided as loading controls. (B) Western blot analysis of lysates from the MCF10 series following growth for 4 days in tissue culture polystyrene. Actin and E-cadherin are provided as loading controls.

FIGURE 1: 14-3-3σ expression follows malignancy in the HMT-3522 model of basal-like breast cancer (BLBC) progression.

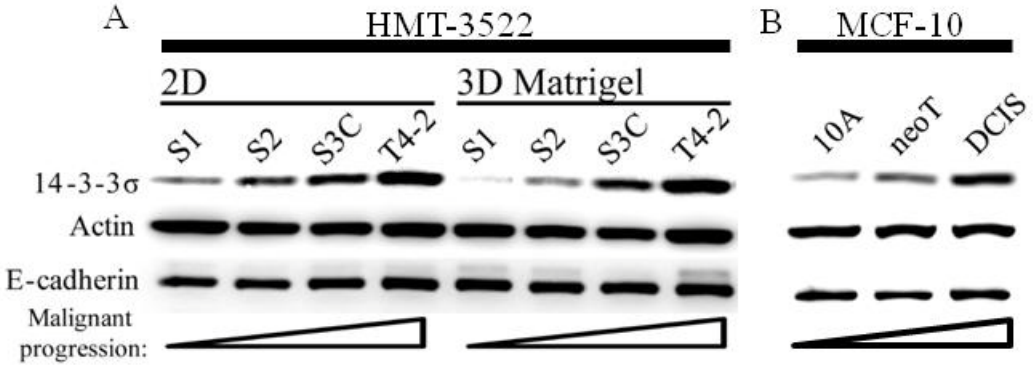

**FIGURE 2: 14-3-3σ expression identifies myoepithelial cells in normal human breast and mouse mammary glands.** Archival formalin-fixed and paraffin-embedded mammary gland sections from an 8 week old mouse (CD1 strain) and tissue sections from a nonmalignant breast reduction (obtained commercially) were dewaxed, stained with 14-3-3σ antibody (clone C-18), and nuclei were counterstained with hematoxylin. Myoepithelial cells were stained ~3-fold more intense than luminal epithelial cells as previously reported in the normal human breast (Moreira et al., 2005; Simpson et al., 2004). Specificity of the staining was verified by excluding the primary antibody (no IgG). Scale bar: 100μm.

FIGURE 2: 14-3-3σ expression identifies myoepithelial cells in normal human breast and mouse mammary glands.

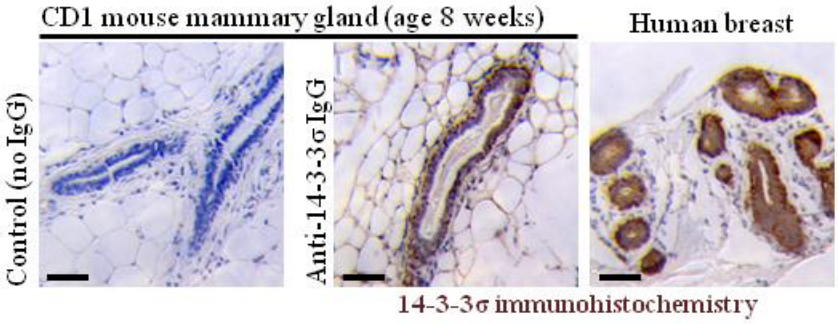

**FIGURE 3: 14-3-3σ expression and distribution is regulated by estrogen signaling.** 16 week old CD1 mice were ovariectomized and administered either estrogen or progesterone (or vehicle) as described in the Materials and Methods. Formalin-fixed, paraffin-embedded tissue sections were dewaxed and stained with 14-3-3σ antibody and counterstained with hematoxylin. 14-3-3σ staining intensity is dramatically higher in both luminal and myoepithelial cells of ovariectomized mice; this is rescued in mice supplemented with estrogen or progesterone. Sham-treated: mice were incised, but ovaries were left intact.

FIGURE 3: 14-3-3σ expression and distribution is regulated by estrogen signaling.

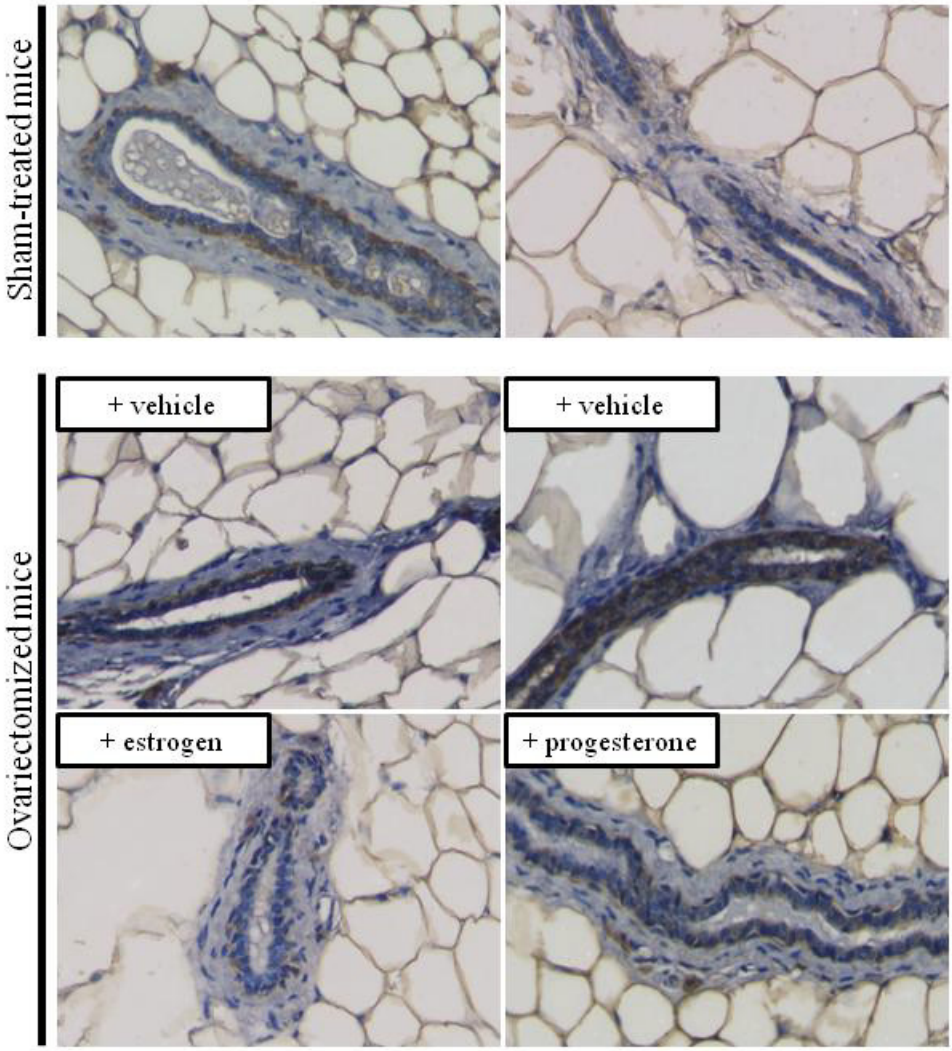


**14-3-3σ immunohistochemistry**

**FIGURE 4: 14-3-3σ expression correlates with ER negative tumors, poor MammaPrint signature, and BLBC molecular subtype.** Microarray data and available clinical information for three breast cancer patient cohorts (Chin et al., 2006; van de Vijver et al., 2002; Wang et al., 2005b) were obtained from public sources as described in the Materials and Methods. Patients were grouped based on ER status (A), MammaPrint signature (B), and molecular subtype (C), and the mean 14-3-3σ expression for each group was calculated. Error bars represent the standard error of the mean, statistical significance was measured using either a two-tailed Mann-Whitney test (A,B), or a one-way analysis of variance (C) with Bonferroni post-test (* $p < 0.05$, ** $p < 0.01$, *** $p < 0.001$).

FIGURE 4: 14-3-3σ expression correlates with ER negative tumors, poor MammaPrint signature, and BLBC molecular subtype.

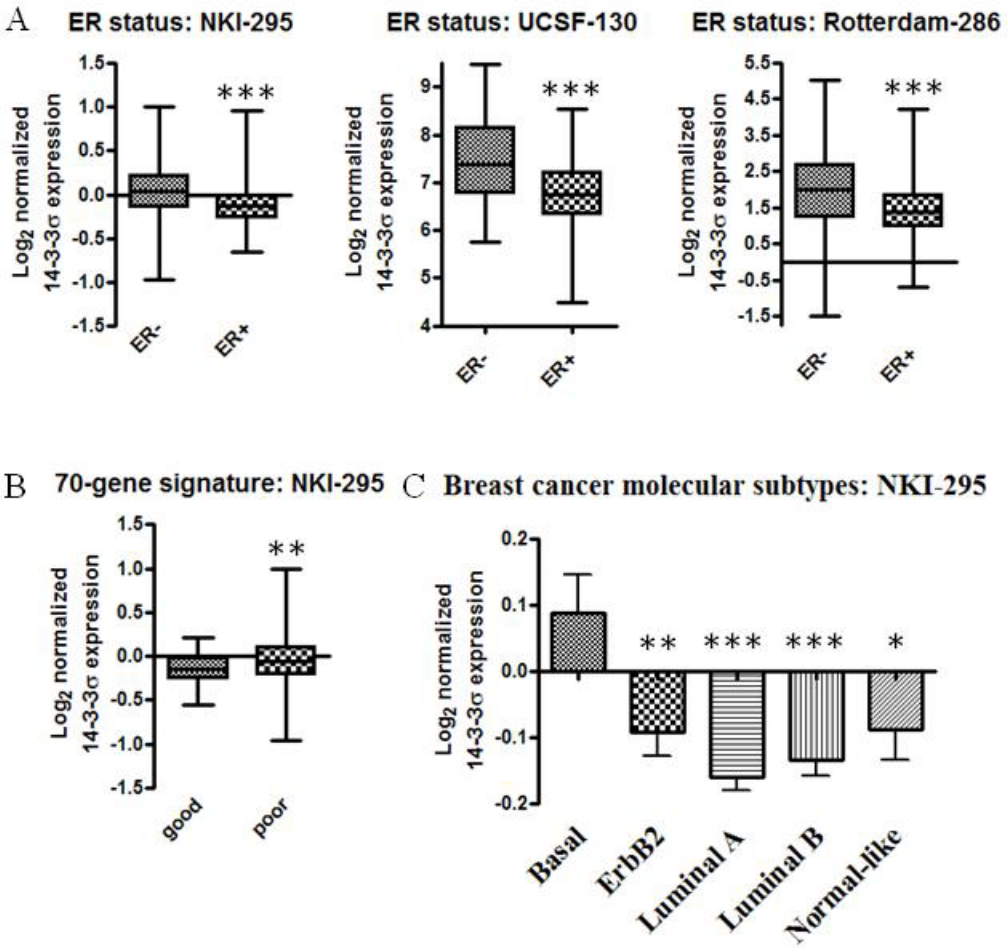

**FIGURE 5: 14-3-3σ nuclear expression correlates with luminal subtype and good clinical outcome in the ICR cohort.** (A) 14-3-3σ immunoreactivity and subcellular distribution (from Table 1 and 2) by tumor subtype. 14-3-3σ cytoplasmic staining correlates with basal subtype, while nuclear or absent staining correlates with luminal subtype. (B) Kaplan-Meier survival analysis of the ICR cohort for patients grouped by 14-3-3σ subcellular distribution. The presence of cytoplasmic 14-3-3σ staining is correlated with poor 5-year clinical outcome. P values were calculated using the log-rank test.

FIGURE 5: 14-3-3σ nuclear expression correlates with luminal subtype and good clinical outcome in the ICR cohort.

A 14-3-3σ subcellular distribution by tumor subtype:

| Tumor subtype | 14-3-3σ Absent | Nuclear only | Nuclear and cytoplasmic | Cytoplasmic only | χ2 p-value |
|---|---|---|---|---|---|
| Luminal | 83 | 39 | 10 | 4 | <0.0001 |
| HER2+ | 14 | 13 | 1 | 0 | |
| Basal | 3 | 4 | 9 | 7 | |

B Overall survival by subcellular distribution

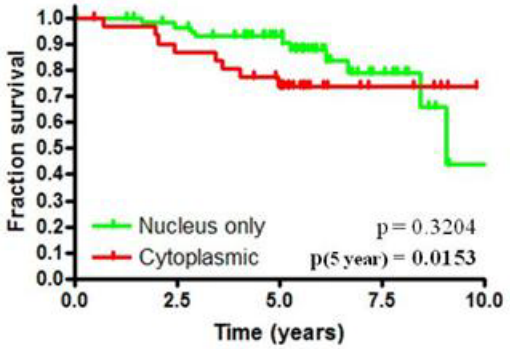

**FIGURE 6: 14-3-3σ expression correlates with decreased overall, recurrence-free, and metastasis-free survival.** (A) Kaplan-Meier survival analysis of the Netherlands Cancer Institute (NKI) and the USCF cohorts for patients grouped by 14-3-3σ expression. (B) Kaplan-Meier recurrence-free survival analysis of the NKI and the USCF patient cohorts for patients grouped by 14-3-3σ expression. (C) Kaplan-Meier metastasis-free survival analysis of the Netherlands NKI and the USCF patient cohorts for patients grouped by 14-3-3σ expression. P values for all survival curves were calculated using the log-rank test. 14-3-3 low: 14-3-3σ mRNA expression levels lower than the median expression of 14-3-3σ in the whole cohort; 14-3-3σ high: 14-3-3σ mRNA expression levels higher than the median expression of 14-3-3σ in the whole cohort.

FIGURE 6: 14-3-3σ expression correlates with decreased overall, recurrence-free, and metastasis-free survival.

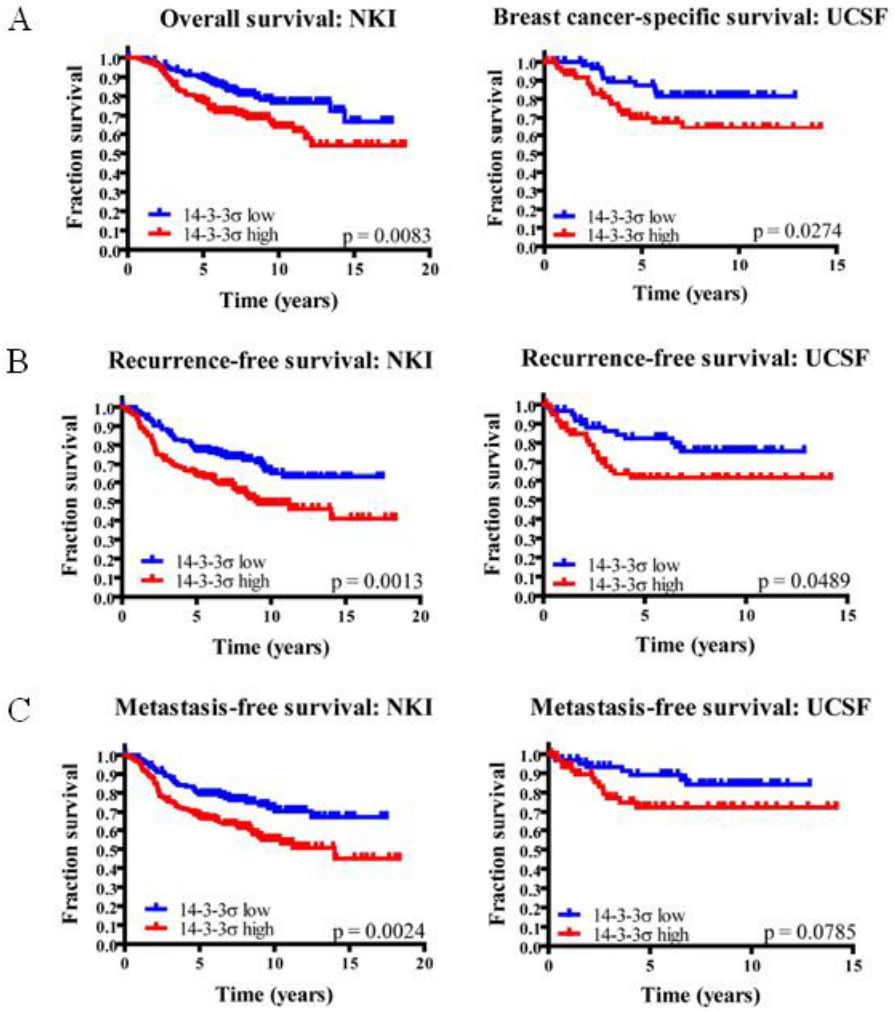

**FIGURE 7: 14-3-3σ immunohistochemical staining is most intense at the invasive front of the tumor in T4-2 xenografts.** T4-2 cells were injected subcutaneously into rear flanks of nu/nu mice and allowed to form tumors for a period of 28 days. The tumors were then were excised and fixed in formalin for immunohistochemical analysis. The surrounding mouse stroma is negative for 14-3-3σ staining (left). A heat map representation of the same tumor section emphasizes the 14-3-3σ distribution at the tumor invasive front (right). Scale bar: 100μm.

FIGURE 7: 14-3-3σ immunohistochemical staining is most intense at the invasive front of the tumor in T4-2 xenografts.

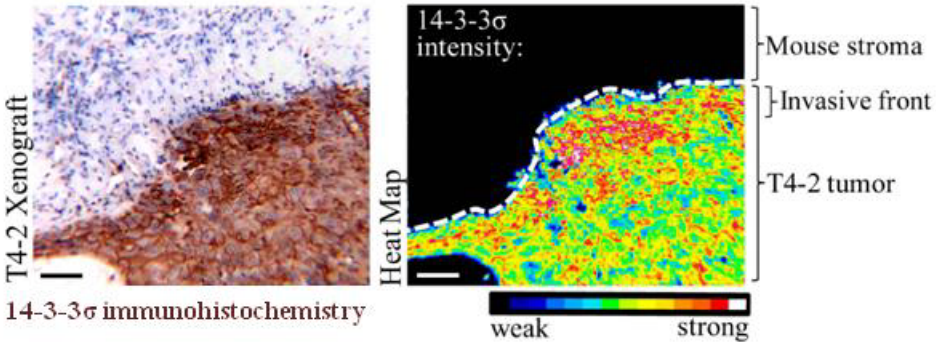

**FIGURE 8: shRNA hairpins targeting 14-3-3σ decrease T4-2 cell motility and invasiveness in culture.** T4-2 cells expressing shRNA hairpins targeting 14-3-3σ (sh-14-3-3σ) have greater than 80% reduction on the protein level (A) relative to cells expressing scrambled shRNAs (sh-scr), have decreased motility in scratch assays (B), and have decreased invasiveness through Matrigel-coated transwell inserts (C). Error bars represent the standard error of the mean (SEM), statistical significance was calculated using a two-tailed Student's t test (* $p < 0.05$, ** $p < 0.01$).

FIGURE 8: shRNA hairpins targeting 14-3-3σ decrease T4-2 cell motility and invasiveness in culture.

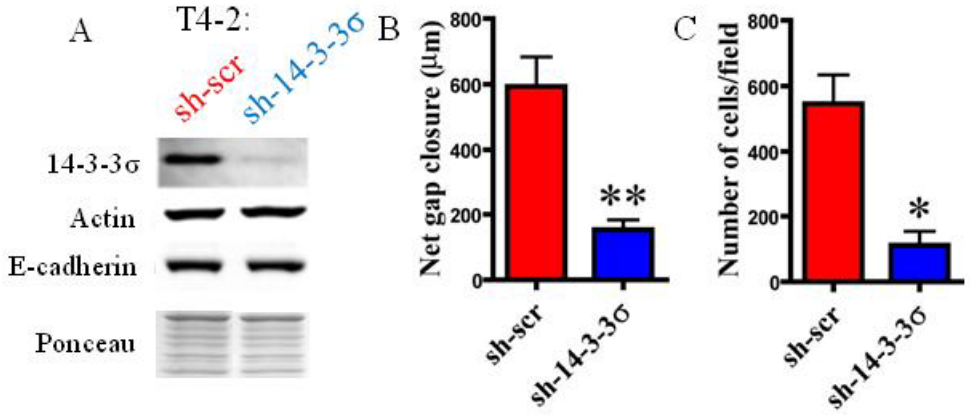

**FIGURE 9: shRNA hairpins targeting 14-3-3σ decrease T4-2 tumor invasion in vivo.** Representative H&E stains of tumors derived from T4-2 sh-scr and sh-14-3-3σ subcutaneous injection, showing the morphology of the tumor and surrounding mouse stroma. Tumors formed by injecting T4-2 sh-scr cells have poor demarcation and frequently disrupt adjacent normal tissues, whereas T4-2 sh-14-3-3σ tumors have much clearer margins and do not disrupt surrounding normal tissue architecture as frequently. Scale bar: 100 μm.

FIGURE 9: shRNA hairpins targeting 14-3-3σ decrease T4-2 tumor invasion in vivo.

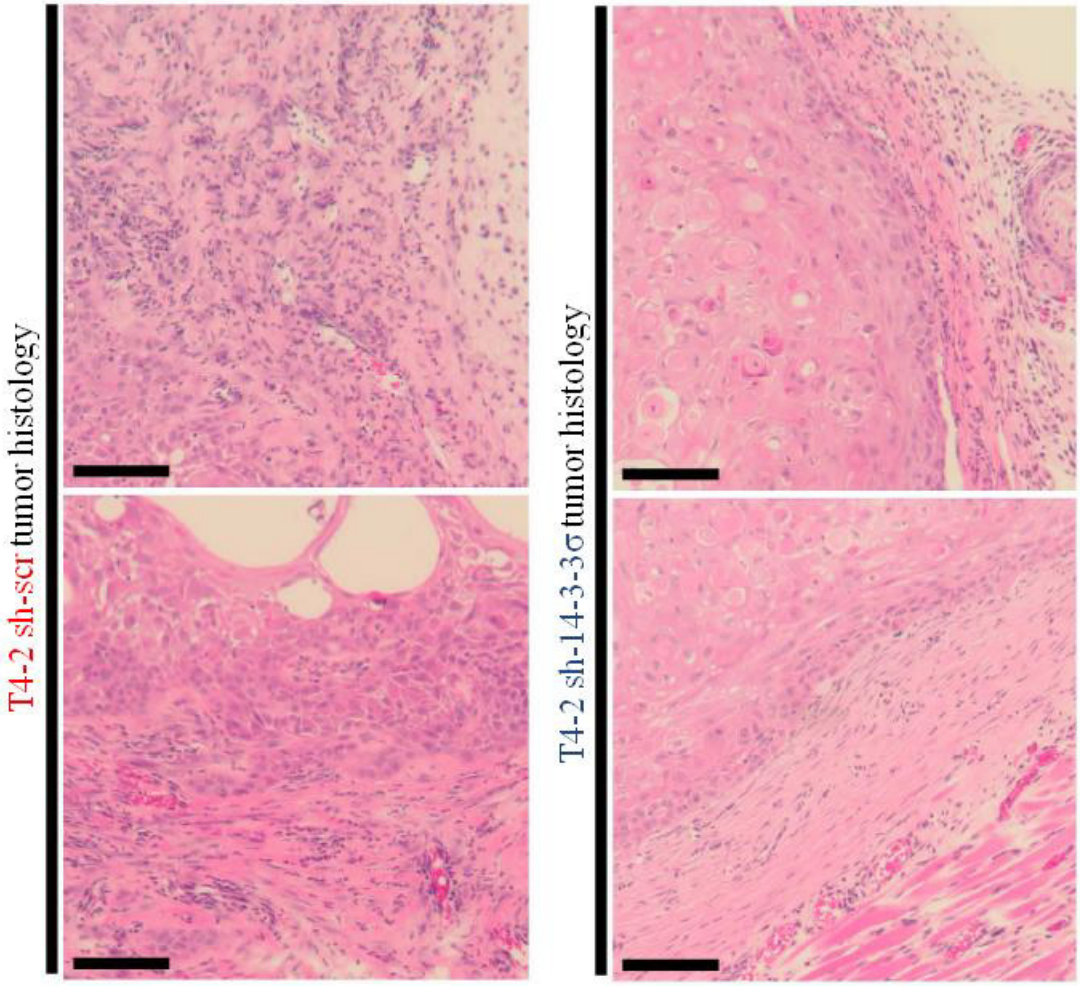

FIGURE 9 (cont.):.

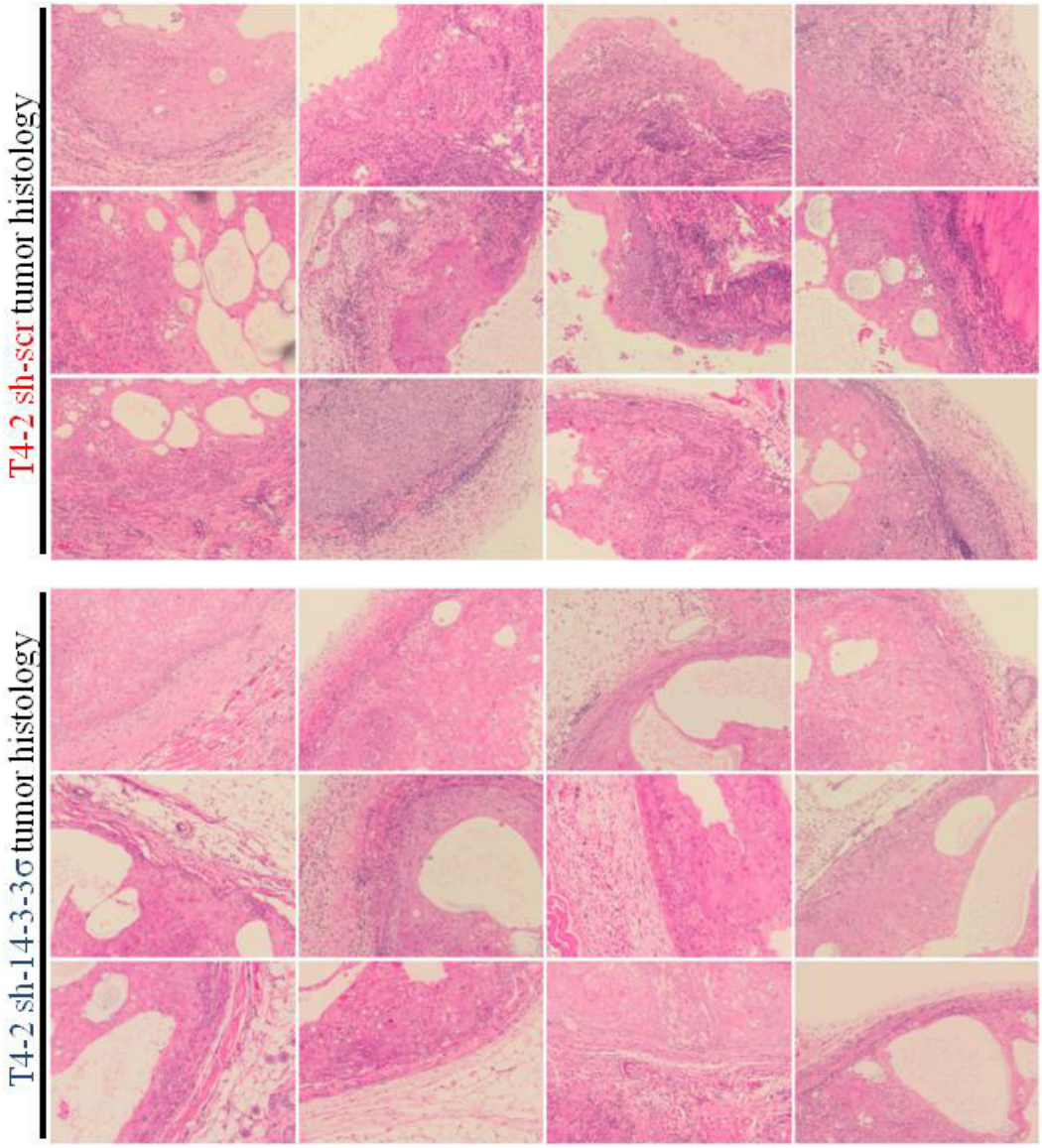

**FIGURE 10: 14-3-3σ knockdown does not influence proliferation in culture or in vivo.** Proliferation of cells in culture (A) and in vivo (B) was not significantly different in the T4-2 sh-14-3-3σ cells relative to the control T4-2 sh-scr cells, as shown by BrdU incorporation and Ki-67 immunohistochemistry, respectively. Examples of nuclei scored as Ki-67 positive (black arrows) and negative (white arrows) are indicated. Error bars represent the standard error of the mean (SEM). (C) T4-2 sh-14-3-3σ cells do not have altered tumor volume in vivo. Tumor growth was measured three times a week. Solid lines represent the best fit exponential growth curve, error bars represent the SEM.

FIGURE 10: 14-3-3σ knockdown does not influence proliferation in culture or in vivo.

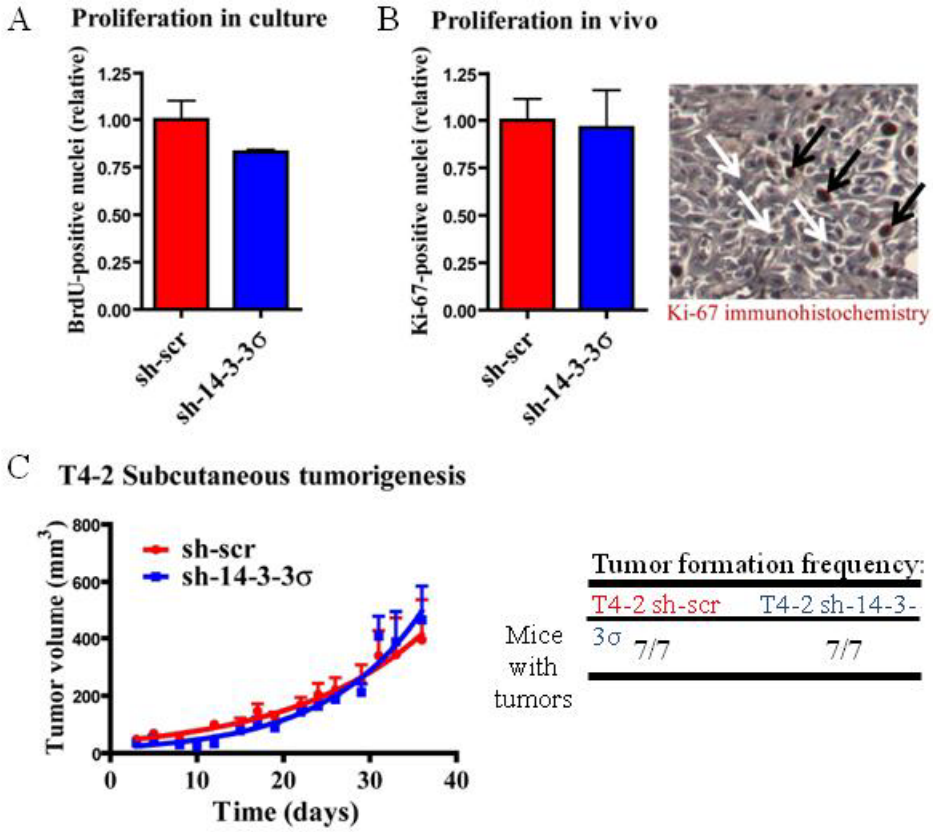


| | Tumor formation frequency: | |
|---|---|---|
| | T4-2 sh-scr | T4-2 sh-14-3-3σ |
| Mice with tumors | 7/7 | 7/7 |

**FIGURE 11: 14-3-3σ contributes to MCF10DCIS cell motility and stellate morphogenesis.** (A) MCF10DCIS.com cells espressing shRNA hairpins (sh-14-3-3σ) targeting 14-3-3σ have greater than 80% reduction on the protein level relative to a scrambled shRNA (sh-scr), have decreased motility in scratch assays (B), and have decreased numbers of invasive and migratory projections per colony when cultured on 3D reconstituted basement membrane (C). Error bars represent the standard error of the mean (SEM), statistical significance was calculated using a two-tailed Student's t test (** $p < 0.01$, *** $p < 0.001$).

FIGURE 11: 14-3-3σ contributes to MCF10DCIS motility and stellate morphogenesis.

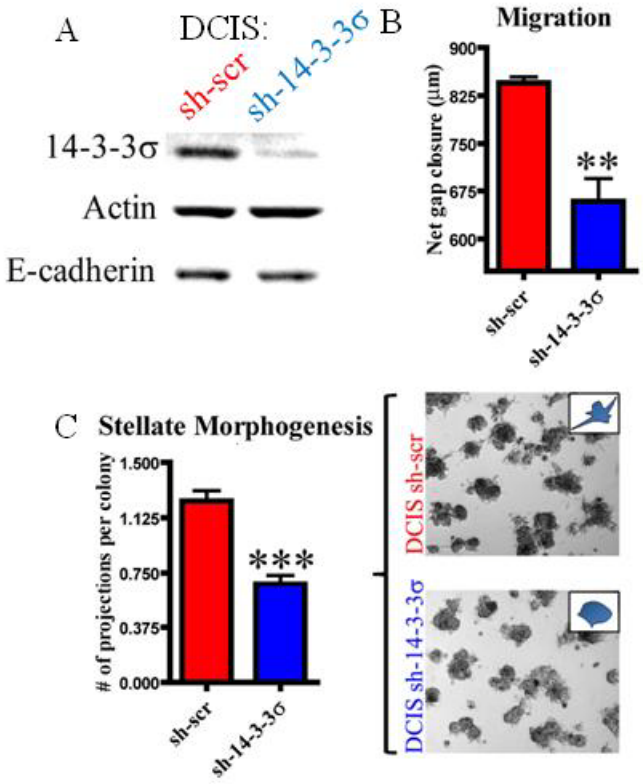

**FIGURE 12: 14-3-3σ shRNA decreases MDA-MB-231 cell migration and invasion without influencing proliferation.** MDA-MB-231 cells espressing shRNA hairpins (sh-14-3-3σ) targeting 14-3-3σ have decreased invasion through Matrigel-coated transwell inserts (A) and decreased chemotaxis towards serum (B) than control cells, but show no differences in proliferation as measured by BrdU incorporation (C). Error bars represent the standard error of the mean (SEM), statistical significance was calculated using a two-tailed Student's t test (* $p < 0.05$, ** $p < 0.01$).

FIGURE 12: 14-3-3σ shRNA decreases MDA-MB-231 cell migration and invasion without influencing proliferation.

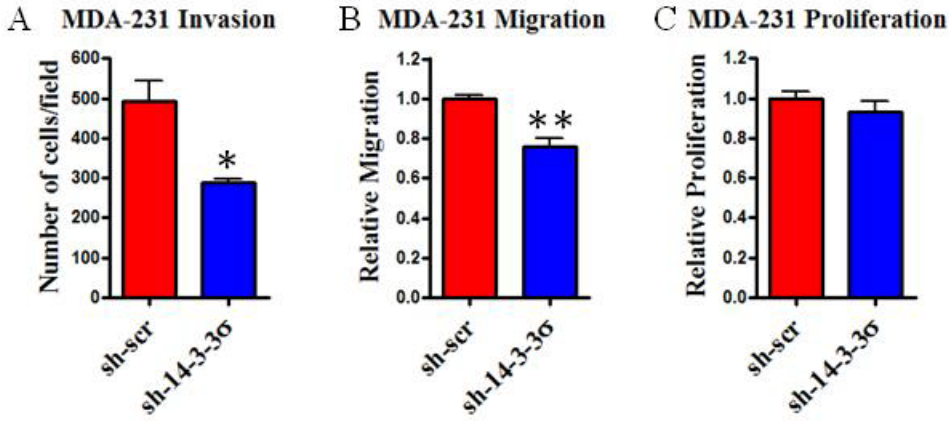

**FIGURE 13: 14-3-3σ knockdown influences motility and invasion without influencing cellular adhesion.** Knockdown and control cells were cultured until 40% confluent, fixed, and stained for the presence of F-actin and beta-catenin at cellular junctions as a measure of cellular adhesion. Junctions were slightly more discontinuous in knockdown cells than control, suggesting the decreased motility and invasion in knockdown cells is not due to increased cellular adhesion.

FIGURE 13: 14-3-3σ knockdown influences motility and invasion without influencing cellular adhesion.

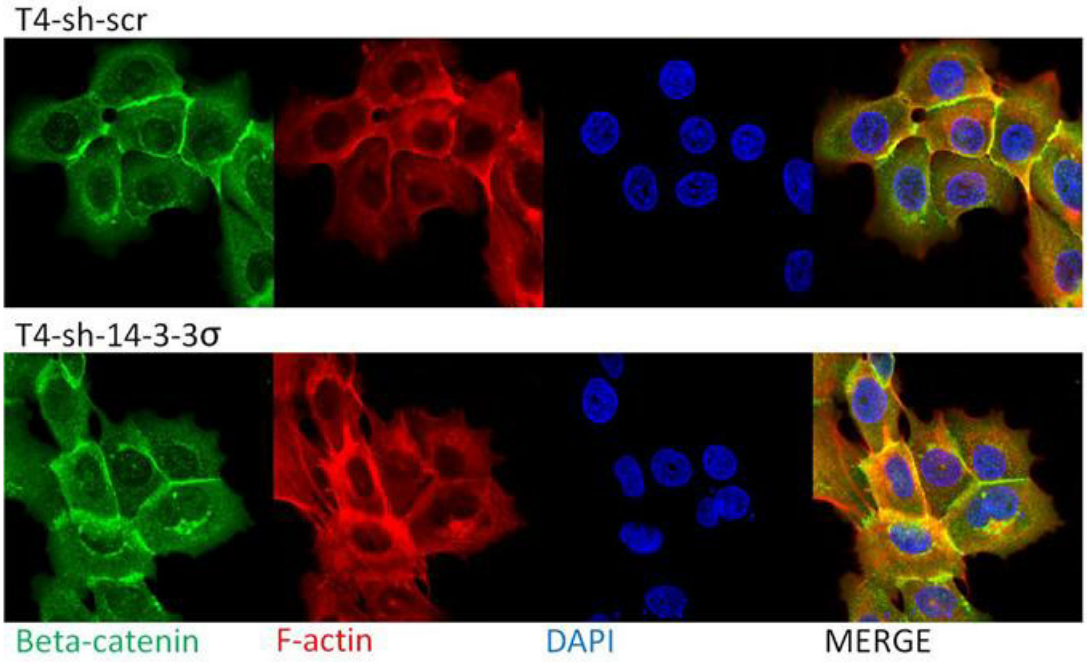

**FIGURE 14: 14-3-3σ knockdown deregulates actin polymerization.** Phalloidin immunofluorescence, showing T4-2 cells with reduced 14-3-3σ (sh-14-3-3σ) have more polymerized actin than cells expressing scrambled hairpins (sh-scr) independent of changes in actin protein levels (see Figure 8). Scale bar: 20μm.

FIGURE 14: 14-3-3σ knockdown deregulates actin polymerization.

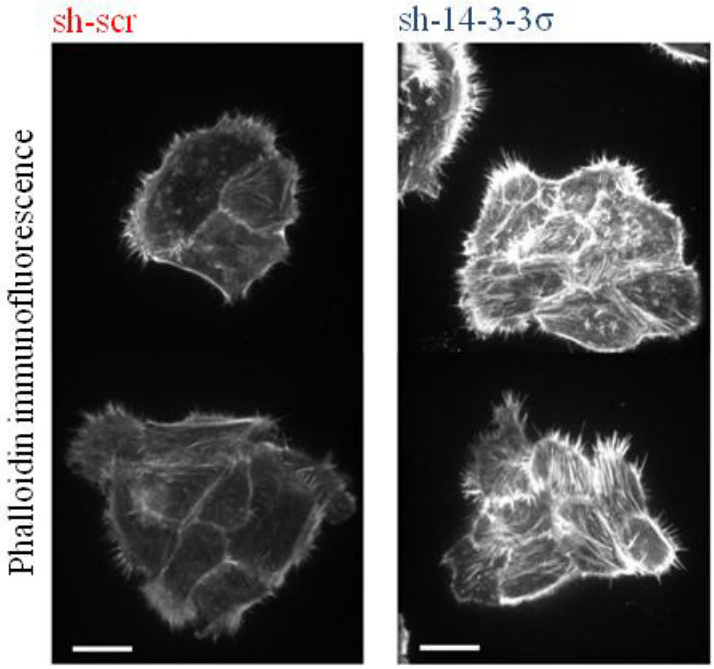

**FIGURE 15: Wild-type 14-3-3σ expression rescues the actin phenotype, while a C-terminal truncation does not.** (A) Schematic depicting the structure of the 14-3-3σ expression constructs, as well as regions influenced in the 14-3-3$\sigma^{\Delta c}$ mutant which is able to dimerize but predicted to be deficient in ligand binding. (B) Phalloidin immunofluorescence depicting the amount of polymeric actin present in the knockdown cells overexpressing an irrelevant gene (Gus) or the 14-3-3σ constructs. Only the wild-type 14-3-3σ is able to rescue the deregulation of actin. Scale bar: 20μm. (C) Quantification of the phalloidin intensity in >20 cells for shRNA and rescue cell lines. Error bars represent the standard error of the mean, statistical significance was measured using a one-way analysis of variance with Bonferroni post-test (* $p < 0.05$, ** $p< 0.01$). Note that the difference in phalloidin intensity between sh-scr versus sh-14-3-3σ + 14-3-3σ was not statistically significant.

FIGURE 15: Wild-type 14-3-3σ expression rescues the actin phenotype, while a C-terminal truncation does not.

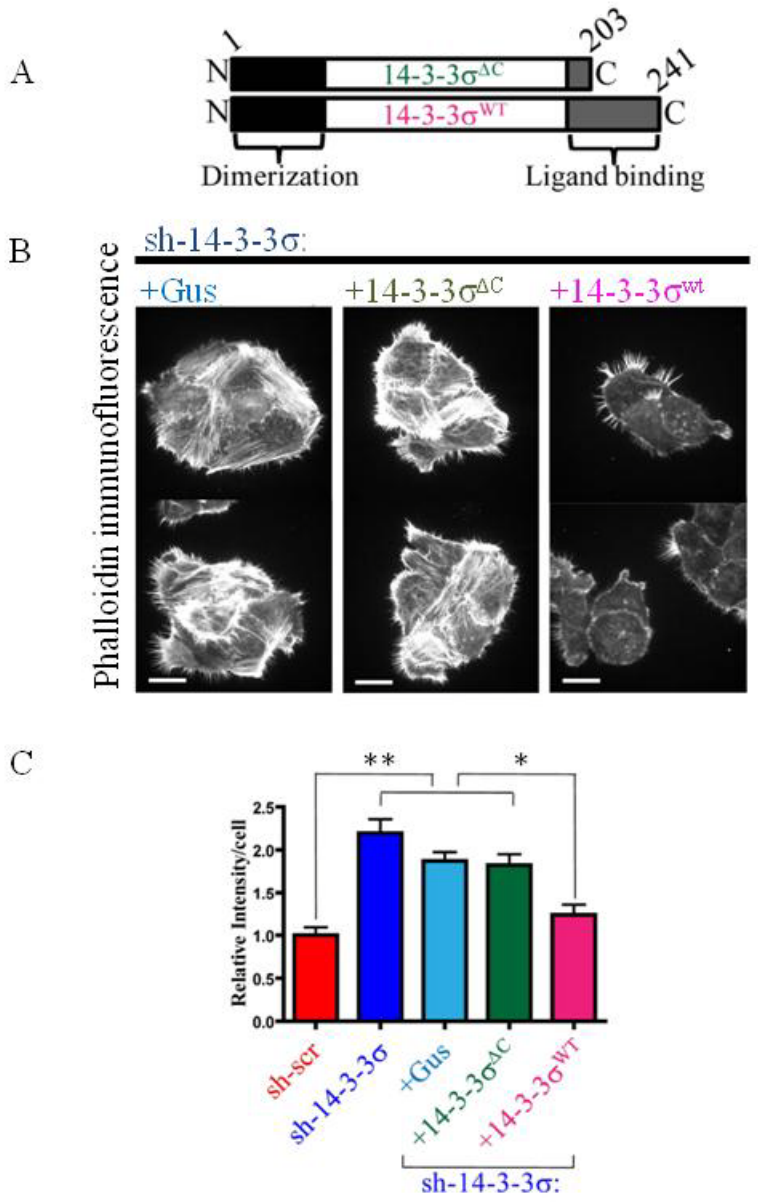

**FIGURE 16: The truncated 14-3-3σ does not act as a dominant negative 14-3-3 with respect to migration and invasion.** (A) Lysates from cell lines expressing the 14-3-3σ constructs were resolved by SDS-PAGE and analyzed for transgene expression using an antibody specifically recognizing the N-terminus of 14-3-3σ (clone N-14; Santa Cruz). Cell lines had transgene expression comparable to endogenous 14-3-3σ levels, but showed no statistically significant differences in transwell migration (B) or Matrigel invasion (C) assays.

FIGURE 16: The truncated 14-3-3σ does not act as a dominant negative 14-3-3 with respect to migration and invasion.

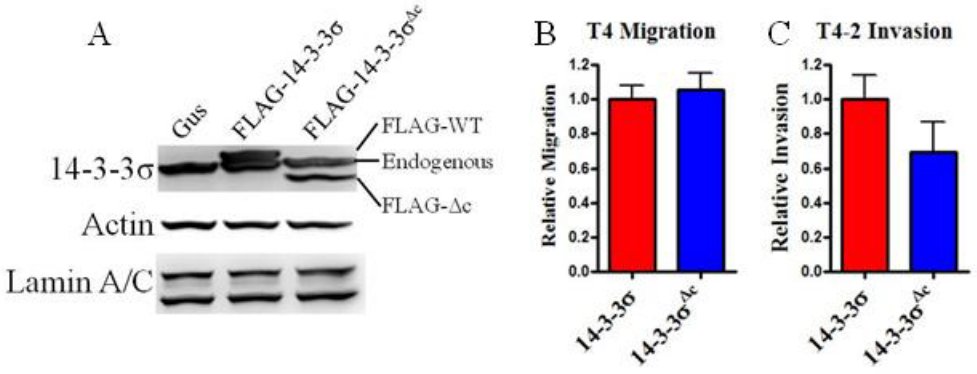

**FIGURE 17: 14-3-3σ regulates actin dynamics downstream of canonical cytoskeletal signaling pathways.** Lysates from sh-14-3-3σ and control cells were resolved by SDS-PAGE and the activity of various signaling molecules implicated in actin dynamics and epithelial to mesenchymal transition were assessed by western blot analysis. Alternatively, the activity of small GTPases (Rac1, RhoA, and cdc42) was assessed as described in the Materials and Methods by performing pull-down assays with GST-PAK1 (Rac1 and cdc42) or GST-RBD (RhoA) prior to SDS-PAGE. No dramatic differences in the activity of any of the biomolecules measured were noted in the knockdown cells.

FIGURE 17: 14-3-3σ regulates actin dynamics downstream of canonical cytoskeletal signaling pathways.

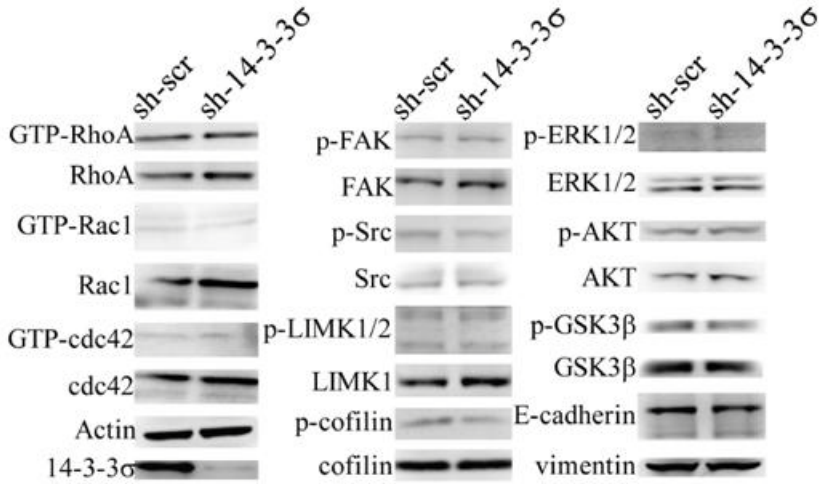

**FIGURE 18: LifeAct decorates F-actin and is mutually exclusive from YFP-14-3-3σ, similar to endogenous F-actin and 14-3-3σ.** (A) Merged green (YFP-14-3-3σ) and red (mCherry) channels in live cells, showing the localization of untagged mCherry (upper panel) versus Lifeact-mCherry (lower panel). Untagged mCherry localizes throughout the cell, whereas LifeAct-mCherry preferentially localizes to actin filaments and is mutually-exclusive from YFP-14-3-3σ similar to the distribution of endogenous 14-3-3σ and F-actin (B). Scale bar: 10μm.

FIGURE 18: LifeAct decorates F-actin and is mutually exclusive from YFP-14-3-3σ, similar to endogenous F-actin and 14-3-3σ.

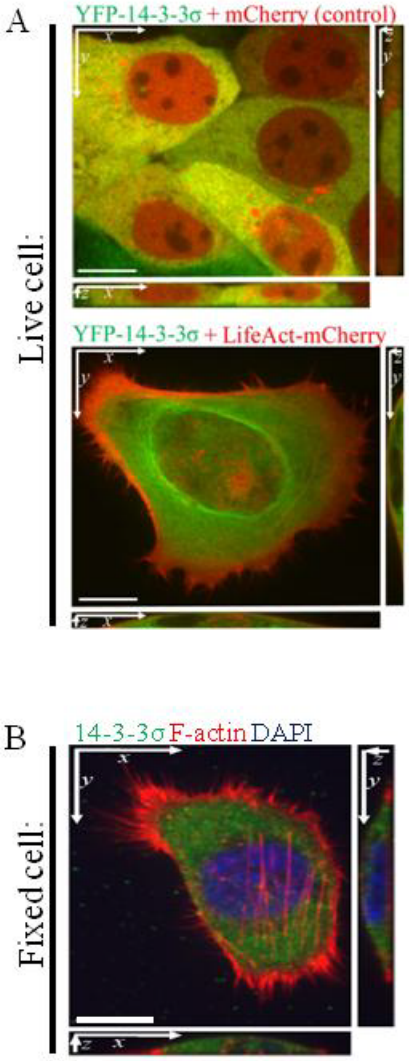

**FIGURE 19: YFP-14-3-3σ localizes away from the F-actin-rich leading edge of a cell during migration.** Representative live cell imaging of a cell expressing LifeAct-mCherry and YFP-14-3-3σ as it migrates over time. Most 14-3-3σ localizes away from the migratory front of the cell, while rapid F-actin remodeling occurs either as lamellipod extension and retraction at the leading edge or as actin turnover at the trailing edge of the cell (A). The 14-3-3σ and F-actin subcellular polarity is emphasized by converting the channels into a differential heat map (B). Black arrows: cell trajectory. Scale Bar: 10μm.

FIGURE 19: YFP-14-3-3σ localizes away from the F-actin-rich leading edge of a cell during migration.

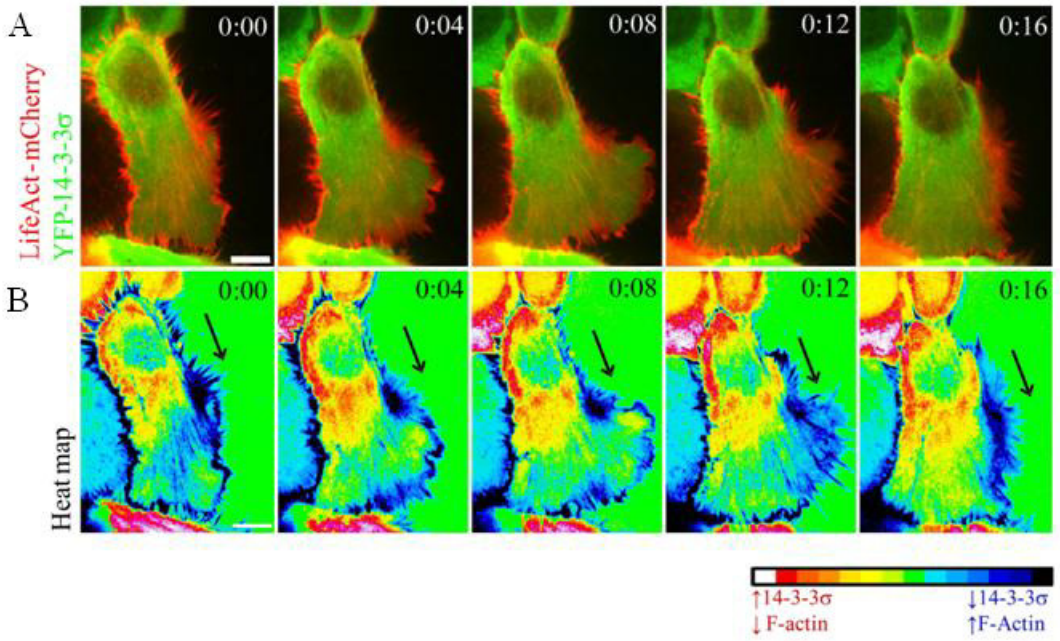

**FIGURE 20: YFP-14-3-3σ subcellular polarity persists throughout cell migration.** Representative pictures of cells expressing YFP-14-3-3σ and LifeAct-mCherry and which are actively migrating after 24 hours. The F-actin and 14-3-3σ distributions remain polarized, suggesting that continual (rather than transient) 14-3-3σ polarization occurs throughout cell migration. Black arrows: trajectory of cells. Scale bar: 20μm.

FIGURE 20: YFP-14-3-3σ subcellular polarity persists throughout cell migration.

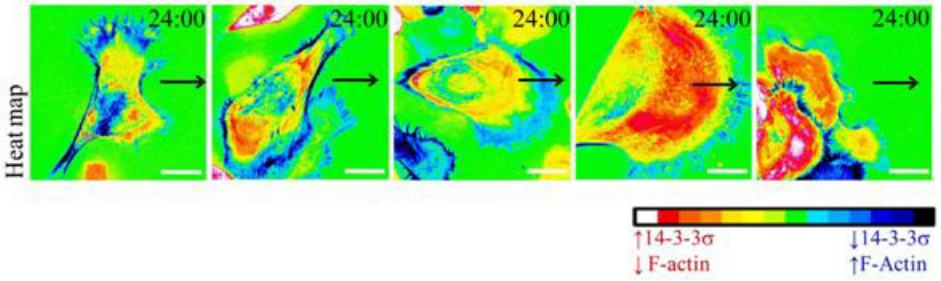

**FIGURE 21: Endogenous 14-3-3σ similarly polarizes away from F-actin during cell migration.** T4-2 cells were grown to a confluent monolayer, scratched with a pipet tip, and migratory cells were fixed and stained 16 hours later to measure endogenous F-actin and 14-3-3σ distributions. Migratory cells facing the scratch area are polarized such that 14-3-3σ is away from the leading edge of cell migration, whereas stationary cells far from the scratch area show no 14-3-3σ polarization. Black arrows: trajectory of cells. Scale bar: 20μm.

FIGURE 21: Endogenous 14-3-3σ similarly polarizes away from F-actin during cell migration.

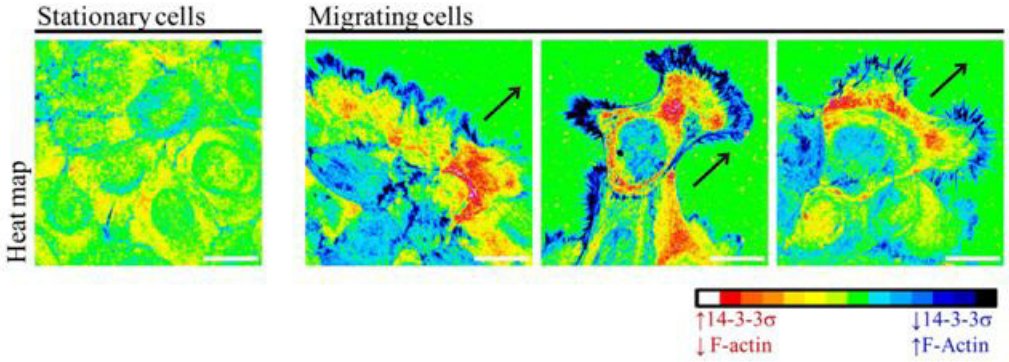

**FIGURE 22: Actin filaments in sh-14-3-3σ cells are more dynamic than in control cells.** (A) Photobleach and fluorescence recovery in a peripheral actin fiber decorated with LifeAct-mCherry, a live cell phalloidin (Riedl et al., 2008). Recovery to equilibrium was reached within ~3 seconds. (B) An example fluorescence recovery curve of the boxed region from (A), in comparison to the lack of recovery observed in a fixed cell (inset). (C) FRAP kinetic constants in cells expressing shRNAs targeting 14-3-3σ versus scrambled control as measured in >20 cells. Knockdown cells show ~2-fold more rapid fluorescence recovery, indicating the F-actin turnover is much more rapid in these cells and supporting that the actin phenotype (Figure 14) is most likely an increased polymerization rate rather than suppressed depolymerization.

FIGURE 22: Actin filaments in sh-14-3-3σ cells are more dynamic than in control cells.

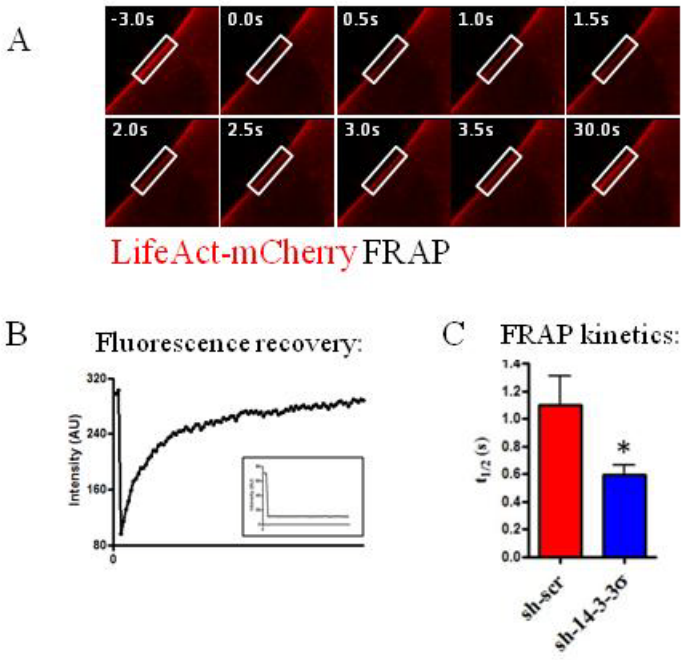

**FIGURE 23: The increased actin filament turnover observed in sh-14-3-3σ cells decreases the pool of soluble actin.** (A) T4-2 sh-14-3-3σ and control cells were grown to 70% confluence, lysed in buffer containing 1% Triton X-100, and the Triton-soluble and insoluble cell fractions were resolved by SDS-PAGE and analyzed for actin expression by western blot. The ratio of soluble to insoluble actin for three independent experiments is shown (B), with knockdown cells having over 2-fold less soluble actin. Error bars represent the standard error of the mean (SEM), statistical significance was calculated using a two-tailed Student's t test (* $p < 0.05$).

FIGURE 23: The increased actin filament turnover observed in sh-14-3-3σ cells decreases the pool of soluble actin.

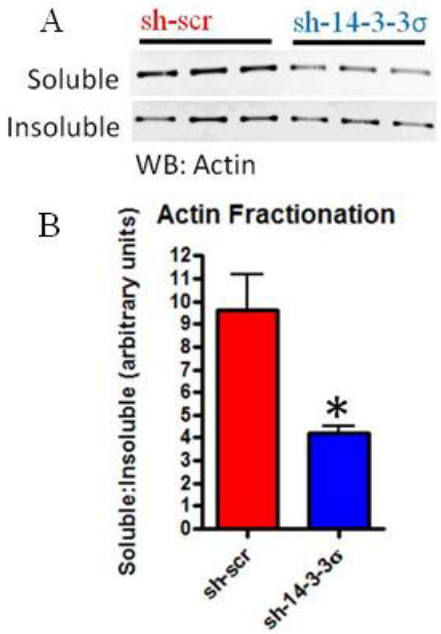

**FIGURE 24: Overexpression of actin, but not a mutant unable to polymerize, rescues migration and invasion in sh-14-3-3σ cells.** 14-3-3σ knockdown cells were stably infected with lentiviruses encoding Gus, wild-type actin, or an actin mutant (R62D) that is unable to polymerize into F-actin (Posern et al., 2002). Expression of wild-type actin restores the pool of polymerization-competent G-actin in knockdown cells and thus rescues the motility (A) and invasion (B) of the cells, whereas the mutant (R62D) protein is unable to. Error bars represent the standard error of the mean, statistical significance was measured using a one-way analysis of variance with Bonferroni post-test (* $p < 0.05$, ** $p < 0.01$). Note that the differences in migration and invasion between cells expressing Gus versus actin (R62D) were not statistically significant.

FIGURE 24: Overexpression of actin, but not a mutant unable to polymerize, rescues migration and invasion in sh-14-3-3σ cells.

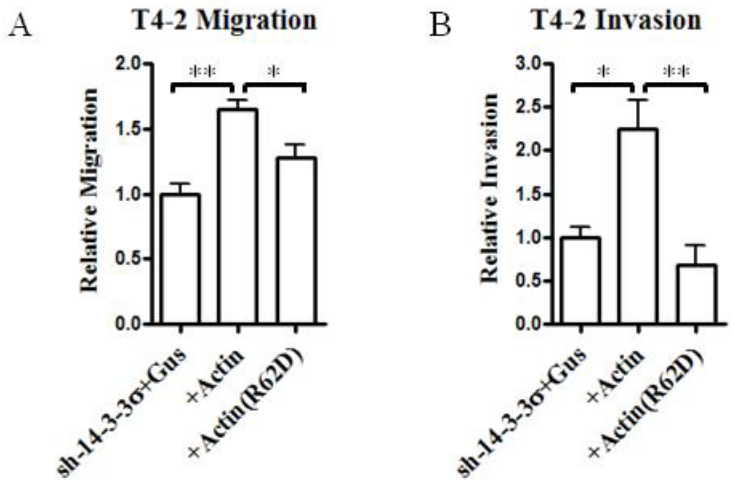

**FIGURE 25: 14-3-3σ interacts directly with actin in cells and in vitro.** (A) T4-2 cells expressing FLAG-14-3-3σ and FLAG-14-3-3$\sigma^{\Delta c}$ were lyzed, and FLAG-tagged proteins and their interacting partners were affinity purified then resolved by SDS-PAGE. Only wild-type 14-3-3σ formed stable complexes with actin despite both the wild-type and the truncated mutant being able to interact with endogenous 14-3-3σ (shown by the asterisk), suggesting that two functional 14-3-3σ monomers are required for stable actin interaction. IP: immunoprecipitation. IB: western blot. (B) A GST pull-down experiment, showing that recombinant GST-14-3-3σ, but not GST tag, interacts directly with purified actin in vitro. Proteins were resolved by SDS-PAGE and visualized by silver staining.

FIGURE 25: 14-3-3σ interacts directly with actin in cells and in vitro.

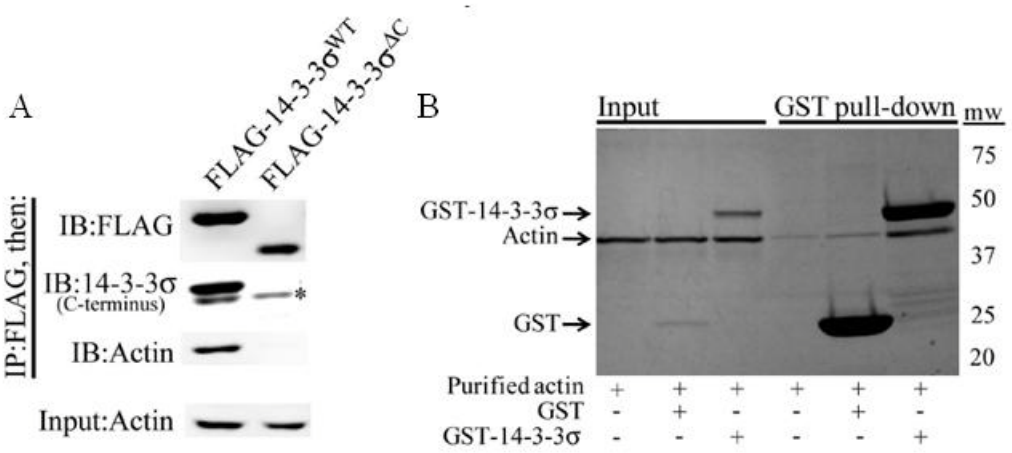

**FIGURE 26: 14-3-3σ inhibits actin polymerization in vitro.** Pretreating G-actin with GST-14-3-3σ inhibits subsequent polymerization into F-actin. This was observed by (A) fractionating the residual G-actin from F-actin following polymerization by ultracentrifugation, and by (B) polymerizing AlexaFluor488-conjugated G-actin (488-G-actin) and imaging F-actin fibrils by confocal microscopy. Depicted is the maximum intensity projection of 20 superimposed fields. The quantification shown (C) is the residual G-actin pool remaining following polymerization of unconjugated actin from (A). Error bars represent the standard error of the mean (SEM), statistical significance was calculated using a two-tailed Student's t test (*** $p < 0.001$).

FIGURE 26: 14-3-3σ inhibits actin polymerization in vitro.

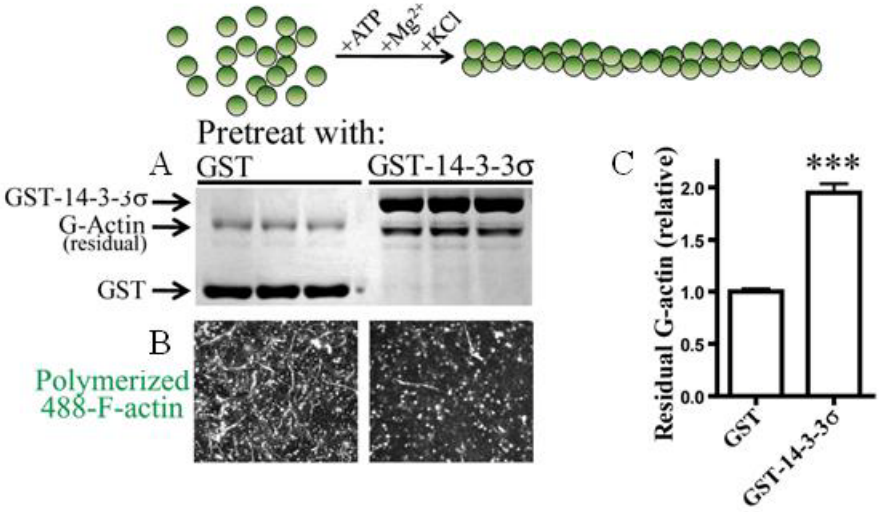

**FIGURE 27: 14-3-3σ inhibits actin polymerization in situ.** De novo actin polymerization was measured by permeabilizing cells with saponin, introducing 488-G-actin in the presence of ATP, fixing the cells, then counterstaining endogenous F-actin with phalloidin. Pretreatment with GST-14-3-3σ significantly inhibits 488-G-actin incorporation in cells with low endogenous 14-3-3σ (BT549). The quantification shown is the ratio of incorporated 488-G-actin to endogenous F-actin, relative to values obtained by pretreating 488-G-actin with GST in the respective cell lines. Error bars represent the standard error of the mean (SEM), statistical significance was calculated using a two-tailed Student's t test (*** $p < 0.001$).

FIGURE 27: 14-3-3σ inhibits actin polymerization in situ.

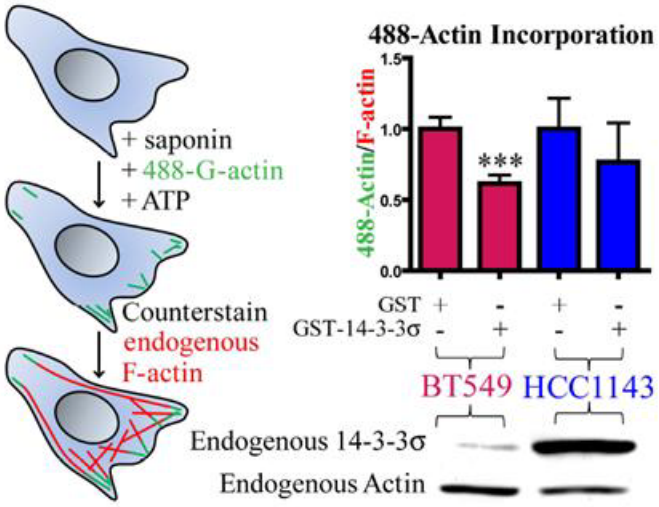

**FIGURE 28: 14-3-3σ decreases the maximum rate of pyrene actin polymerization and shifts the equilibrium towards G-actin.** The pyrene actin polymerization kinetics are markedly different in the presence of GST versus GST-14-3-3σ. GST-14-3-3σ decreases the maximum rate of polymerization (apparent by the decreased slope of the linear region prior to the plateau in the curves) and shifts the equilibrium towards more G-actin (decreased height of the plateau in the GST-14-3-3σ curve). Fluorescence ($A_{410}$) measurements were conducted in 30s intervals in triplicate. Error bars represent the standard error of the mean (SEM), statistical significance was calculated using a two-tailed Student's t test for every time point (* $p < 0.05$, ** $p < 0.01$, *** $p < 0.001$).

FIGURE 28: 14-3-3σ decreases the maximum rate of pyrene actin polymerization and shifts the equilibrium towards G-actin.

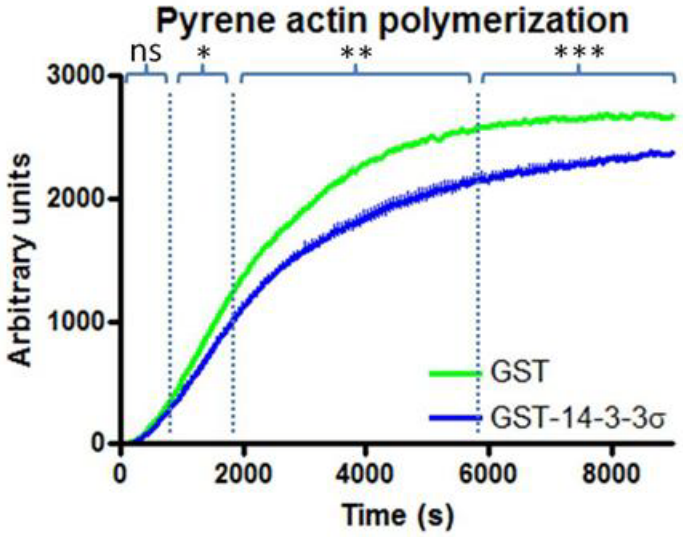

**FIGURE 29: 14-3-3σ does not inhibit actin polymerization by capping F-actin, as it does not co-sedimentation with filaments.** An actin sedimentation assay, in which actin is polymerized into F-actin (Polymerization) or left as G-actin (No polymerization), is subsequently incubated with GST-14-3-3σ, and lastly fractionated by centrifugation. The localization of 14-3-3σ to the supernatant was unchanged in the presence of F-actin (there was no co-sedimentation with actin filaments), indicating that 14-3-3σ does not interact with F-actin and thus does not inhibit actin polymerization by capping F-actin.

FIGURE 29: 14-3-3σ does not inhibit actin polymerization by capping F-actin, as it does not co-sedimentation with filaments.

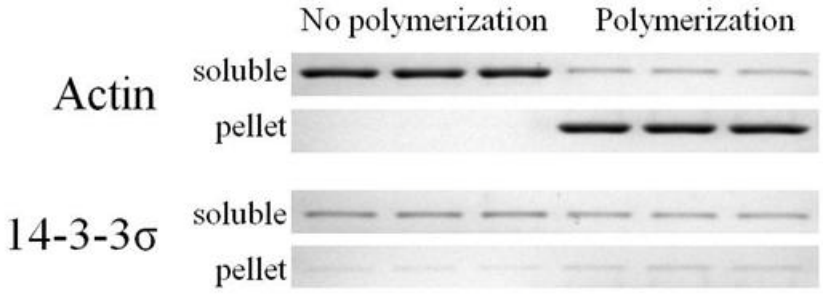

**FIGURE 30: 14-3-3σ and F-actin are mutually-exclusive, while 14-3-3σ has significant cytoplasmic colocalization with G-actin.** Cells were fixed and stained using an antibody recognizing 14-3-3σ (clone C18), a monoclonal antibody against beta-actin, and phalloidin to decorate F-actin. Both antibodies showed negligible colocalization with F-actin, validating earlier data showing that 14-3-3σ and F-actin are mutually-exclusive (Figure 18), and demonstrating that the actin mAb specifically recognizes non-filamentous actin (ie soluble actin) by immunofluorescence. In contrast, both antibodies showed a high degree of cytoplasmic colocalization (>75% for n = 10 independent cells), suggesting that 14-3-3σ colocalizes with G-actin in cells and likely inhibits actin polymerization by sequestering G-actin rather than capping actin filaments (Figures 25-29). Colocalization analysis was performed using automated thresholds detection as described in the Materials and Methods.

FIGURE 30: 14-3-3σ and F-actin are mutually-exclusive, while 14-3-3σ has significant cytoplasmic colocalization with G-actin.

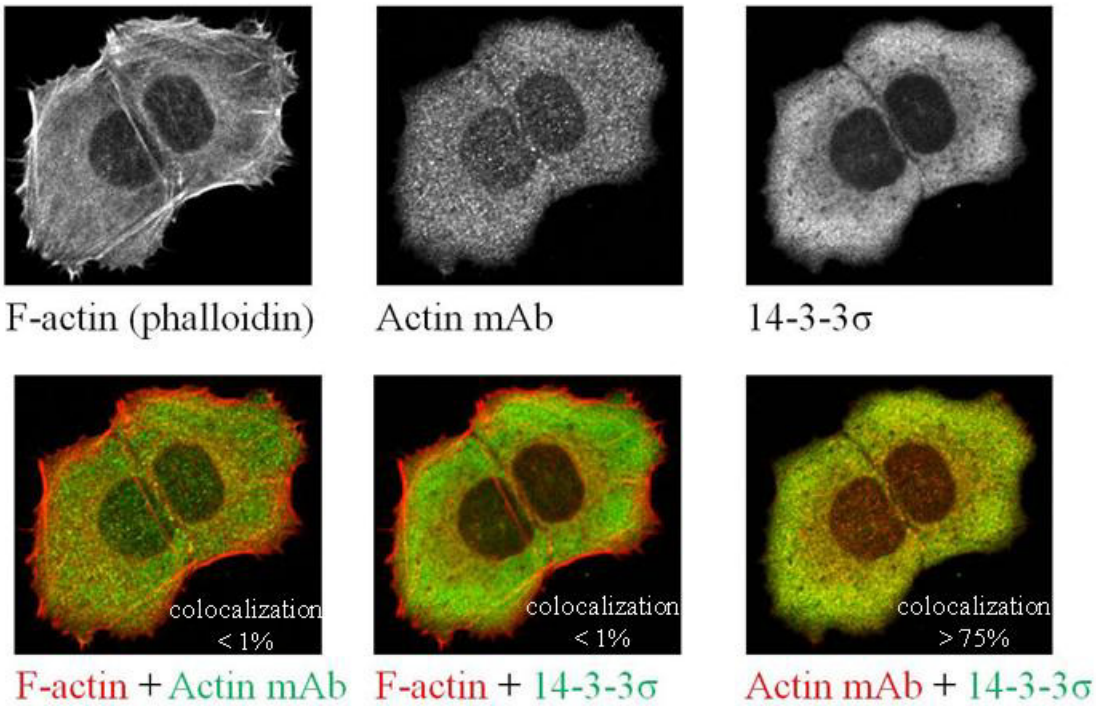

**FIGURE 31: Profilin and F-actin are mutually-exclusive, while 14-3-3σ has significant cytoplasmic colocalization with profilin.** Cells were fixed and stained using antibodies recognizing 14-3-3σ (clone C18), the G-actin binding protein, profilin, as well as phalloidin to decorate F-actin. Profilin distribution mirrors that of 14-3-3σ, as profilin and F-actin are mutually-exclusive and show no statistically significant colocalization. However, both antibodies showed a high degree of cytoplasmic colocalization (>80% for n = 10 independent cells), providing further evidence that 14-3-3σ colocalizes with G-actin and suggesting that 14-3-3σ may interact with both G-actin and profilin as a complex. Colocalization analysis was performed using automated thresholds detection as described in the Materials and Methods.

FIGURE 31: Profilin and F-actin are mutually-exclusive, while 14-3-3σ has significant cytoplasmic colocalization with profilin.

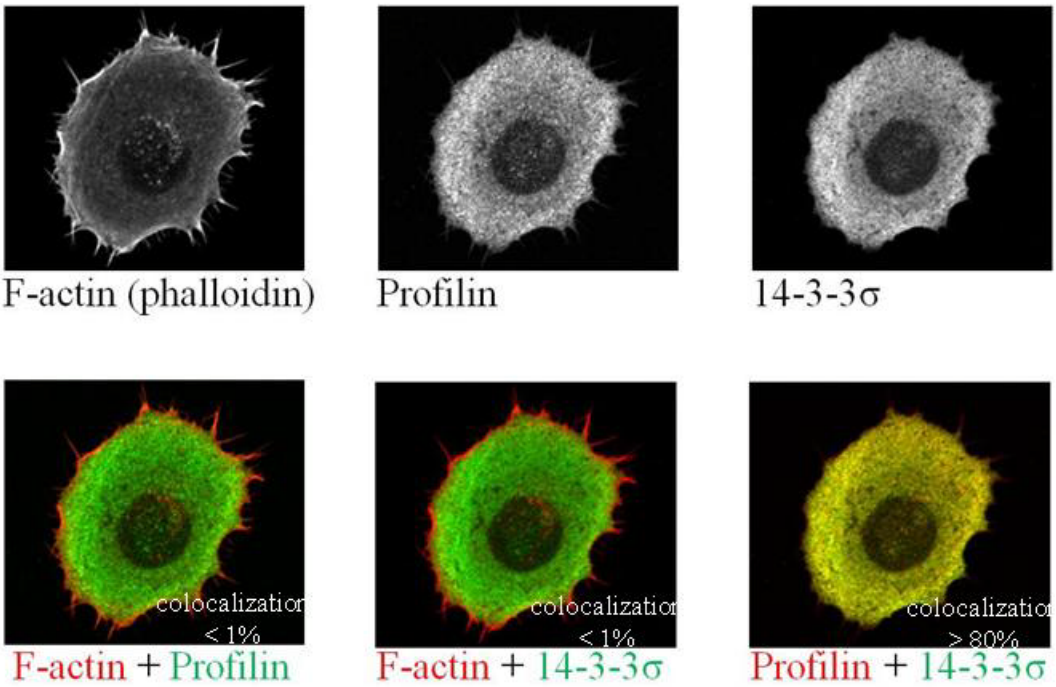

**FIGURE 32: Overexpression of profilin, but not a mutant unable to bind actin, decreases cell motility and deregulates actin polymerization.** (A) Western blot analysis of lysates from cells stably overexpressing Gus, profilin, or a mutant profilin that is unable to bind to actin (S137D) (Shao et al., 2008), showing a ~two-fold overexpression of profilin compared to endogenous levels. (B) Profilin overexpression suppresses cell migration, whereas cells expressing the mutant profilin show no statistically significant difference in migration versus cells overexpressing Gus. Error bars represent the standard error of the mean, statistical significance was measured using a one-way analysis of variance with Bonferroni post-test (* $p < 0.05$, ** $p < 0.01$). (C) Immunofluorescence of cells stained with phalloidin and an antibody recognizing profilin. Cells overexpressing profilin (top panels) have deregulated actin polymerization (similar to 14-3-3σ knockdown cells) in comparison to neighboring cells that do not overexpress profilin; this was not observed in cells expressing profilin S137D (bottom panels).

FIGURE 32: Overexpression of profilin, but not a mutant unable to bind actin, decreases cell motility and deregulates actin polymerization.

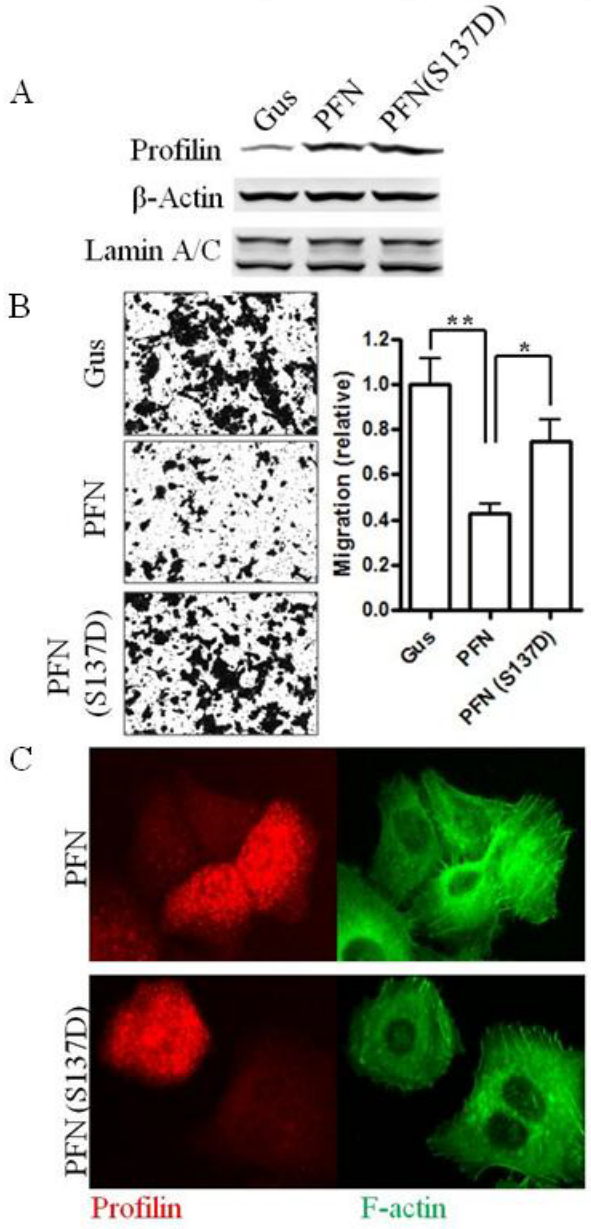

Table 1: Correlations between 14-3-3σ staining intensity, clinicopathological parameters, and other immunohistochemical markers in 245 cases of invasive breast carcinoma.

| Parameter | | N | 14-3-3σ negative | 14-3-3σ strong | P value |
|---|---|---|---|---|---|
| **Size – TNM** | | 198 | | | NS * |
| | T1 | | 84 | 17 | |
| | T2 | | 70 | 13 | |
| | T3 | | 12 | 2 | |
| **Grade** | | 194 | | | 0.0010 ** |
| | 1 | | 18 | 0 | |
| | 2 | | 53 | 3 | |
| | 3 | | 91 | 29 | |
| **Type** | | 197 | | | NS * |
| | IDC | | 118 | 26 | |
| | ILC | | 29 | 1 | |
| | Mixed | | 12 | 3 | |
| | Other | | 6 | 2 | |
| **LVI** | | 197 | | | NS ** |
| | - | | 53 | 11 | |
| | + | | 112 | 21 | |
| **LN mets** | | 192 | | | NS ** |
| | - | | 53 | 12 | |
| | + | | 107 | 20 | |
| **ER** | | 195 | | | <0.0001 ** |
| | - | | 19 | 17 | |
| | + | | 144 | 15 | |
| **PgR** | | 195 | | | <0.0001 ** |
| | - | | 33 | 19 | |
| | + | | 130 | 13 | |
| **HER2** | | 193 | | | NS ** |
| | - | | 135 | 30 | |
| | + | | 26 | 2 | |
| ***HER2* CISH** | | 188 | | | NS ** |
| | Not amp | | 131 | 29 | |
| | Amp | | 27 | 1 | |
| **EGFR** | | 198 | | | <0.0001 ** |
| | - | | 160 | 21 | |
| | + | | 6 | 11 | |
| **Ck 14** | | 197 | | | <0.0001 ** |
| | - | | 160 | 22 | |
| | + | | 5 | 10 | |
| **Ck 5/6** | | 191 | | | <0.0001 ** |
| | - | | 155 | 17 | |
| | + | | 7 | 12 | |
| **Ck 17** | | 195 | | | <0.0001 ** |
| | - | | 153 | 20 | |
| | + | | 10 | 12 | |
| **Basal cytokeratins** | | 197 | | | <0.0001 ** |
| | - | | 153 | 16 | |
| | + | | 12 | 16 | |
| **Basal cytokeratins or EGFR** | | 197 | | | <0.0001 ** |
| | - | | 152 | 13 | |
| | + | | 13 | 19 | |

| Parameter | | N | 14-3-3σ negative | 14-3-3σ strong | P value |
|---|---|---|---|---|---|
| **Nielsen groups** | | 187 | | | <0.0001 * |
| | Basal | | 7 | 16 | |
| | Luminal | | 122 | 14 | |
| | HER2 | | 27 | 1 | |
| **Triple negative** | | 195 | | | <0.0001 ** |
| | No | | 152 | 19 | |
| | Yes | | 11 | 13 | |
| **P53** | | 186 | | | 0.0275 ** |
| | - | | 117 | 17 | |
| | + | | 38 | 14 | |
| **Ki-67** | | 186 | | | 0.0001 * |
| | <10% | | 69 | 8 | |
| | 10-30% | | 71 | 11 | |
| | >30% | | 15 | 12 | |
| **Topoisomerase IIα** | | 178 | | | 0.0017 ** |
| | Low | | 82 | 6 | |
| | High | | 68 | 22 | |
| ***TOP2A* CISH** | | 190 | | | NS ** |
| | Not amp | | 141 | 32 | |
| | Amp | | 17 | 0 | |
| **Cyclin D1** | | 186 | | | <0.0001 * |
| | Low | | 11 | 10 | |
| | Intermediate | | 32 | 7 | |
| | High | | 113 | 13 | |
| ***CCND1* CISH** | | 168 | | | NS ** |
| | Not amp | | 114 | 26 | |
| | Amp | | 26 | 2 | |
| ***MYC* CISH** | | 165 | | | NS ** |
| | Not amp | | 124 | 24 | |
| | Amp | | 14 | 3 | |
| **Caveolin 1** | | 198 | | | <0.0001 ** |
| | - | | 158 | 22 | |
| | + | | 8 | 10 | |
| **Caveolin 2** | | 179 | | | 0.0023 ** |
| | - | | 146 | 22 | |
| | + | | 5 | 6 | |
| **FOXA1** | | 158 | | | 0.0318 ** |
| | - | | 28 | 10 | |
| | + | | 107 | 13 | |

Ck: cytokeratin; ER: estrogen receptor; IDC: invasive ductal carcinoma; ILC: invasive lobular carcinoma; LN mets: lymph node metastasis; LVI: lympho-vascular invasion; Nielsen groups: immunophenotypic groups defined based upon the expression of ER, HER2, Ck 5/6 and EGFR; PgR: progesterone receptor

*: $\chi^2$ p values (two-tailed, 95% confidence interval)

**: Fisher's exact test p values (two-tailed, 95% confidence interval)

Table 2: Correlations between 14-3-3σ nuclear staining, clinicopathological parameters, and other immunohistochemical markers in 245 cases of invasive breast carcinoma.

| Parameter | | N | 14-3-3σ negative | 14-3-3σ (nucleus) | P value |
|---|---|---|---|---|---|
| **Size – TNM** | | 198 | | | NS * |
| | T1 | | 64 | 37 | |
| | T2 | | 41 | 42 | |
| | T3 | | 11 | 3 | |
| **Grade** | | 194 | | | NS * |
| | 1 | | 12 | 6 | |
| | 2 | | 37 | 19 | |
| | 3 | | 64 | 56 | |
| **Type** | | 197 | | | NS * |
| | IDC | | 89 | 55 | |
| | ILC | | 17 | 13 | |
| | Mixed | | 6 | 9 | |
| | Other | | 4 | 4 | |
| **LVI** | | 197 | | | NS ** |
| | - | | 42 | 22 | |
| | + | | 73 | 60 | |
| **LN mets** | | 192 | | | NS ** |
| | - | | 33 | 32 | |
| | + | | 80 | 47 | |
| **ER** | | 195 | | | 0.0229 ** |
| | - | | 15 | 21 | |
| | + | | 98 | 61 | |
| **PgR** | | 195 | | | NS ** |
| | - | | 30 | 22 | |
| | + | | 83 | 60 | |
| **HER2** | | 193 | | | NS ** |
| | - | | 96 | 69 | |
| | + | | 16 | 12 | |
| ***HER2* CISH** | | 188 | | | NS ** |
| | Not amp | | 96 | 64 | |
| | Amp | | 14 | 14 | |
| **EGFR** | | 198 | | | NS ** |
| | - | | 109 | 72 | |
| | + | | 7 | 10 | |
| **Ck 14** | | 197 | | | NS ** |
| | - | | 108 | 74 | |
| | + | | 7 | 8 | |
| **Ck 5/6** | | 191 | | | 0.0378 ** |
| | - | | 105 | 67 | |
| | + | | 7 | 12 | |
| **Ck 17** | | 195 | | | 0.00151 ** |
| | - | | 109 | 64 | |
| | + | | 6 | 16 | |
| **Basal cytokeratins** | | 197 | | | NS ** |
| | - | | 103 | 66 | |
| | + | | 12 | 16 | |
| **Basal cytokeratins or EGFR** | | 197 | | | 0.0080 ** |
| | - | | 103 | 62 | |
| | + | | 12 | 20 | |

| Parameter | | N | 14-3-3σ negative | 14-3-3σ (nucleus) | P value |
|---|---|---|---|---|---|
| **Nielsen groups** | | 187 | | | NS * |
| | Basal | | 10 | 13 | |
| | Luminal | | 87 | 49 | |
| | HER2 | | 14 | 14 | |
| **Triple negative** | | 198 | | | NS ** |
| | No | | 109 | 71 | |
| | Yes | | 7 | 11 | |
| **P53** | | 186 | | | NS ** |
| | - | | 85 | 49 | |
| | + | | 26 | 26 | |
| **Ki-67** | | 186 | | | NS * |
| | <10% | | 50 | 27 | |
| | 10-30% | | 42 | 40 | |
| | >30% | | 17 | 10 | |
| **Topoisomerase IIα** | | 178 | | | NS ** |
| | Low | | 46 | 42 | |
| | High | | 58 | 32 | |
| ***TOP2A* CISH** | | 190 | | | NS ** |
| | Not amp | | 101 | 72 | |
| | Amp | | 9 | 8 | |
| **Cyclin D1** | | 186 | | | 0.0322 ** |
| | Low | | 7 | 14 | |
| | Intermediate | | 24 | 15 | |
| | High | | 80 | 46 | |
| ***CCND1* CISH** | | 168 | | | NS ** |
| | Not amp | | 79 | 61 | |
| | Amp | | 20 | 8 | |
| ***MYC* CISH** | | 165 | | | NS ** |
| | Not amp | | 88 | 60 | |
| | Amp | | 11 | 6 | |
| **Caveolin 1** | | 198 | | | NS ** |
| | - | | 109 | 71 | |
| | + | | 7 | 11 | |
| **Caveolin 2** | | 179 | | | NS ** |
| | - | | 100 | 68 | |
| | + | | 5 | 6 | |
| **FOXA1** | | 158 | | | NS ** |
| | - | | 21 | 17 | |
| | + | | 78 | 42 | |

Ck: cytokeratin; ER: estrogen receptor; IDC: invasive ductal carcinoma; ILC: invasive lobular carcinoma; LN mets: lymph node metastasis; LVI: lympho-vascular invasion; Nielsen groups: immunophenotypic groups defined based upon the expression of ER, HER2, Ck 5/6 and EGFR; PgR: progesterone receptor

*: $\chi^2$ p values (two-tailed, 95% confidence interval)

**: Fisher's exact test p values (two-tailed, 95% confidence interval)